2012

REGENERATION OF ELECTROSPUN BIORESORBABLE VASCULAR GRAFTS: A PHENOMENON ASSOCIATED WITH VASCULAR GRAFT PROPERTIES AND MACROPHAGE PHENOTYPES (M1/M2)

Koyal Garg
Virginia Commonwealth University

REGENERATION OF ELECTROSPUN BIORESORBABLE VASCULAR GRAFTS: A PHENOMENON ASSOCIATED WITH VASCULAR GRAFT PROPERTIES AND MACROPHAGE PHENOTYPES (M1/M2)

A dissertation submitted in partial fulfillment of the requirements for the degree of Doctor of Philosophy at Virginia Commonwealth University.

by

Koyal Garg
M.S., Biomedical Engineering, 2008

Director: Dr. Gary L. Bowlin
Professor, Department of Biomedical Engineering
Co-director: Dr. John J. Ryan
Professor, Department of Biology

Virginia Commonwealth University
Richmond, VA
August 2012

Acknowledgements

There are countless wonderful people who deserve recognition for their guidance and support. I would like to start by thanking my dissertation advisor, Dr. Gary L. Bowlin. I will be eternally grateful to his understanding, encouraging, and appreciative yet challenging mentorship. I cannot thank him enough for the numerous opportunities he has provided me throughout my graduate career. I extend my utmost gratitude to Dr. Bowlin for always being there for me, for believing in me and for guiding me in the right direction to realize my dream. Over the years, Dr. Bowlin has played multiple roles in my life and I have learned a lot from him, but most importantly I have learned the importance of creative and independent thinking.

I owe immense gratitude to my dissertation co-advisor, Dr. John J. Ryan. I have been truly blessed to have had his guidance and support from the conception to the completion of this dissertation. I am indebted to Dr. Ryan for training and teaching me to be a better scientist. Dr. Ryan has taught me to critically analyze results and figure out the next direction by asking the most important and thought intensive questions. I also thank him for the invaluable lessons about mast cell and macrophage biology, or just life in general. I highly appreciate his kindness and patience and I am very grateful for the time and effort he took to discuss at length all my problems and questions in our weekly meetings – he is an outstanding teacher and mentor. He has provided me with guidance in the lab and in life that I will certainly use all through my future endeavors.

Dr. Carole Oskeritzian, who has been a motherly figure to me, deserves a giant thank you. Dr. Oskeritzian's methodical approach to problems has been very inspiring. I have sought her guidance at every step of my dissertation project and she has been most gracious and helpful with her time and resources. A special thanks for patiently training me in the *in vivo* angiogenesis study. I have learned from Dr. Oskeritzian, the art of proper experimental design and interpreting and explaining data in the correct context.

Although I have not worked very closely with Dr. David Simpson, Dr. Hu Yang and Dr. Thomas Haas, I would like to thank you for being on my committee, for always being available to answer questions and for your support with my efforts to earn this doctoral degree. I also offer deep thanks to Dr. Jorge Almenara for his help with histology and immunohistochemistry.

I have been privileged to work with passionate and intelligent engineers and scientists in Dr. Bowlin's and Dr. Ryan's laboratories. A special thanks goes to Dr. Nicholas Pullen from Dr. Ryan's laboratory. The majority of the experiments described in this document would not have been possible without his expert technical guidance and training. I highly admire Dr. Pullen's deep understanding of various biochemical topics and techniques, not to mention the uncanny knack of getting difficult and complex experiments to work. His excellent sense of humor made learning a fun, enjoyable and comfortable experience. I would like to acknowledge the personal and professional support extended to me by Travis Faber, Tenchee Lama Tamang, Brigitte Engelmann, Yves Falanga, Brian Barnstein, Motunrayo Kolawole and Johanna Morales from Dr. Ryan's laboratory. I would also like to thank my fellow tissue-engineers; Scott Sell, Parthasarathy Madurantakam, Yas

Moghaddam, Anna Bulysheva, Michael McClure, Isaac Rodriguez, Jennifer McCool, Michael Francis and Patricia Wolfe in Dr. Bowlin's laboratory for all their support and help.

Thank you to all of my delightful friends, who have enriched my life with their endless care and emotional refueling. In particular I would like to thank Ravi Bhadauria, Meha Kohli and Leena Joseph. These individuals have been rock-solid pillars of support and their love and friendship is what I have looked forward to every evening after a hard day of work. I would also like to thank Gaurav Gupta, Arunvel Kailasan and Lathika Mohanraj for always being there for me.

Last but not the least, I would like to thank and dedicate this dissertation to my life's greatest blessing; my family. My parents (Col Vinod Garg and Dr. Meena Garg) and brother (Madhur Garg) have been a perpetual source of wisdom, encouragement and inspiration throughout my life. Their love empowers me to follow my dreams. Thank you for believing that I can achieve anything, if I set my mind to it.

Table of Contents

List of Figures

List of Abbreviations

1,1,1,3,3,3-hexafluoro-2-propanol (HFP)

Angiopoietin (Ang)

Arginase (Arg1)

basement membrane extract (BME)

basic fibroblast growth factor (bFGF)

bone marrow derived murine mast cells (BMMC)

bovine serum albumin (BSA)

C-X-C ligand 4 (CXCL4)

dinitrophenol-conjugated albumin (DNP)

Directed *in vivo* angiogenesis assay (DIVAA™)

endothelial cells (ECs)

extracellular matrix (ECM)

fluorescein isothiocyanate (FITC)

foreign body giant cells (FBGCs)

hematoxlin and eosin (H&E)

hydrogen peroxide (H_2O_2)

IL-1 receptor associated kinase 4 (IRAK-4)

immunohistochemistry-paraffin (IHC-P)

inducible nitric oxide synthase (iNOS)

Insulin-like growth factor-I (IGF-I)

inteleukin-1beta (IL-1β)

interferon response factor (IRF)

interferon–gamma (IFN-γ)

Interleukin-6 (IL-6)

Jun N-terminal kinase (JNK)

knockout (KO)

lipopolysaccharide (LPS)

macrophage inflammatory protein (MIP)-1α

Macrophages (MΦ)

matrix metalloproteases (MMPs)

monocyte chemoattractant protein -1 (MCP-1)

Myeloid differentiation factor-88 (MyD88)

natural killer (NK)

Nitric oxide (NO_2^-)

nuclear factor kappa B (NFκB)

peroxynitrite ($ONOO^-$)

platelet derived growth factor (PDGF)

poly (glycolic acid) (PGA)

poly(tetrafluoroethylene) (e-PTFE)

polycaprolactone (PCL)

polydioxanone (PDO)

resistin like molecule-α (RELMα)

silk fibroin (SF)

stem cell factor (SCF)

superoxide (O_2)

T helper 1 (T_H1)

TAK1 (transforming growth factor-β-activated kinase 1)

TIR domain containing adapter inducing interferon-beta (TRIF)

tissue culture plastic (TCP)

tissue inhibitor of metalloproteinase (TIMP)

toll-like receptors (TLRs)

TRAF6 (TNF receptor associated factor 6)

Transforming Growth Factor – beta1 (TGF-β1)

Tris-buffered saline containing 0.05% tween-20 (TBST)

Tumor Necrosis Factor – alpha (TNF-α)

vascular basement membrane (VBM)

Vascular Endothelial Growth Factor (VEGF)

Abstract

REGENERATION OF ELECTROSPUN BIORESORBABLE VASCULAR GRAFTS: A PHENOMENON ASSOCIATED WITH VASCULAR GRAFT PROPERTIES AND MACROPHAGE PHENOTYPES (M1/M2)

By Koyal Garg, M.S.

A dissertation submitted in partial fulfillment of the requirements for the degree of Doctor of Philosophy at Virginia Commonwealth University.

Virginia Commonwealth University, 2012

Director: Dr. Gary L. Bowlin
Professor, Department of Biomedical Engineering
Co-director: Dr. John J. Ryan
Professor, Department of Biology

Macrophages (MΦ) and mast cells are important cell types in the context of tissue remodeling and regeneration. Mast cells participate in the early stages of wound healing and modulate the acute inflammatory responses to biomaterials. Mast cells can secrete a myriad of different cytokines by the process of degranulation; the process of regulated secretion in which preformed contents stored in their granules are rapidly released by exocytosis. Some of these cytokines such as IL-4, IL-13 and TNF-α can modulate the MΦ

phenotype. Macrophages (MΦ) are innate immune cells, crucial for tissue homeostasis, presentation of foreign and self-antigens following infection/injury, pathogen clearance, inflammation resolution, angiogenesis, and wound healing. MΦ display plasticity and can acquire pro-inflammatory (M1) or angiogenic/wound healing (M2) phenotypes depending upon the environmental stimuli. The phenotypic profile of MΦ as M1 or M2 following exposure to the biomaterial can dictate the downstream processes of tissue remodeling and angiogenesis. An analysis of how these two cell types interact with electrospun biomaterials and how different properties of an electrospun biomaterial impacts the MΦ phenotype is the focus of this thesis.

Mast cells synthesize several potent angiogenic factors and can also stimulate fibroblasts, endothelial cells and macrophages. An understanding of how they participate in wound healing and angiogenesis is important to further our knowledge about *in situ* vascular prosthetic regeneration. The adhesion, proliferation and cytokine secretion of bone marrow derived murine mast cells (BMMC) on electrospun polydioxanone (PDO), polycaprolactone (PCL) and silk scaffolds, as well as tissue culture plastic (TCP) has been investigated in the presence or absence of IL-3, SCF, IgE and IgE with a crosslinking antigen, dinitrophenol-conjugated albumin (DNP). It was previously believed that only activated BMMCs exhibit adhesion and cytokine secretion. However, this study shows non-activated BMMC adhesion to electrospun scaffolds. Silk scaffold was not found to be conducive for mast cell adhesion and cytokine secretion. Activation by IgE and DNP significantly enhanced mast cell adhesion, proliferation, migration and secretion of TNF-α, MIP-1α and IL-13. This indicates that mast cells might play a role in MΦ polarization

(M1/M2), biomaterial integration into the host tissue, regeneration, and possibly angiogenesis.

In the next study, bone marrow derived murine macrophages (BMMΦs, 10^6 cells) were seeded on TCP (24 well plate) and PDO scaffolds (15 mm discs) electrospun from varying polymer concentrations (60, 100, and 140 mg/ml). Scaffold evaluation showed that large polymer concentrations led to larger fiber diameters, which in turn led to larger pore-sizes and porosity but a smaller surface area to volume ratio. After 24 hrs of culture, the cell lysates were analyzed for Arginase (Arg1) and inducible nitric oxide synthase (iNOS) expression by western blot and cell culture supernatants were analyzed for Nitric oxide (NO_2^-), Tumor Necrosis Factor – alpha (TNF-α), Interleukin-6 (IL-6), Vascular Endothelial Growth Factor (VEGF), Transforming Growth Factor – beta1 (TGF-β1) and basic fibroblast growth factor (bFGF) levels. The results indicated a correlation between Arg1 expression and increasing fiber/pore-size, indicating that the larger fiber/pore-sizes polarize towards a M2 phenotype. Also, the expression of iNOS was downregulated on the larger fiber/pore-size. The levels of NO_2^- were significantly higher on the lower fiber/pore-sizes indicating an M1 phenotype. The levels of VEGF, TGF-β1 and bFGF increased with increasing fiber/pore-sizes. The results showed higher Arg1 expression in M2s on the 60 mg/ml scaffold created by the air-flow impedance method compared to the 60 mg/ml scaffold created on the solid mandrel created by traditional electrospinning. The Arg1 expression was reduced on the compressed 140 mg/ml PDO scaffold compared to the normal 140 mg/ml scaffold. This result indicates that pore-size might be playing a greater role compared to fiber diameter in BMMΦ phenotype modulation.

In order to assess the angiogenic potential of BMMΦs cultured on PDO scaffolds, a 3D angiogenesis bead assay was performed using conditioned media from the BMMΦ:PDO interaction. The results of the 3D angiogenesis bead assay showed that the conditioned media from BMMΦs of M0 and M2 phenotypes cultured on the 140 mg/ml PDO scaffold induced larger sprouting and higher percentage density of sprouts when compared to the 60 mg/ml PDO scaffold and TCP.

To investigate the signaling mechanism involved in this phenotypic switch, BMMΦs were isolated from the bone marrow of MyD88 knockout (KO) mice (Jackson Laboratories) and cultured on PDO (60 and 140 mg/ml) scaffolds (10^6 /disc) and TCP for 24 hrs and their Arg1 and iNOS expression was analyzed by western blot. The expression of Arg1 and iNOS was severely impaired on the BMMΦs from MyD88$^{-/-}$ mice cultured on the 140 mg/ml scaffold when compared to the 60 mg/ml PDO scaffold and TCP. This result indicates that scaffolds with different fiber/pore-sizes signal differently.

A subcutaneous mouse model (described in Chapter 6) was used to evaluate the angiogenic and regenerative potential of PDO scaffolds *in vivo*. The DIVAA assay showed statistically higher FITC-dextran signal intensity for the 140 mg/ml scaffold compared to the 60 mg/ml scaffold indicating greater angiogenic response in the 140 mg/ml tube. However, problems of high background were observed in this assay with the use of electrospun PDO. The observed high background was probably due to the formation of complexes between dextran and adsorbed plasma proteins on the surface of the PDO. More studies are needed to optimize this assay for use with biomaterials such as PDO. H&E staining of the harvested PDO tubes (60 mg/ml and 140 mg/ml) was also performed. The

cross-sections of these tubes showed greater cell recruitment and infiltration into the fibrous structures of the 140 mg/ml tube compared to the 60 mg/ml tube. This result corroborates the *in vitro* result of BMMΦ infiltrating deeper into the structures of the 140 mg/ml scaffold compared to the 60 mg/ml scaffold. The scaffolds were also analyzed by immunostaining for iNOS (indicative of M1 phenotype of MΦs). The results showed statistically higher ratios of iNOS positive:negative areas on the 60 mg/ml scaffold compared to the 140 mg/ml scaffold. Overall, these studies indicate that 140 mg/ml scaffold supports greater cell recruitment and cell infiltration *in vivo* but a smaller ratio of iNOS positive:negative areas compared to the 60 mg/ml scaffold, which supports a predominately M1 MΦ phenotype.

The studies indicate that varying properties of PDO can alter both the phenotype and function of BMMΦs *in vitro* and *in vivo*. We have also shown that the 140 mg/ml scaffold signal BMMΦs through MyD88-dependent mechanisms. A complete understanding of the way materials signal would allow us to control or modulate undesirable immune reactions to biomaterials *in vivo*. These studies would also help engineer biomaterials that promote angiogenesis and regeneration *in vivo*.

Chapter I: Introduction

I.1 Host Response to Biomaterials

The host response to tissue injury or implanted biomaterials occurs in four main stages: hemostasis, inflammation, proliferation, and remodeling (Figure 1). In the very early process of implantation, injury to the tissue and vasculature activates platelets. The activation of platelets results in the release of clotting factors that initiate hemostasis. A provisional matrix forms on the surface of the biomaterials consisting of fibrin and entrapped erythrocytes. This provisional matrix provides structural, biochemical and cellular components to the process of wound healing. It serves as a substrate for cell migration and a medium for cell signaling. In addition to the activation of clotting factors, platelets also release several cytokines and chemokines such as platelet derived growth factor (PDGF), Transforming growth factor beta (TGF-β1), C-X-C ligand 4 (CXCL4) and inteleukin-1beta (IL-1β). These factors contribute to tissue repair by recruiting several different cell types including neutrophils, macrophages and fibroblasts. Neutrophils are the first inflammatory cell type to arrive at the wound site. They phagocytose and destroy foreign material, bacteria and dead cell debris. Mast cells also mediate acute inflammatory responses to implanted biomaterials by releasing granules containing enzymes, histamine, and other factors such as IL-4 and IL-13 that modulate the inflammatory response. Neutrophils are quickly replaced by monocytes as the predominant cell type. Three reasons account for this phenomenon: (1) Neutrophils have a short half-life and disintegrate and disappear after 24-48h. (2) The chemotactic factors for neutrophil migration are activated early in the inflammatory response. (3) After emigration from the vasculature, monocytes

differentiate into Macrophages (MΦ) and these cells have a much longer life span (~months). MΦ begin to dominate the cell population by day 48-72 h post-injury.

MΦ continue the process debridement and disinfection by removing apoptotic neutrophils and bacteria. In response to microbial products such as lipopolysaccharide (LPS) and cytokines such as interferon–gamma (IFN-γ), MΦ acquire an M1 phenotype. These MΦ destroy pathogens by phagocytosis and by production of reactive nitrogen and oxygen species, including nitric oxide (NO), peroxynitrite ($ONOO^-$), hydrogen peroxide (H_2O_2) and superoxide (O_2). M1s also produce a myriad of enzymes such as matrix metalloproteases (MMPs), collagenase, elastase and hyaluronidase and are crucial in matrix destruction and tissue reorganization at the injured tissues. This also allows them to quickly migrate through the injured tissues to clear pathogens and debris. Prolonged activation of M1s can lead to tissue injury. Therefore, this phenotype must be quickly abolished to make way for a tissue regenerative M2 phenotype. The size, shape, dimensions and chemical and physical properties of the biomaterial may be responsible for variations in the intensity and time duration of the inflammatory and wound healing processes. M2 macrophages are induced by a variety of signals such as IL-4, IL-13 and IL-10. M2s produce arginase, which allows them to convert arginine to ornithine, a precursor of polyamines and collagen, thereby contributing to the production of extracellular matrix (ECM). M2s also produce large amounts of chitinase and chitinase-like molecules including YM1 and YM2. These chitinase –like molecules have carbohydrate and matrix binding activity and play a role in matrix reorganization and wound healing. M2 macrophages also release several growth factors such as VEGF, TGF-β1 and bFGF which play a key role in the next stage of wound healing; the proliferative phase.

The proliferative phase of wound healing involves cellular proliferation, angiogenesis, new ECM deposition and formation of granulation tissue. Granulation tissue derives its name from the pink, soft granular appearance on the surface of healing wounds. Its characteristic histological features include the proliferation of new blood vessels and fibroblasts. The process of formation of new blood vessels from pre-existing vasculature is angiogenesis (or neovascularization). Angiogenesis involves proliferation, maturation and organization of endothelial cells into capillary tubes. The development of granulation tissue also involves proliferating fibroblasts which actively synthesize collagen and proteoglycans. In the early stages of granulation tissue development, proteoglycans predominate; however at later stages collagen type I predominates and forms the fibrous capsule. In the granulation tissue, some fibroblasts may take up the features of smooth muscle cells and these cells are termed myofibroblasts. These cells are believed to be responsible for wound contraction seen during the development of the granulation tissue. Fibrous materials generally have a surface response composed of multinucleated giant cells. These cells are formed by the fusion of MΦ in an attempt to phagocytose the material and are called foreign body giant cells. These cells may persist on the tissue-biomaterial interface for the lifetime of the biomaterial. Adherent human MΦ/foreign body giant cells (FBGCs) on biomaterials produce MMP-9, tissue inhibitor of metalloproteinase (TIMP)-1 and TIMP-2 *in vitro*. The adherent MΦ/FBGCs on a biomaterial surface can modulate ECM remodeling/fibrosis and therefore affect biomaterial performance [1-4]. Typically biomaterials heal with a fibrous encapsulation surrounding the biomaterial with its interfacial foreign body reaction. This encapsulation isolates the biomaterial from the surrounding tissue and prevents its integration with the native tissue. In normal wound

healing, after the deposition of new ECM, the remodeling phase of wound healing begins. This phase is characterized by MMP and TIMP-mediated degradation and remodeling of the newly deposited ECM, usually resulting in scar tissue formation/maturation.

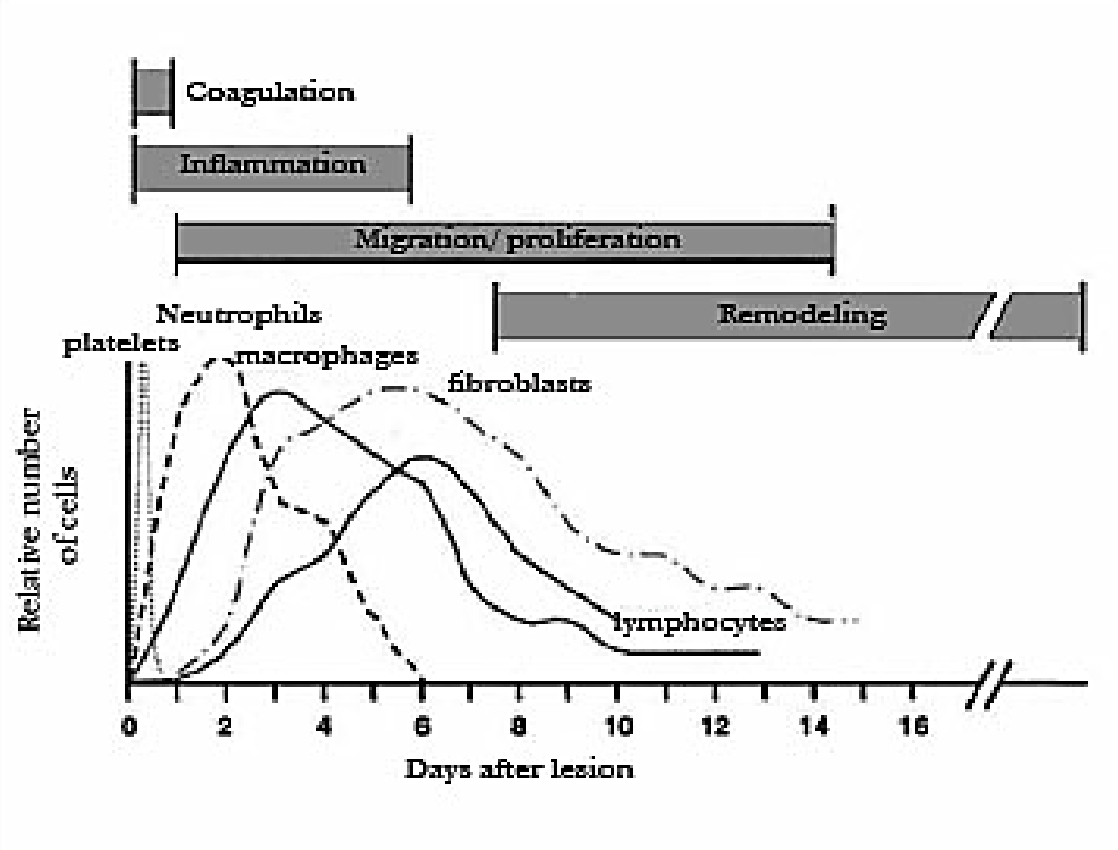

Figure 1 The stages of wound healing [5].

I.2 Macrophage Polarization in Wound Healing

Macrophages belong to the mononuclear phagocyte system. This system comprises the bone marrow monoblasts, pro-monocytes, peripheral blood monocytes and tissue macrophages. They share a common progenitor cell with granulocytes in the bone marrow. This common progenitor is called the colony-forming unit, granulocyte-macrophage (CFU-

GM) because of its ability to give rise to colonies of monocytes and neutrophils in a semi-solid marrow cultures. When monocytes enter the blood stream and migrate into tissues, they undergo final differentiation to tissue macrophages. Macrophages are present ubiquitously in all tissues and display great structural and functional heterogeneity as histiocytes, alveolar macrophages (lungs), Kupffer cells (liver), osteoclasts (bone), peritoneal macrophages (peritoneum), synovia type A cells (synovium), or microglia (central nervous system). Macrophages are set into different functional states by a process known as activation. Activation of macrophages entails increased phagocytic or microbicidal activities and alteration of their chemotactic response and secretory activities. Activation is a complex process involving different stimuli. Macrophages increase performance of some functions and down regulate others. Macrophages can secrete a repertoire of proteases and growth factors such as bFGF, GM-CSF, transforming growth factor- alpha (TGF-α), TGF-β, insulin-like growth factor-I (IGF-I), platelet-derived growth factor (PDGF), VEGF, and other cytokines such as IL-1, IL-6, IL-8 and TNF- α. They also secrete neurotransmitter such as substance P, lipid mediators such as prostaglandins, interferons, and anti-angiogenic substances such as thrombospondin 1 [6].

The specialization and activation of these cells are mainly influenced by local stimuli [7, 8]. Classically activated macrophages (M1) are produced during cell mediated immunity. They can arise in response to IFN-γ, which can be produced during an adaptive immune response by T helper 1 (T_H1) cells or $CD8^+$ T cells or during an innate immune response by natural killer (NK) cells. Alternatively activated macrophages (or wound healing macrophages, M2) arise in response to IL-4, which can be produced during an adaptive immune response by T_H2 cells or during an innate response by granulocytes. IFN-

γ can prime macrophages to secrete pro-inflammatory cytokines, produce increased amounts of superoxide anions and oxygen and nitrogen radicals (e.g. iNOS) to increase killing ability. M1 macrophages produce high levels of IL-12 and modest levels of IL-10. They also secrete IL-1, IL-6 and IL-23. M2 macrophages produce low levels of both IL-12 and IL-10. These macrophages fail to present antigen to T cells, produce minimal amounts of pro-inflammatory cytokines and are less efficient than M1 macrophages at producing toxic oxygen and nitrogen radicals. The M2 macrophages also have increased arginase activity that allows them to convert arginine to ornithine, a precursor to of polyamines and collagen, thereby contributing to the production of extracellular matrix. M2 macrophages also produce large amounts of chitinase like molecules like YM1 and YM2. These molecules lack chitin degrading ability, but they have carbohydrate and matrix binding ability. They also express the antigen resistin like molecule-α (RELMα; also known as FIZZ1) [8-12]. The activation states of MΦ are hypothetical ends of a spectrum. The actual MΦ phenotype is viewed as a continuum of functional states.

Recently M2s were further divided into M2a, M2b and M2c based on their different roles in tissue remodeling (Figure 2). M2a phenotype arises in response to IL-4 and IL-13 and these MΦ are associated with Th2 responses. The M2b phenotype is induced by immune complexes as well as agonists of TLRs or IL-1 receptors and these MΦ secrete high amounts of IL-10 but reduced IL-12. M2c phenotype is induced by IL-10 or glucocorticoids. They produce elevated levels of IL-10 and TGF-β1 and are associated with immune suppression and remodeling [3, 13]. In contrast, INF-γ or TNF-α primed MΦs are grouped as M1s. These MΦs have decreased phagocytic capability and (FcγR)II expression. M1s secrete pro-inflammatory cytokines, such as TNF-α, IL-1, IL-6, IL-12, and IL-23, possess

anti-proliferative functions and induce Th1 responses. In addition, M1s are also crucial in matrix destruction and tissue reorganization at injured tissues via the production of a variety of enzymes such as MMPs, collagenase, elastase and hyaluronidase. This allows M1s to quickly migrate through injured tissues to clear pathogens and debris [3]. Mosser *et al.* suggested a spectrum of MΦ phenotypes and characterized MΦ populations based on three fundamental homeostatic activities, including host defense, wound healing, and immune regulation. MΦ are grouped into three primary phenotypes: classically activated MΦ for microbicidal activity, wound-healing MΦ for tissue repair, and regulatory MΦ for anti-inflammatory activity [12].

MΦ phenotypes exhibit plasticity, meaning that a classically activated M1 can switch to an alternatively activated M2 (Figure 3). Prolonged activation of M1s can lead to tissue injury. Therefore, after disinfecting and debriding the wound site, the M1s must switch over to M2s at later stages to facilitate proper tissue remodeling.

It has been established from previous studies that the fate of a tissue engineered implant depends upon the kind of MΦ response it elicits [14]. Biological responses to implanted materials involve neutrophil mediated detoxification, followed by MΦ activity to phagocytize debris and co-ordinate remodeling events. Several different cell types including natural killer (NK) cells, basophils, mast cells and innate lymphoid cells can polarize macrophages to either a M1 or M2 phenotype (Figure 3). Mast cell derived Interleukin-4 (IL-4) and IL-13 were found to be inductors of MΦ fusion while TNF-α was responsible for biomaterial adherent MΦ apoptosis [15]. Mast cell derived IL-4 and IL-13

can also lead to alternatively activated MΦ (M2 phenotype) which play a role in matrix remodeling, angiogenesis and elimination of parasites [13].

It has been demonstrated that mast cell derived TNF-α is a crucial component of host defense against bacterial infection and is involved in recruitment of leukocytes by establishing cytokine networks [17, 18]. MΦ may also be responsible for the development of mast cells, since removal of MΦs greatly reduced the mast cell development *in vitro* [19].

In a recent study skin biopsies from human patients were obtained and gene expression was analyzed on early (Day 1-2) and late stages (Day 4-8) of cutaneous wound healing (Figure 4). It was observed that the early stage included a mix of M1 and M2 markers (11 M1 genes and 7 M2 genes) whereas the late stage expressed predominately M2 markers (1 M1 gene and 9 M2 genes) [20].

It has been shown by Greisler *et al.* [21-25], Valentin *et al.* [26], Roh *et al.* [27], and Brown *et al.* [28] that macrophages play a key role in the success and potential failure of any vascular prosthetic. Tissue regeneration begins with phagocytosis of debris and ECM remodeling and reorganization through enzymes released by the macrophage which include proteinase, collagenase, elastase and hyaluronidase [29].

The second step involves cell recruitment, migration, proliferation and ECM formation via the spectrum of cytokines produced by the macrophage. The third and final step of tissue regeneration is angiogenesis, a process by which new capillaries are generated from a pre-existing vascular system.

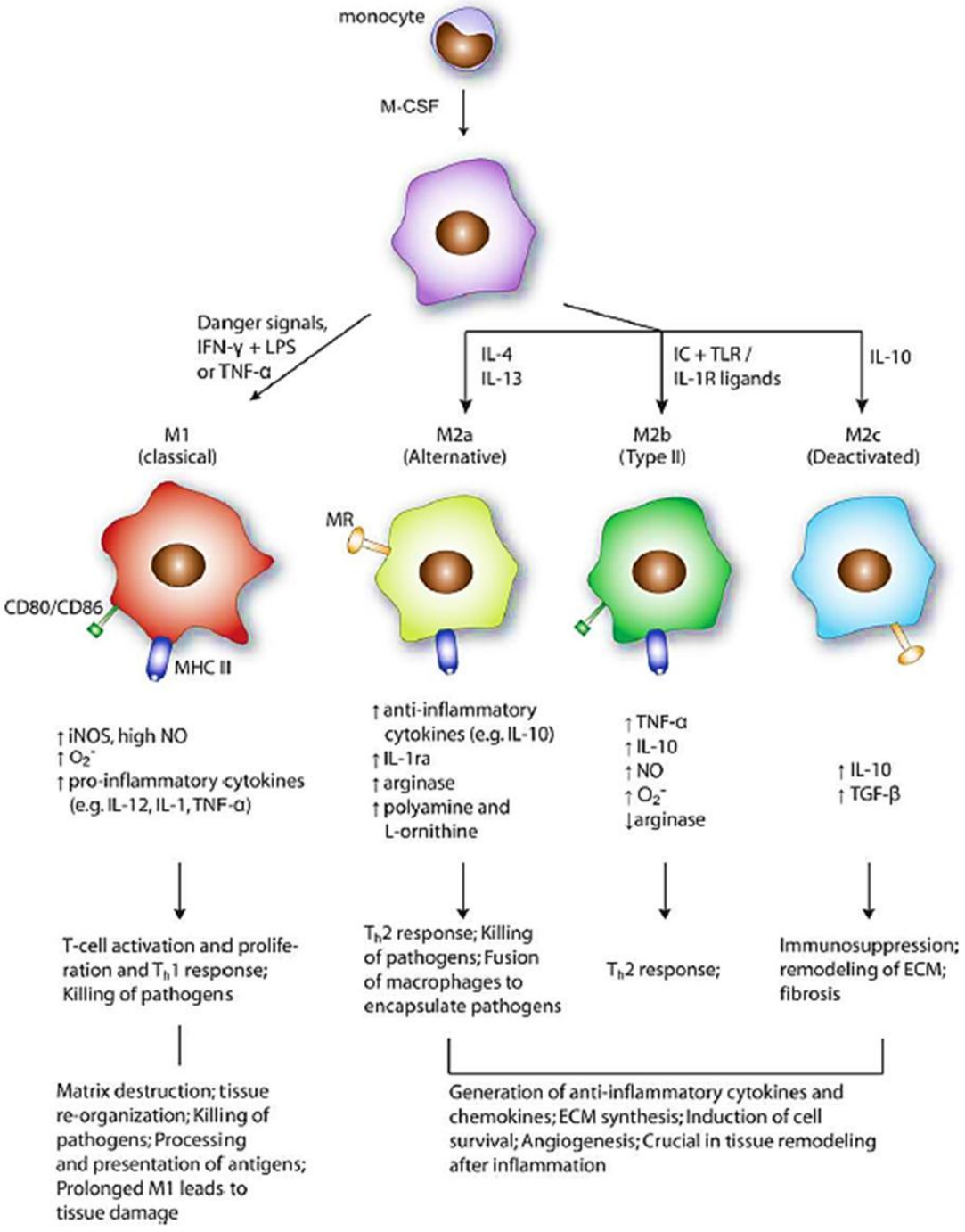

Figure 2 An illustration of macrophage phenotypes, their inducers, phenotype and functions as depicted by Kou *et al.* [3].

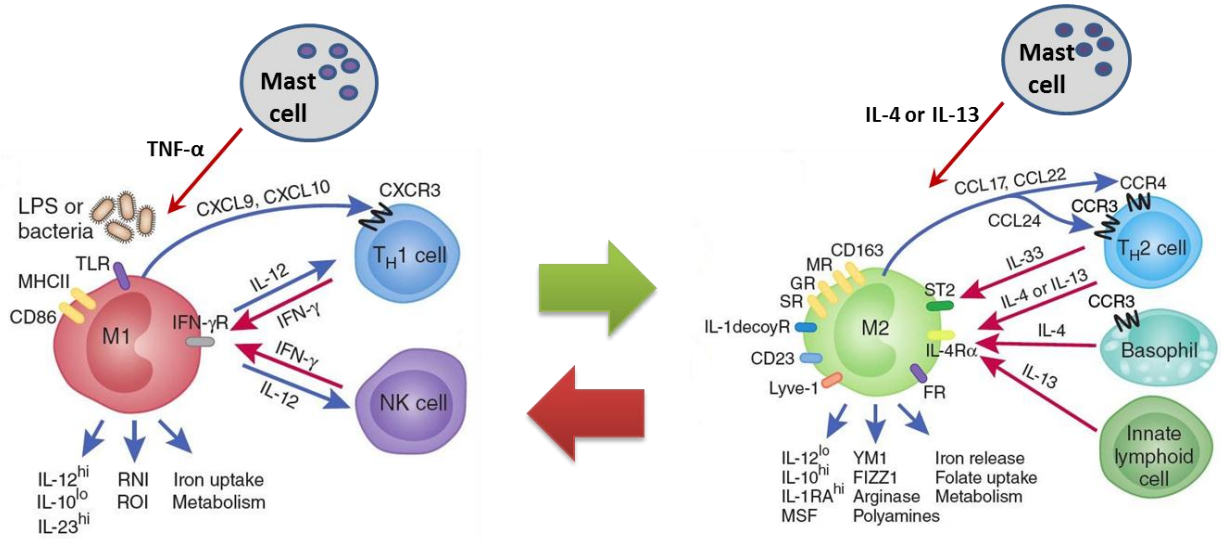

Figure 3 Macrophage polarization in wound healing [16].

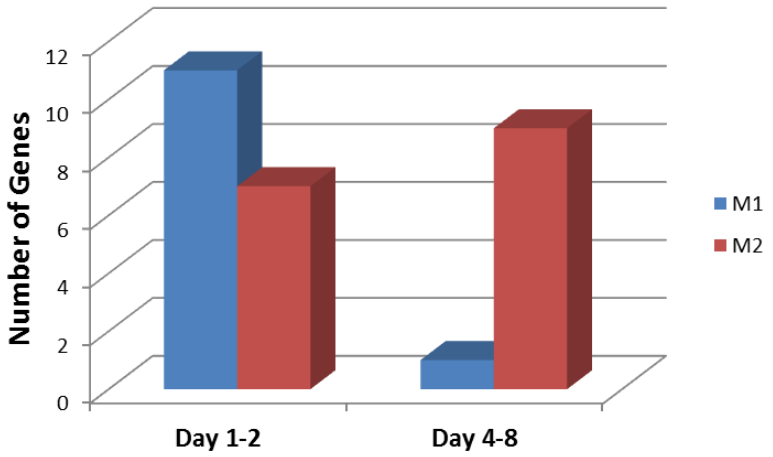

Figure 4 Gene Expression Profiling of Macrophages in cutaneous wound healing [17].

Angiogenesis is fundamental to wound healing, reproduction and embryonic development [18]. It results from stimulation of endothelial cells, which causes them to proliferate and migrate towards the source of pro-angiogenic molecules. On reaching a certain appropriate density, junctions between endothelial cells are formed, components of ECM are produced and a new basal membrane is formed [19]. The endothelial cells then progress to form a hollow tube. All steps in this transformation are induced by the myriad of growth factors derived from the macrophage. The outstanding role of macrophages in angiogenesis can be attributed to their much longer half-life as compared to granulocytes and platelets and secretion of myriad growth factors for initiation, maintenance and termination of the angiogenic process. Also, macrophages are resident in all tissues in greater numbers than other blood borne cells and the distinct subtypes can always be recruited from the blood stream. They have heterogeneous functionality and can be activated from an inactive non-angiogenic stage to an angiogenic stage [6].

MΦs bind to foreign surfaces such as biomaterials via integrin-mediated interactions with the adsorbed protein layer on the material surfaces. MΦs express integrins with three different types of β chains: β1, β2, and β3. MΦs have three β1 integrins, including α4/β1 that binds fibronectin and VCAM-1, α5/β1 that binds fibronectin and α6/β1 that binds laminin. There are four β2 integrins, including αD/β2 and αL/β2 that bind ICAMs, αM/β2 that binds ICAMs and various other ligands such as fibrinogen, Factor X, elastase, and complement fragment C3bi, and αX/β2 that binds C3bi, fibrinogen, and LPS. MΦs have only one β3 integrin, αV/β3, that binds vitronectin, entactin, and ECM proteins containing RGD- and KGAGDV- sequences. These interactions between MΦ integrins and the adsorbed cell-adhesive proteins provide intracellular signals that are crucial in

regulating the functions of MΦs, including cytoskeletal remodeling, gene transcription, spreading, motility, proliferation, apoptosis, survival, and fusion [1, 3, 20].

MΦ response to biomaterials is also dependent on their size. It has been shown that when foreign materials are < 10 μm, MΦ can effectively phagocytose them. The process of phagocytosis leads to the formation of membrane bound phagosomes in the cytoplasm. The phagosomes fuse with endosomes and lysosomes to form phagolysosomes, which contain proteolytic and microbicidal substances to kill, digest and degrade the internalized particles. On encountering larger foreign materials (10-100 μm) that cannot be engulfed by a single MΦ, multinucleated MΦs or FBGCs are formed by the fusion of multiple MΦs. These FBGCs then phagocytose and digest the foreign materials. When FBGCs encounter bulk materials that even they cannot effectively engulf, they undergo a process called "frustrated phagocytosis". In this process MΦs release an array of substances such as cytokines, reactive oxygen species and proteolytic enzymes in an attempt to degrade the implanted materials [1].

I.3 Signaling Mechanisms Involved In Macrophage Polarization

Within the array of MΦ surface molecules, the toll-like receptors (TLRs), specialized membrane proteins that recognize pathogen-specific antigenic patterns, are the likely candidates for mediating biomaterial- MΦ interactions (key MΦ activators). TLRs may be found on the cell surface (TLR-1, 2, 4, 5 and 6) or intracellular (TLR-3, 7, 9). Upon ligand exposure, TLRs couple to signaling adaptors to induce two major downstream signaling pathways, nuclear factor kappa B (NFκB) and interferon response factor (IRF). Myeloid

differentiation factor-88 (MyD88) is an essential adapter protein involved in TLR signaling pathways (except TLR-3) leading to the activation of NFκB.

Different TLRs use different combinations of adaptor proteins to determine downstream signaling. TLR4 is the only known TLR which utilizes all these adaptor proteins [21]. The majority of TLR's signal through MyD88, which couples the TLR to downstream signaling kinases, eventually leading to the activation of NFκB by translocation from the cytoplasm to the nucleus. However, MyD88 independent signaling pathways do exist for TLR3 and TLR4. TLR4 possesses two options for signal transduction, either to signal through MyD88 or through TIR domain containing adapter inducing interferon-beta (TRIF), while TLR3 can signal only through TRIF [22].

MyD88 contains a death domain (DD), which can recruit other DD-containing molecules through homotypic interactions. Upon LPS stimulation, MyD88 recruits and activates IL-1 receptor associated kinase 4 (IRAK-4). IRAK-4 is responsible for the subsequent recruitment, activation and degradation of IRAK-1. Another adaptor protein TRAF6 (TNF receptor associated factor 6), is critical for the MyD88 dependent pathway downstream of IRAK4 and IRAK1. TRAF 6 activates TAK1 (transforming growth factor-β-activated kinase 1). TAK1 then activates downstream IKK (inhibitor of κ light chain gene enhancer in B cells (IκB) kinase) and MAPK (mitogen-activated protein kinase) pathways. IKK complex phosphorylates IκB proteins. This phosphorylation leads to the degradation of IκB proteins and subsequent translocation of the transcription factor NFκB, which controls the expression of proinflammatory cytokines, in addition to other immune related genes. The MyD88-dependent pathway can also activate p38 and c-Jun N-terminal kinase (JNK),

leading to AP-1 activation followed by transcription of genes involved in regulation of cell proliferation, morphogenesis, apoptosis, and differentiation.

TLR4 can also signal via a MyD88-independent pathway to stimulate the production of the antiviral protein interferon (IFN)-β. TLR4 can recruit another TIR-domain-containing adaptor called TRIF. Like MyD88, activated TRIF can bind to TRAF-6 to activate NFκB. Unlike MyD88, TRIF can also bind to kinases called IκKε and TBK1. These kinases activate transcription factors called IRFs (interferon regulatory factors) that are involved in stimulating IFN-β transcription. Thus, the adaptor TRIF enables TLR4 signaling to induce production of IFN-β in addition to activation of NFκB [23].

It is known that wound healing is impaired in MyD88 deficient mice, characterized by delayed wound closure and granulation tissue formation and a decreased density of new blood vessels [24]. In a recent study, it was demonstrated that dendritic cells can sense polymers through a mechanism involving multiple TLR/MyD88-dependent pathways (TLR-2, 4, 6). These TLR-polymer interactions also induced the expression of activation markers (e.g. MHC II, CD80, CD86) and pro-inflammatory cytokines (e.g. IL-1β and TNF-α) [25].

I.4 Angiogenesis

Endothelial cells are one of the major cell types that are involved in the inflammatory and repair processes that occur after scaffold implantation. They participate in these processes by releasing pro-inflammatory factors and expressing cell adhesion molecules [44]. Endothelial cells line up the internal surface of the blood vessels that supply the cells in organs and tissues with oxygen and nutrients to survive and which

remove waste products. These cells are also the primary cells involved in the formation of new blood vessels from pre-existing vasculature, a process known as angiogenesis [45]. Vasculogenesis on the other hand, refers to the first stages of vascular development, through which precursor cells of vascular endothelium suffer differentiation, expansion and coalescence to form a network of primitive tubules in the organism [26]. Under normal conditions in an adult organism, angiogenesis occurs only in the reproductive cycle of females. Angiogenesis occurs in the uterus, with the formation of the endometrium, and in the ovaries, in the formation of corpora lutea. Therefore, the vascular network remains quiescent, but it has the capability to start angiogenesis, especially during the process of healing [27].

New vessels participate in the formation of temporary granulation tissue and supply nutrients and oxygen to the growing tissue. Angiogenesis, in response to tissue damage, is a dynamic process, fine regulated by signs present both in serum and in the local ECM. During the healing process, the formation of new blood vessels becomes necessary to form new granulation tissues, in which the blood vessel cells correspond to about 60% of the repair tissue. Angiogenesis occurs in the ECM of the wound bed with the migration and the mitogenic stimulation of endothelial cells.

The process of angiogenesis begins with the release of angiogenic factors from MΦ, platelets or ECM. Angiogenic factors are then transported to existing blood vessels in the vicinity. At the blood vessel, the angiogenic factors bind to the receptors on the endothelial cells. Factors such as VEGF increase vascular permeability, thereby allowing extravasation of plasma proteins that lay down a provisional matrix for the migrating endothelial cells

(Figure 5). However, excessive permeability of blood vessels is bad as it may lead to circulatory collapse. Angiopoietin (Ang) 2, an inhibitor of the Tie2 signaling, loosens the surrounding ECM by detaching smooth muscle cells. The release of matrix metalloproteases (MMPs) which degrade the surrounding ECM, facilitate endothelial cell migration and further proliferation. Ang 1, a ligand of the endothelial Tie2 receptor, does not initiate endothelial network organization, but stabilizes the networks presumably by stimulating the interaction between endothelial and periendothelial cells. Endothelial cells assemble as solid cords that eventually acquire a lumen.

Finally, the newly formed vessels are stabilized by the recruitment of the surrounding smooth muscle cells and pericytes that provide structural support. An effective wound healing and long-term implant stability and survival require maintenance of an optimal environment for endothelial cell viability and a rapid formation of functional blood vessels. Angiogenic sprouting is controlled by a balance of activators and inhibitors. Angiogenesis inhibitors suppress the proliferation or migration of endothelial cells include angiostatin, endostatin, antithrombin III, interferon-β, leukemia inhibitory factor and platelet factor 4 [26].

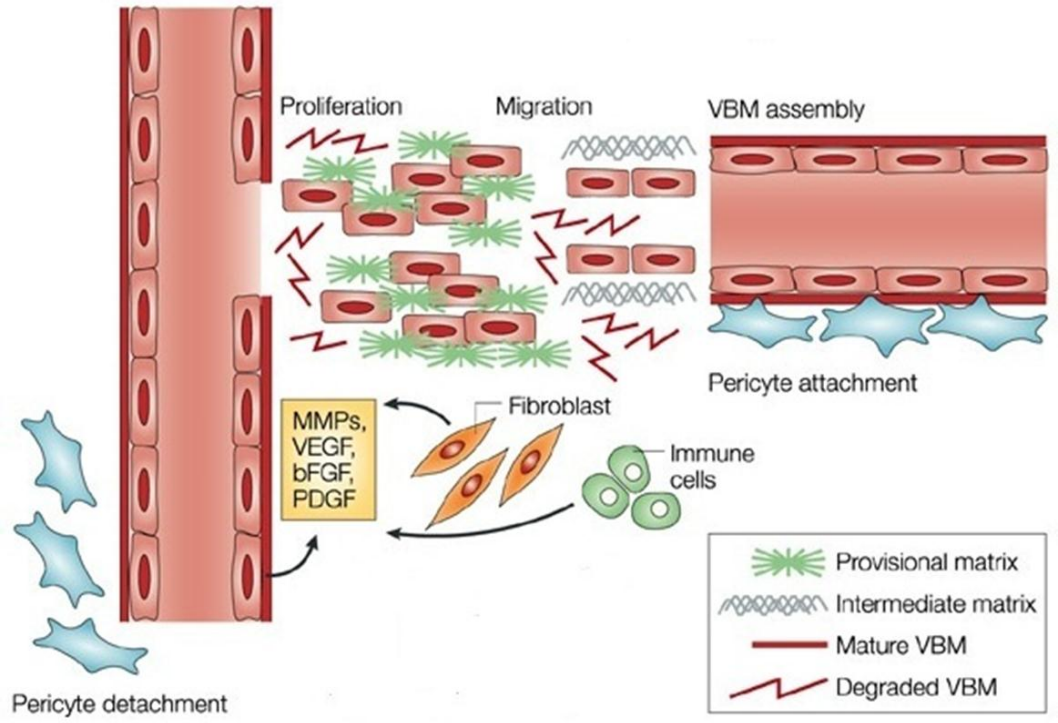

Figure 5 The process of angiogenesis [28].

I.5 Electrospinning for Tissue Engineering Applications

This section has been taken from the review article published in Biomicrofluidics, 2011 Mar 30; 5(1):13403 entitled 'Electrospinning jets and nanofibrous structures'.

A number of processing techniques such as drawing, template synthesis, phase separation, self-assembly and electrospinning have been utilized to synthesize polymer nanofibers for tissue engineering. Drawing is a process that can make one-by-one very long single nanofibers. However, only a viscoelastic material that can undergo very strong deformations can be made into nanofibers through drawing. Template synthesis uses a nanoporous membrane as a template to make nanofibers of a solid or hollow shape. A major drawback of the method is the inability to synthesize one-by-one continuous

nanofibers. The phase separation method consists of dissolution, gelation, extraction using a different solvent, followed by freezing and drying. In self-assembly procedure, pre-existing, individual components organize themselves into desired patterns and functions. However, both phase separation and self-assembly processes are very time consuming in processing continuous polymer nanofibers. Electrospinning is an advantageous processing method for synthesizing one-by-one continuous nanofibers from various different polymers [29]. It's also a very simple, straight forward, cost-effective method to generate different types of scaffolds.

The most basic electrospinning set up consists of three major components: a high voltage power supply, electrically conducting spinneret and collector separated at a defined distance (Figure 6). In the laboratory, the most common set up is the syringe that holds the polymer solution with a blunt tip needle as the spinneret. With the use of a syringe pump, the solution can be fed at a constant and controllable rate. The electrode from the power supply is connected to the needle holding the spinning solution to charge the polymer solution and the other is attached to an opposite polarity collector (usually a grounded conductor). When the high voltage (typically in the range of 0-30kV) is applied to the spinneret, the surface of the fluid droplet held by its own surface tension gets electrostatically charged at the spinneret tip. As a result, the drop comes under the action of two types of electrostatic forces: mutual electrostatic repulsion between the surface charges and the coulombic force applied by the external electric field. Due to these electrostatic interactions, the liquid drop elongates into a conical object known as the Taylor cone. Once the intensity of the electric field attains a certain critical value, the electrostatic forces overcome the surface tension of the polymer solution and force the

ejection of the liquid jet from the tip of the Taylor cone. The liquid jet continues to be ejected in a steady manner and the surface tension causes the droplet shape to relax again. Before reaching the collector screen, the liquid jet elongates and solvent evaporates, leading to the formation of a randomly oriented, non-woven mat of thin polymeric fibers on the collector. Initially the solution jet follows a linear trajectory, but the jet begins to whip out in chaotic fashion at some critical distance from the capillary orifice. This is referred to as the bending instability. At the onset of this instability, the jet follows a diverging helical path. As the jet spirals towards the collection mechanism, higher order instabilities manifest themselves resulting in a completely chaotic trajectory. There are great advantages of using electrospinning for tissue engineering applications. Electrospinning is capable of producing extremely thin fibers with diameters ranging from microns down to few nanometers. In native tissues, cells are typically about one to two orders of magnitude bigger than the structural ECM proteins (50-300 nm). This allows the cells to be in direct contact with many ECM fibers. Therefore, the small-size fibers mimic the structural dimension of the ECM of several native tissues which are deposited and characterized by well-organized hierarchical fibrous structures realigning from nanometer to millimeter scale. The scaffolds produced by electrospinning possess a highly porous microstructure with interconnected pores and extremely high surface-area-to-volume ratio, which is conducive to tissue growth. In addition, it is a very versatile technique and allows the use of a variety of polymers, blends of different polymers, and inorganic materials. Recent advances in electrospinning have shown that integration of various substances such as additives, biomolecules, and living cells is possible in scaffolds for tailoring different application requirements [30].

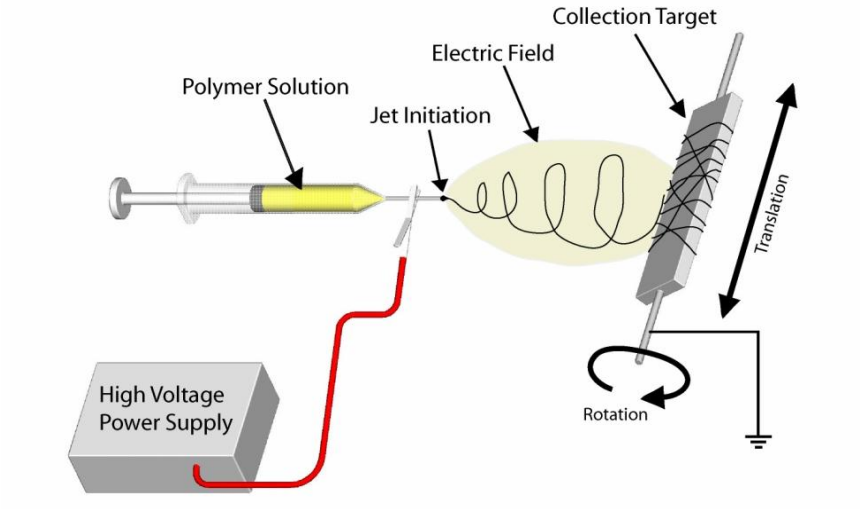

Figure 6 Basic Electrospinning set up.

The typical approach in tissue engineering is to use electrospun scaffolds as ECM analogues or support substrates for the cells that have been seeded on them. The electrospun scaffold is then expected to facilitate the anchorage, migration and proliferation of the cells to reproduce the three dimensional structure of the tissue to be regenerated. Electrospun scaffolds are attractive to tissue engineering because they have biomimetic properties, characterized by fiber diameters in the sub-micron range, large surface to volume ratio, high porosity, variable pore size distribution and the ability to be tailored into a variety of sizes and shapes. In addition, scaffold composition and fabrication can be controlled to match the desired properties and functionality [31-33]. A variety of cell-electrospun matrix interactions have been reported in the literature. Typically, the fiber diameters of these matrices conform to the structural properties of the ECM and are on the order of 80-500 nm. It has also been reported that biocompatibility of a material improves with decreasing fiber diameter [34]. Another parameter very crucial for cell growth is the degree of porosity and the average pore dimension of the nanofibrous

scaffold. Depending upon the cell type, the optimal pore diameters are 20-100 μm [35]. It has also been reported that cells are able to easily migrate to a depth of only about 100 μm[36]. The role of fiber orientation has also been investigated. It has been observed that growing cells tend to follow the orientation of the fibers. In addition, the production of ECM is greater on oriented rather than non-oriented matrix fibers [37].

Several natural and synthetic electrospun polymers have been used to engineer both hard and soft tissues. Natural polymers often lack sufficient strength upon hydration. The mechanical stability of these natural polymers can be improved by either cross-linking or mixing with synthetic polymers [38, 39]. One of the most plentiful proteins in the human body is collagen. Collagen fibers display several attractive biological and structural properties. They transmit forces, dissipate energy, prevent premature mechanical failure, and have high water affinity, low antigenicity and good cell compatibility [40]. Various labs have worked extensively on the electrospinning of collagen (Type I [41], II [42], III [43] and IV [43]) and blends of collagen with both synthetic and natural polymers to produce scaffolds for vascular [38, 44-52], skin [53-58], cartilage [59], bone [60, 61] and ligament [62, 63], nerve [64] tissue engineering applications. Elastin is another key protein found in the native ECM of connective tissues where elasticity and recoil are critical parameters. As collagen and elastin are two of the most predominant proteins in the native vessel, they are often used together as tissue engineering scaffolds for vascular scaffolds, with or without synthetic polymers [50, 65-69]. Elastin has also been blended with PLA for urologic tissue engineering [70]. Recently, silk fibroin (SF) has gained immense popularity in the field of tissue engineering. SF exhibits good biocompatibility, significant crystallinity, high elasticity, good tensile strength, toughness and resistance to failure in compression. SF was

originally electrospun for ligament [71-78] tissue engineering but has also been used for vascular [79-81], bone [82, 83] and skin [84] tissue engineering. For a detailed review of both synthetic and natural electrospun polymers in tissue engineering, the readers are referred to the works of Sell *et al.* [38, 39, 85, 86], Ashammakhi *et al.* [32] and Kumbar *et al.* [87].

The technique of electrospinning has also been used extensively for drug delivery applications. Nanofiber systems for the release of drugs are required to fulfill diverse functions. The matrices should be able to protect the compound from decomposition, should allow for controlled release in the targeted tissue, over a desired period of time at a constant release rate. Kenawy *et al.* demonstrated the release of tetracycline hydrochloride from electrospun matrices composed of Poly[ethylene-co-(vinyl acetate)] (PEVA), PLA, and a 50:50 mixture of the two polymers. The fastest drug release was observed with PEVA, as compared to PLA or the blend. Burst release was observed with PLA, and release properties of the blend were found to be intermediate to those of the pure polymers [88]. It was concluded that release kinetics can be altered by changing the polymer used for the fabrication of the nanofibers. Other parameters that can impact the release kinetics include; the morphology of the fibers, their interaction with the drug and the drug concentration in the fibers. It has been observed that with higher drug concentration, more amount of drug gets enriched on the nanofiber surface, leading to a burst release [89].

In another study, water insoluble antitumor drug called paclitaxel and the antituberculosis drug called rifampin were electrospun onto PLA nanofibers. In the presence of proteinase K, it was found that drug release was nearly linear over time. The

drug release was attributed to the polymer degradation by the proteinase [90]. However, in the case of the hydrophilic drug doxorubicin, burst release was observed. It was reasoned that the hydrophilic nature of the drug caused its accumulation on the surface of the nanofibers, leading to burst release [91]. To circumvent this problem, Xu *et al.* [92] electrospun water-oil emulsions, in which the drug was contained in the aqueous phase and a PLA-co-PGA copolymer was contained in the oil phase. This method showed a biomodal release pattern in which burst release was observed initially through diffusion from the fibers, followed by linear drug release through enzymatic degradation of the polymer by proteinase K.

Coaxial electrospinning technique has also been utilitized for drug delivery. In this system, core immobilizes the drugs and the shell controls their diffusion out of the fibers. Huang *et al*. used coaxial electrospinning to prepare PCL as the shell and two medically pure drugs, Resveratrol and Gentamycin Sulfate, as the cores. The drugs were released in a controlled way without any initial burst effect [93].

Environmentally sensitive polymer drug delivery systems, which can release drugs when triggered by a stimulus (such as pH or temperature), have also been reported. Chunder *et al.* demonstrated that ultrathin fibers composed of two weak polyelectrolytes poly(acrylic acid) (PAA) and poly(allylamine hydrochloride) (PAH) could be used for the controlled release of methylene blue (MB) through pH changes. They also showed that temperature sensitive drug release can be obtained by depositing temperature sensitive PAA/poly(*N*-isopropylacrylamide) (PNIPAAM) multilayers onto the fiber surfaces [94].

I.6 Electrospun Bioresorbable Vascular Grafts

The native blood vessel is a highly complex and crucial organ. The complex vascular network of the human body serves two main functions, delivery of oxygen and nutrients to the tissues and removal of metabolites for clearance or re-oxygenation. As shown in figure 7, the artery is composed of three different layers or tunics of different compositions which surround a hollow core or lumen through which the blood flows. The innermost layer, surrounding the lumen is known as the intima and is made up of single layer of endothelial cells on a basement membrane rich in collagen IV and elastin. This layer contacts the bloodstream and endothelial cells provide a crucial barrier to platelet activation by secreting specific molecules like nitric oxide and prevent thrombus formation. The thick middle layer, the media, is composed of several layers of smooth muscle cells in an extracellular matrix of collagen types I and III, elastin and proteoglycans. In elastic arteries like the aorta, the elastic lamellae allow the artery to maintain sufficient blood pressure with variations in hemodynamic stress of the cardiac systole and diastole. In muscular arteries, elastin is assembled as fibers. The outermost adventitial layer is composed of fibroblasts and randomly arranged collagen type I. This, collagen provides tensile support and prevents vessel rupture. The proteoglycans contribute to the compressibility and the elastin fibers give elasticity to the vessel and provide the ability to recover from pulsatile deformations. Its elastic nature dominates the low strain mechanical response of the vessel to blood flow and prevents pulsatile energy from being dissipated as heat The ideal vascular prosthetic must have the following performance characteristics: ease of handling, suture retention, ease of suture replacement, flexibility with kink resistance, biocompatibility, durability after implantation and association with surrounding

connective tissue, compliance matching that of the native artery, and resistance to aneurysm formation. Also, the graft must be easily manufactured, economical, easily stored and available in a variety of sizes [7].

Initial graft research focused on Poly(ethylene terephthalate) (Dacron) and expanded poly(tetrafluoroethylene) (e-PTFE) as prosthetic vascular grafts. Both Dacron and e-PTFE react with blood components and perigraft tissues in both advantageous and injurious ways. It has been documented that monocytes and macrophages produce cytokines such as IL-1β, IL-6, and TNF-α when incubated with Dacron and e-PTFE [8]. However, these prostheses remained permanently within the host after implantation. The concept of a slowly absorbable graft that could stimulate rapid and controlled regenerative process producing a "neoartery" was first described by Wesolowski *et al.* [9] and Ruderman *et al.* [10]. These grafts were partially bioresorbable and composed of Dacron and polylactide yarns. Bowland *et al.* described the use of Vicryl (a copolymer of polyglycolide and polylactide) as a fully bioresorbable vascular graft [11]. These early grafts were susceptible to aneurismal rupture and dilation.

Greisler *et al.* evaluated woven poly (glycolic acid) (PGA) grafts in a rabbit model. Four weeks after implantation, these grafts were shown to contain an inner capsule composed of a confluent layer of endothelial cells and smooth muscle like myofibroblasts in the midst of dense collagen fibers. Similarly constructed and implanted Dacron grafts failed to show the results described above [12, 13]. It is also important for the bioresorbable graft to regenerate a complex tissue of sufficient strength before prosthetic degradation so as to

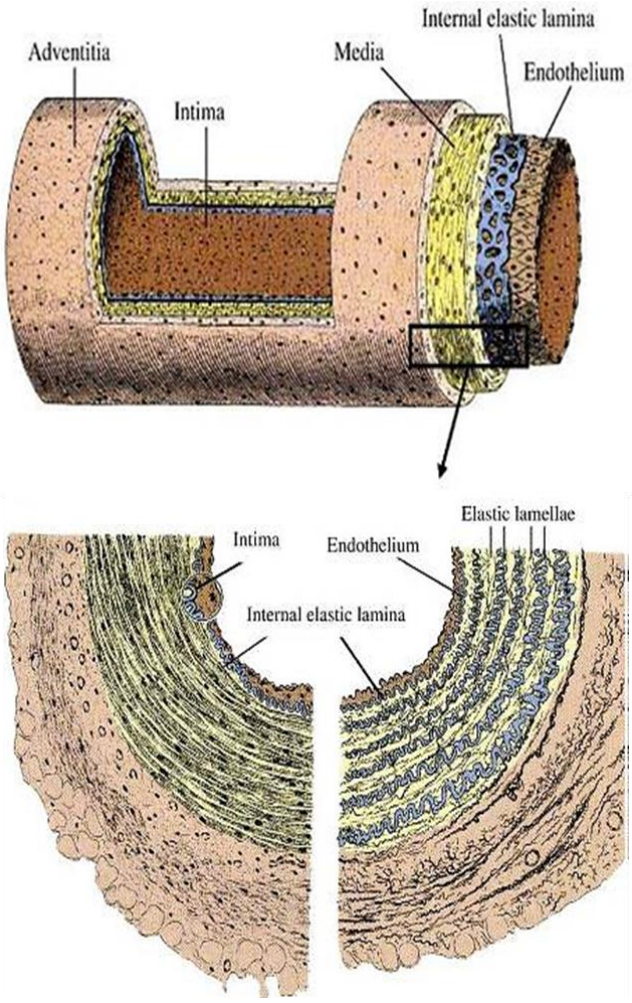

Figure 7 Architecture of the native artery.

minimize the risk of aneurismal dilation. To circumvent this problem two or more bioresorbable materials with different resorption rates can be combined so that the more rapidly absorbed material induces rapid tissue ingrowth while the second material provides structural support [14]. Such composite grafts containing 69% polyglactin 910 (PG910) and 31% polypropylene were implanted into rabbit and dog arteries [15]. These grafts demonstrated 100% one-year patency with no aneurysms. In another study,

composite grafts of 74% PG910 and 26% polydioxanone (PDO/PDS) also showed 100% patency with no aneurysms one year after implantation [16]. PDO is a colorless, crystalline, biodegradable polymer that was developed for wound closure sutures. It exhibits high flexibility, higher strength retention, slower absorption rate, and lower inflammatory response as compared to poly(glycolide lactide) and poly(glycolic acid) [7]. Greisler *et al.* published results utilizing PDO absorbable vascular prosthetics in a rabbit aortic model of regeneration. The results showed no perigraft hematomas and the myofibroblast migration paralleled the macrophage–mediated degradation of the PDO structure. A confluent EC lining was present within two weeks, with the compliance of the explants at 1 year resembling an artery [17]. Greisler *et al.* demonstrated that PDO grafts had the highest production ratio of PGI2/TxA2 at a seven fold increase versus PGA and approximately equal to the native aorta control. The study showed a tissue dependence response in terms of thrombogenicity and the grafts containing PDO were less thrombogenic [18]. PDO can be reproducibly electrospun. It is readily dissolvable in 1,1,1,3,3,3-hexafluoro-2-propanol (HFP) and has been electrospun at concentrations between 42 and 167 mg/ml, producing fibers diameters ranging from 180 nm to 1.4 μm respectively. Uniaxial tensile testing performed on PDO revealed a modulus ranging from 2.0 to 46 MPa, a peak stress ranging from 1.7 to 12.0 MPa, and a percent strain at break ranging from 31 to 240% [7, 19].

I.7 Pore-size/Porosity: a crucial material property for tissue regeneration

From the early stages of vascular prosthetic use, porosity emerged as the design focus, out-ranking material properties. The complex nature of most prosthetic designs makes it difficult to determine the “porosity” or basic void space requirements (defined by

water permeability) for healing and transmural endothelialization. In many prosthetic designs, it has been seen that the porosity is supportive of MΦs and other inflammatory cells to infiltrate, but connective tissue cells (similar cell diameters) were noticeably absent. It was determined that the connective tissue cells (i.e. smooth muscle cells) trail the endothelial cells (ECs) during healing. Thus, an important prosthetic design variable is that the wall pores permit capillaries (average 10 μm diameter) to sprout while leaving room for accompanying cells to trail.

Pore size, pore interconnectivity, and net porosity have always been a focus of tissue engineering scaffolds and have been shown to be key determinants of a scaffold's success through their influence on cell infiltration, nutrient/oxygen exchange, and angiogenesis [95, 96]. The success of electrospun scaffolds has been minimal due to the inability to directly control pore size and overall net porosity due to fiber diameters and the subsequent tight packing of the fibers. Because the fine pore structure restricts cell migration into the structure, it has been suggested that the pore size should at least be the size of the cell of interest to allow infiltration [66, 97, 98]. An additional challenge is that the "optimal" pore size for cell adhesion, proliferation and migration varies by material composition and cell type from 5 to 500 μm [99]. A review by Szentivanyi *et al.* [100] showed that for electrospun scaffolds composed of 0.25 and 2 μm diameter fibers that a 10-50 μm pore size was necessary for cell infiltration. Above 2 μm diameter fibers (resulting pore size >10 μm [97]), the scaffolds were all conducive to cell infiltration. In order to get 50 μm pores, Pham *et al.* [97] showed that one needs 10 μm diameter fibers (pore size is a function of fiber diameter). Electrospun scaffolds composed of submicron diameter fibers generally result in pore dimensions of 1-5 μm. Thus, a fabrication technique that offers

direct control of pore dimension, yet allows for the use of submicron diameter fibers without significantly compromising structural integrity is needed. In terms of maximizing angiogenesis, it has been suggested that optimal physical properties (i.e. pore size, 0.8 to 8 μm) are critical [101]. Soliman *et al.* [102] showed for electrospun PCL that a 50-60 μm pore size enhanced EC infiltration versus a scaffolding composed of 10 μm pores (no infiltration). Lowery *et al*. [103] showed an optimal pore size of 6-20 μm (±50% seeded cell diameter) for electrospun PCL with cells unable to bridge the gaps in larger pores between fibers.

To overcome electrospun scaffold pore size limitations, scaffolds composed of blended synthetic and natural polymers (native integrin binding sites) have been created [104-106]. While cell adhesion was enhanced, these structures had limited success in improving cellular infiltration. The use of porogens in electrospun scaffolds has also been utilized. Zhang *et al.* electrospun a blend of PCL and gelatin without cross-linking, allowing a large percentage of the gelatin to dissolve when immersed in an aqueous media [30]. Baker *et al.* electrospun poly(ethylene oxide) (PEO) fibers intermingled with simultaneously electrospun PCL fibers, with the water-soluble PEO "sacrificial fibers" removed by post-processing [107]. Results showed that the greater the PEO in the scaffold, the greater the cellular infiltration (majority of cells remained in the upper 25%) but at the expense of a significant reduction in the scaffolds' modulus and maximum stress. Nam *et al.* introduced salt crystals amongst the fibers that were removed by post-processing to create void areas that enhanced cell infiltration [108]. The major concerns with this method include the uneven distribution of crystals and loss of scaffold integrity (macroscopic scaffold delamination). The common result of these studies is that enhanced

porosity/cell infiltration comes at the expense of decreased mechanical properties/scaffold integrity. McClure *et al.* [109] recently published a method for scaffold fabrication that allows consistent control over electrospun scaffold porosity by the use of an air flow impedance mandrel. The scaffolds' fabricated possess two seemingly contradictory properties by having both 1) porous regions which permit rapid cell infiltration, and 2) dense fiber regions which are less amenable to cell infiltration, but which provide ample structural integrity. Scaffolds with these properties are made using a mandrel that is perforated. During the electrospinning process, as fibers are deposited onto the perforated mandrel, pressurized air emanating from the mandrel perforations is introduced into the developing fibrous structure that are located at or near the perforation, causing the fibers in those areas to be less dense, creating regions of increased scaffold porosity. In contrast, fibers deposited on solid, non-perforated sections of the mandrel (e.g. located between and adjacent to the perforations) are, in comparison, densely packed. The scaffold thus contains regions in which the fibers are porous and regions in which the fibers are densely packed, all within a single contiguous, seamless structure prepared during a single deposition event, thus not requiring multiple deposition steps and/or processing steps. This now overcomes the major limitation pertaining to the lack of control over scaffold porosity and potentially creates an environment (defined fiber diameters and scaffold porosity) capable of promoting MΦ-mediated angiogenesis and *in situ* tissue regeneration.

I.7 Hypothesis and Thesis Objectives

The host response to implanted biomaterials is a complex multi-step process consisting of various different cell types. MΦ can play both beneficial and detrimental roles

in the process of tissue remodeling due to their inherent plastic nature. An essential and timely phenotypic switch is required for proper and functional remodeling of the tissue as opposed to a scar tissue outcome with a loss of function. Thus, MΦ can decide the fate of the implanted biomaterial. Mast cell is another important cell type in the context of tissue healing. Mast cells participate in the early stages of wound healing and modulate the acute inflammatory responses to biomaterials. Mast cells can secrete a myriad of different cytokines by the process of degranulation; the process of regulated secretion in which preformed contents stored in their granules are rapidly released by exocytosis. Some of these cytokines such as IL-4, IL-13 and TNF-α can modulate the MΦ phenotype. The phenotypic profile of MΦ as M1 or M2 following exposure to the biomaterial (electrospun PDO) can dictate the downstream processes of tissue remodeling and angiogenesis. MΦ participating in the host response to an implanted biomaterial are exposed to numerous cytokines and effector molecules secreted by several types of cells. In addition, MΦ are also exposed to microbial agents, epitopes associated with the implanted biomaterial and the degradation products of the biomaterial. The host MΦ response is modulated via "cross-talk" between MΦ and other cells (e.g. endothelial cells) as well as factors within the local environment. Therefore, a complete understanding how mast cells and MΦ interact with biomaterials is crucial.

This thesis aims to gather insight into the mast cell and MΦ activity on electrospun biomaterials. A detailed analysis of mast cell interaction with electrospun PDO, PCL and Silk is given in Chapter 2. The adhesion, proliferation and cytokine secretion of mast cells on electrospun bioresorbable grafts was investigated in the presence or absence of IL-3, SCF, IgE and IgE with a crosslinking antigen, DNP. We attempted to modulate the behavior

of mast cells on electrospun scaffolds by adding these stimulating agents using tissue TCP as the control. The stimulating agents were chosen and combined according to their proliferation and attachment-inducing potential. The hypothesis in this study is that mast cells would secrete more pro-M2 or pro-wound healing cytokines after interacting with biomaterials and would thereby assist MΦ and other cell types in tissue remodeling.

The next study (Chapter 3) involves the identification of the macrophage phenotype (M1 or M2) promoted by electrospun PDO of varying fiber diameter, pore-size, surface area to volume ratio and porosity. The hypothesis in this study is that differences in pore-size and fiber diameters of electrospun PDO would modulate MΦ phenotype (M1/M2) and thus influence the MΦ mediated angiogenesis and regeneration. A relationship between the M1/M2 profile of MΦs and the downstream angiogenic responses has also been determined using a 3D angiogenesis bead assay described previously [110]. This study is described in detail in Chapter 4. We hypothesized that the bigger fiber/pore-size PDO scaffolds would shift the MΦs to a functionally active M2-like phenotype, which would support angiogenesis.

We have also tried to understand the signaling mechanism by which PDO composed of small or large fiber/pore-size signals MΦ phenotypic responses in Chapter 5. The potential candidates tested in this study were MyD88 and TLR4. The hypothesis for this study was that materials with different fiber/pore-sizes would signal through different mechnisms. A complete understanding of these signaling mechanisms would allow for development of strategies that control the regeneration of biomaterials *in vivo*.

In order to evaluate the angiogenic and regeneration potential of electrospun PDO *in vivo,* we used a subcutaneous directed *in vivo* angiogenesis assay. We hypothesized that electrospun PDO of bigger fiber/pore-size would lead to greater angiogenic response *in vivo.* Furthermore, immunostaining of electrospun PDO would allow for quantification of M1:M2 phenotype ratios. We expected the bigger fiber/pore-size PDO would support a predominately M2 phenotype compared to the small fiber/pore-size PDO.

Recognition of the predominant MΦ phenotypic profile will provide a tool by which a tissue regenerative outcome can be predicted and possibly promoted [111]. Overall, these studies would provide an insight into the mechanisms by which biomaterials heal. These studies would allow biomedical researchers to create better materials for tissue engineering, that self-heal and integrate with the host tissue without any undesirable immune reactions.

Chapter II: Modulation of Mast Cell Adhesion, Proliferation and Cytokine Secretion on Electrospun Bioresorbable Vascular Grafts

This study has been published in the *Journal of Biomedical Materials Research Part A, 2011, 97(4):405-13*.

Koyal Garg*, John J. Ryan# and Gary L. Bowlin*

*Department of Biomedical Engineering, Virginia Commonwealth University

#Department of Biology, Virginia Commonwealth University

II.1 Abstract

Mast cells synthesize several potent angiogenic factors and can also stimulate fibroblasts, endothelial cells and macrophages. An understanding of how they participate in wound healing and angiogenesis is important to further our knowledge about *in situ* vascular prosthetic regeneration. The adhesion, proliferation and cytokine secretion of bone marrow derived murine mast cells (BMMC) on electrospun polydioxanone (PDO), polycaprolactone (PCL) and silk scaffolds, as well as tissue culture plastic (TCP) has been investigated in the presence or absence of IL-3, SCF, IgE and IgE with a crosslinking antigen, dinitrophenol-conjugated albumin (DNP). It was previously believed that only activated BMMCs exhibit adhesion and cytokine secretion. However, this study shows non-activated BMMC adhesion to electrospun scaffolds. Silk scaffold was not found to be conducive for mast cell adhesion and cytokine secretion. Activation by IgE and DNP significantly enhanced mast cell adhesion, proliferation, migration and secretion of TNF-α, MIP-1α and IL-13. This indicates that mast cells might play a role in the process of biomaterial integration into the host tissue, regeneration, and possibly angiogenesis.

II.2 Introduction

An understanding of how mast cells participate in angiogenesis is important to further our knowledge about vascular development and remodeling [112]. Mast cells are important to the pathogenesis of allergic, autoimmune and cardiovascular diseases, and cancer. However, in addition to playing a critical role in host defense, they are also involved in various physiological processes such as angiogenesis, tissue remodeling and collagen production [113-116].

Biological responses to implanted materials involve neutrophil mediated detoxification, followed by macrophage activity to phagocytize debris and coordinate remodeling events. It was reported by Ashley *et al.* that these events occur in the presence of both eosinophils and mast cells [15]. They are known to mediate acute inflammatory responses to the implanted biomaterials [1]. Mast cell-derived Interleukin-4 (IL-4) and IL-13 were found to induce macrophage fusion while tumor necrosis factor alpha (TNF-α) was responsible for biomaterial adherent macrophage apoptosis. IL-4 and IL-13 lead to alternatively activated macrophages which play a role in allergic responses, elimination of parasites and matrix remodeling [13]. Using implantation of fibrinogen coated polyethylene terephthalate (PET) disks in mice, it was found that this biomaterial triggers the activation of mast cells shortly after implantation, releasing granular products including histamine. Mast cell-deficient mice exhibited reduced phagocyte accumulation on the implants. Administration of histamine receptor antagonists also greatly decreased recruitment and adhesion of neutrophils and monocytes/macrophages to implants [117].

Mast cells can be activated by physical stimuli, immunogenic stimuli (Immunoglobulin E (IgE), complement, cytokines and growth factors) and neurogenic stimuli (neuropeptides) [113]. Exposure of mast cells to an allergen leads to cross linking of the IgE-loaded surface receptor, $Fc_{\varepsilon}RI$, with at least three biological effects. First, they can undergo degranulation; the process of regulated secretion in which preformed contents stored in their granules are rapidly released by exocytosis. Granule associated mediators include proteases, histamine, proteoglycans and cytokines such as TNF-α and IL-16. Following degranulation is the rapid enzymatic synthesis of lipid mediators derived from precursors stored in the cell membranes and in lipid bodies. These include, the

arachidonic acid metabolites prostaglandin (PG) D2, leukotrienes (LT) $B4^{+}$ and C4, and platelet activating factor (PAF). Lastly, activated mast cells initiate transcription, translation and secretion of a variety of cytokines and chemokines depending on the mast cell type and stimulus. These include, TNF-α, granulocyte-macrophage colony-stimulating factor (GM-CSF), stem cell factor (SCF), IL-3, IL-4, IL-5, IL-6, IL-10, IL-13, IL-14 and IL-16, and chemokines, such as macrophage inflammatory protein (MIP)-1α, MIP-1β, T-cell activation gene 3, lymphotactin and monocyte chemoattractant protein -1 (MCP-1) [118-121]. Under physiological conditions in several organs, mast cells are found in close vicinity to capillaries and lymphatic vessels and a direct correlation between the number of mast cells and blood vessel density has been demonstrated in the dermis[122]. Mast cells synthesize several potent angiogenic factors such as vascular endothelial growth factor (VEGF), basic fibroblast growth factor (bFGF), heparin, histamine, tumor necrosis factor (TNF-α) and IL-8. On the other hand, endothelial cells may also express the mast cell growth and chemotactic factor, SCF. This shows that endothelial cells may also elicit mast cell chemotaxis and survival, demonstrating a two way relationship between them [123, 124]. It has been shown that SCF is the primary cytokine involved in mast cell differentiation and activation [125-128]. SCF (or c-kit ligand) is critical for mast cell survival, as mast cells cultured without SCF undergo apoptosis [129]. In addition to acting on the vasculature, mast cells may augment wound healing by promoting extracellular matrix deposition. In fibroblasts, mast cell extracts elicit collagen synthesis and activate an enzyme involved in matrix remodeling; gelatinase A [130]. The addition of histamine to cultured fibroblasts has been shown to stimulate proliferation and collagen synthesis [131, 132]. It has also been reported that tryptase, which is abundantly expressed in mast cells,

can act as a growth factor for human fibroblasts and can stimulate collagen type I synthesis [133]. Similar to mast cell-endothelial cell interactions, mast cells can be attracted to fibroblasts via their SCF expression as both membrane-bound and secreted forms.

In this study, an investigation of mast cell interaction with electrospun scaffolds has been performed. The biomaterials chosen for this study were polycaprolactone (PCL), PDO, and silk fibroin (silk). PCL exhibits properties (i.e. compliance) that are conducive to arterial tissue engineering with an extended degradation time, and compatibility for endothelial cells and smooth muscle cells [106, 134-136]. PDO has been extensively studied by our laboratory and has shown promise *in vitro* [105, 106, 137-141]. Its flexibility, excellent strength retention, shape memory, low inflammatory response and slow degradation rate make it a suitable candidate for vascular tissue engineering. The use of silk as a vascular tissue engineering scaffold has escalated recently. Zhang *et al.* demonstrated the bioactivity of human aortic endothelial cells and human coronary artery smooth muscle cells on electrospun silk [142]. It was established by Soffer *et al.* that electrospun tubular silk constructs can withstand native arterial pressures while behaving in a similar manner to native vessels during creep testing [143].

The adhesion, proliferation and cytokine secretion of mast cells on electrospun bioresorbable grafts was investigated in the presence or absence of IL-3, SCF, IgE and IgE with a crosslinking antigen, dinitrophenol-conjugated albumin (DNP). We attempted to modulate the behavior of mast cells on electrospun scaffolds by adding these stimulating agents using tissue culture plastic (TCP) as the control. The stimulating agents were chosen and combined according to their proliferation and attachment-inducing potential. It is widely accepted that IL-3 alone is capable of maintaining mouse mast cell survival.

However, SCF is required for mast cell attachment to substrates. The presence of IgE and antigen can further enhance the survival and attachment of mast cells induced by IL-3 and SCF. The results of various studies show conflicting reports on the effects of IgE in the absence of antigen. Its impact on mast cell survival and attachment has not been clearly defined yet [144]. Overall, our data demonstrate mast cell adhesion, survival and IgE responsiveness when cultured with bioresorbable polymers, supporting the utility of these polymers in tissue grafts.

II.3 Materials and Methods

II.3.1 Electrospinning

Electrospinning was used to generate nanofibrous scaffolds of PCL, PDO, and silk. Silk fibroin was extracted from the cocoons of Bombyx mori silkworms (The Yarn Tree) through an established protocol [145]. PCL (MW 60,000 kDa, Sigma Aldrich), PDO (Ethicon, Inc.) and silk polymer concentrations used in the study were 250, 100 and 100 mg/ml respectively in 1,1,1,3,3,3, Hexafluoro-2-propanol (HFP) to form flat sheets on a stainless steel mandrel (0.5 cm x 3cm x 15 cm). Disks 6 mm in diameter were punched out of these scaffolds and were placed in a 96 well plate. Fibronectin (100 µl) at a concentration of 50 µg/ml was added on top of the disk and the plate was allowed to sit in the incubator at 37°C for an hour. After an hour, the disks were moved to a new well. The scanning electron micrographs of the uncoated scaffolds are shown in Figure 9.

II.3.2 Cell Culture and Seeding

Bone marrow derived murine mast cells (BMMCs) were derived from C57BL/6 mice as described previously [146]. Briefly, BMMC cultures were derived from bone marrow

harvested from C57BL/6 mouse femurs and tibias (Jackson Labs, Bar Harbor, ME). BMMC cultures were maintained in cRPMI supplemented with IL-3 containing supernatant from WEHI-3B and SCF containing supernatant BHK-MKL cells. The final concentration of IL-3 and SCF was adjusted to 1 ng/ml and 10 ng/ml, respectively [147]. After 3-4 weeks in culture, these populations were >99% mast cells, as judged by morphology and flow cytometry staining for expression of $Fc_{\varepsilon}RI$, and Kit (data not shown). The resulting populations were generally used between weeks 4-12. The cells were rinsed with phosphate buffered saline (PBS) and cultured in complete RPMI (cRPMI) 1640 medium (Invitrogen Life Technologies) (10% FBS, 2 mM L-glutamine, 100 U/ml penicillin, 100 µg/ml streptomycin, 1 mM sodium pyruvate, and 1 mM HEPES; Biofluids), supplemented with 5 ng/ml of IL-3 (R&D systems) and 50 ng/ml of SCF (PeproTech) . The cells were then divided into four groups and cultured for 18 hours in the presence of IL-3 (group 1), IL-3+SCF (group 2) and IL-3+SCF+IgE (1µg/ml, clone C38-2, BD Biosciences) (group 3). After 18 hours, Group 3 was centrifuged and suspended in media containing dinitophenyl-human serum albumin (DNP) antigen (100 ng/ml, Sigma-Aldrich) (group 4). This was done to cross link the IgE-loaded cell surface receptor $Fc_{\varepsilon}RI$, triggering BMMC activation prior to scaffold seeding.

II.3.3 Cell Adhesion

Disks 6 mm in diameter were punched from the scaffolds, disinfected (by soaking in ethanol for 10 min followed by repeated rinses in PBS) and placed in a 96 well plate. Each disk was then coated with 100 µl of fibronectin (50 µg/ml) and placed in the incubator at 37°C for an hour. The disks were then moved to a clean well and BMMCs were seeded on fibronectin-coated electrospun PDO, PCL, and silk scaffolds and uncoated tissue culture

plastic (TCP) under four different culture conditions. The culture conditions were; cRPMI media supplemented with IL-3 (group 1), IL-3+SCF (group 2), IL-3+SCF+IgE (group 3) and IL-3+SCF+IgE+DNP (group 4) as described in section 2.2. In all groups, mast cells were seeded at a density of 50,000 cells/well with 170 µL of media. The cells were allowed to attach for 7 hours in the incubator. At 7 hours, the cell seeded scaffold was moved to a clean well and the number of attached cells was quantified by MTS assay as described below.

II.3.4 Cell Proliferation

The numbers of cells on the scaffold were determined with a colorimetric cell titer assay (CellTiter 96® AQ_{ueous}; Promega Corp., Madison, WI). The assay is composed of solutions of a tetrazolium compound, MTS [3-(4,5-dimethylthiazol-2-yl)-5-(3-carboxymethoxyphenyl)-2-(4-sulfophenyl)-2H-tetrazolium] and an electron coupling reagent, PMS (phenazine methosulfate). Metabolically active cells convert MTS into the aqueous soluble formazan product. The quantity of formazan product can be measured by the amount of 490 nm absorbance. It is directly proportional to the number of living cells in culture. For this assay, disks 6 mm in diameter were punched from the scaffolds, disinfected (by soaking in ethanol for 10 min followed by repeated rinses in PBS) and placed in a 96 well plate. Each disk was then coated with 100 µl of fibronectin (50 µg/ml) and placed in the incubator at 37°C for an hour. The disks were then moved to a clean well and BMMCs were seeded on fibronectin-coated electrospun PDO, PCL, and silk scaffolds and uncoated tissue culture plastic (TCP) under four different culture conditions. The culture conditions were; cRPMI media supplemented with IL-3 (group 1), IL-3+SCF (group 2), IL-3+SCF+IgE (group 3) and IL-3 + SCF +IgE+DNP (group 4) as described in section 2.2.

In all groups, mast cells were seeded at a density of 50,000 cells/well with 170 µL of media. In order to exclude any cells attached to TCP, the scaffold disks were moved to a new well plate and 100 µl of fresh media with 20% MTS solution (20 µl) was added and placed in the incubator for 2 hours. Simultaneously, standards were made with mast cells starting with a concentration 200,000 cells/well to zero (media alone). The number of cells was determined by interpolation from the standard curve by using a log-log fit. The assay was performed on day 1, 3 and 5. Each data point was calculated from triplicate wells.

II.3.5 Histology

For histological evaluation, disks of PDO, PCL and silk of all four groups were fixed in formalin on day 3. The paraffin embedded disks were cross-sectioned and stained with hematoxlin and eosin (H&E) to examine cell infiltration into the scaffolds.

II.3.6 Quantification of TNF-α, MIP-1α and IL-13

10 mm disks (disinfected) of fibronectin-coated (50 µg/ml) electrospun PDO and PCL scaffolds were placed in a 48 well plate and an 8 mm cloning ring was placed on top of the scaffolds to retain the cells during scaffold seeding within a defined circumference. Cells were seeded on fibronectin-coated electrospun PDO, PCL, and silk scaffolds and uncoated tissue culture plastic (TCP) at a concentration of ~$1x10^6$ cells/ml. Media was added in the center of each scaffold (100 µl of cells in media incubated for 45 min and followed by 200 µl of media). Cell culture supernatants were collected after 24 hours and stored frozen at -20°C until analyzed by enzyme linked immunosorbent assay (ELISA). The amounts of TNF-α, MIP-1α, IL-13 (PeproTech) secreted by the mast cells due to their

interaction with the electrospun scaffold were quantified by ELISA as per the manufacturer's instructions.

II.3.7 Statistical Analysis

Data expressed in this paper is in the format of means ± standard error of mean (S.E.M). Data of one representative experiment carried out in triplicates are given. Each experiment was reproduced at least twice. All statistical analysis of the data was based on a Kruskal-Wallis one-way analysis of variance on ranks and a Tukey-Kramer pairwise multiple comparison procedure (α=0.05) performed with JMP®IN 8 statistical software (SAS Institute).

II.4 Results

II.4.1 Mast Cell Adhesion and Proliferation

The percentage of adherent mast cells at the end of 7 hours on polymeric scaffolds and TCP are shown in Figure 10. On PCL, PDO and TCP, cells exposed to IgE alone (group 3) displayed greater attachment as compared to group 1 (IL-3) and group 4 (IL-3+SCF+IgE+DNP). Silk exhibited little to no attachment in all groups. SCF +IL-3 (group 2) promoted cell attachment at levels comparable to IgE on TCP and PDO.

Mast cell proliferation on the three scaffolds and TCP was studied at day 1, 3 and 5 with the results shown in Figure 11. Cells stimulated with IgE+DNP (group 4) showed significantly higher proliferation on day 5 as compared to groups 1 and 3 on the PCL and PDO scaffolds. By day 5, the group 4 cells proliferated 2-fold on PCL, 1.7-fold on PDO and 3.3-fold on TCP. Exposure of mast cells to IgE+DNP leads to cross linking of the IgE-loaded surface receptor $Fc_{\varepsilon}RI$. Figure 3 demonstrates that although mast cells exposed to IgE+DNP

initially adhered less than the cells exposed to IgE alone, antigen stimulation allowed for enhanced proliferation and a net gain in cell numbers over the IgE alone group. In fact, IgE in the absence of antigen did not support long-term proliferation and survival of mast cells in this assay. It has been reported that FcεRI aggregation enhances mast-cell proliferation, perhaps owing to the autocrine effects of IL-3 and IL-4 [148]. Our data are consistent with these findings.

SCF is a powerful mast cell co-mitogen. Mast cells treated with IL-3+SCF (Group 2) showed a steady increase in proliferation from day 1 to day 5 for the PDO and PCL scaffolds as well as TCP. Two pieces of data from figure 3 were notable. First, IgE crosslinkage was a stronger mitogen than SCF when used in the presence of PDO or PCL. Second, silk not only offered poor adhesion (Figure 2) but also failed to support mast cell proliferation even in response to SCF or IgE crosslinkage. These data demonstrate the differential ability of the polymer substrates to support mast cell adhesion and expansion.

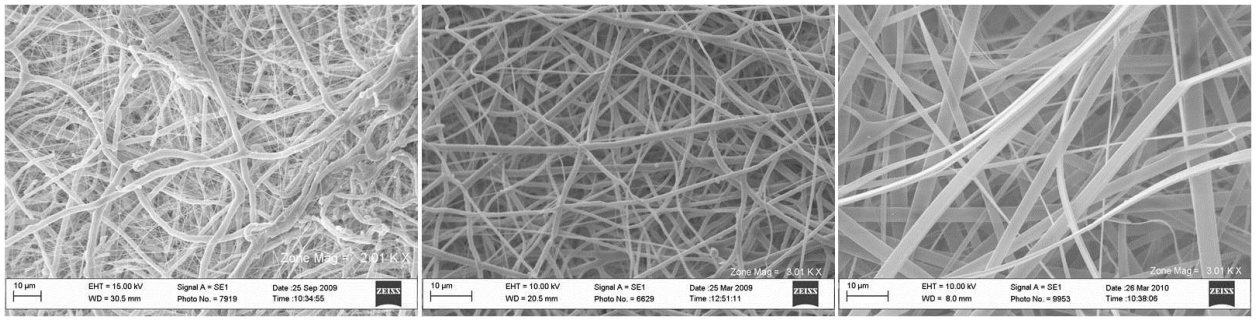

Figure 8 SEM images of PCL (left) PDO (middle) and silk (right).

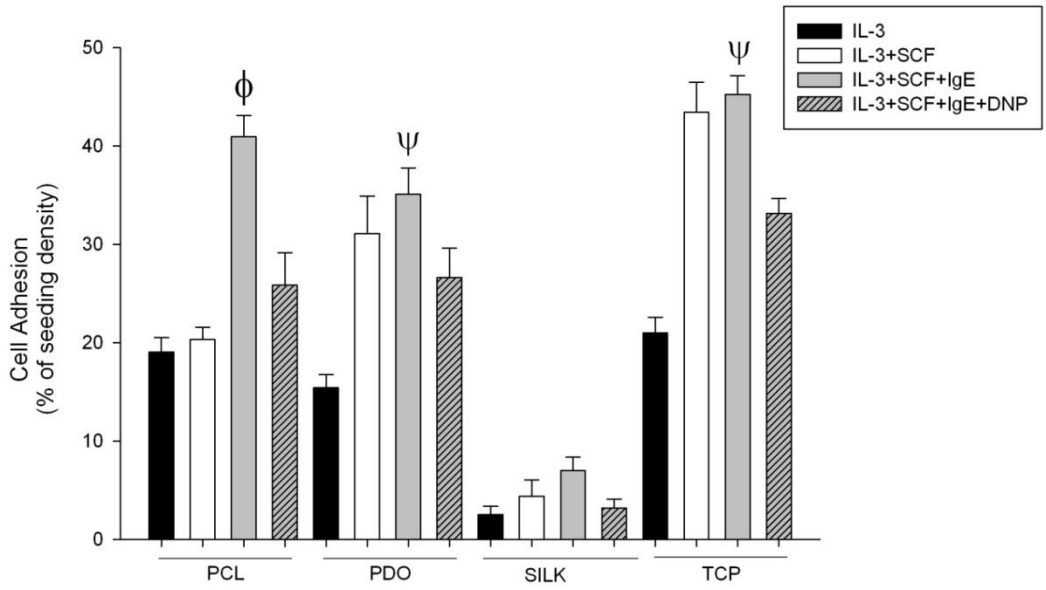

Figure 9 Adherent cells expressed as percentage of seeded cells after 7 hours of culture. Symbols 'Ψ' indicate a statistically significant difference from group 1 (IL3) and group 4 (SCF+IL-3+IgE+DNP) for a particular material. Symbol 'Φ' indicates statistical difference from all groups for that particular material.

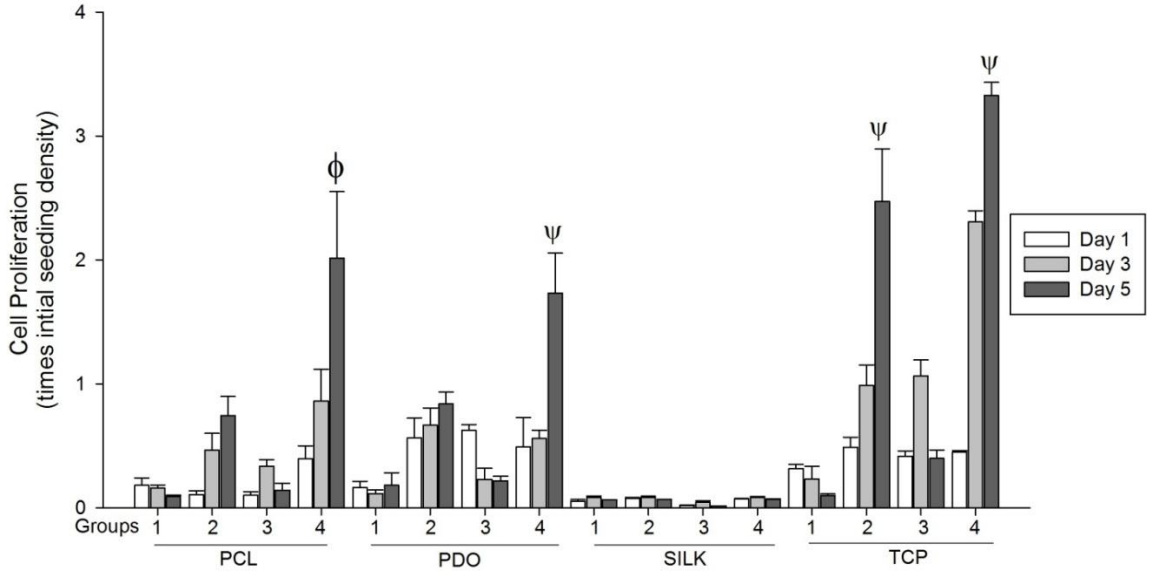

Figure 10 Mast cell proliferation on scaffolds and TCP. Symbols 'Ψ' indicate a statistically significant difference from group 1 (IL-3) and group 3 (SCF+IL-3+IgE) for a particular material. Symbol 'Φ' indicates statistical difference from all groups for that particular material.

II.4.2 Histology

H&E staining revealed cell infiltration into the fibrous structures of PDO (Figure 12h) and PCL (Figure 12d) on day 3. Consistent with the poor cell binding in short-term assays, no cells were observed on the silk scaffold using H&E staining (Figure 12i, j, k, l). Mast cell adhesion molecules include various integrins, intercellular adhesion molecule-1 (ICAM1) and c-kit. It has been shown that mast cells adhere to plate bound laminin, fibronectin and vitronectin only when activated through FcεRI or by pharmacological stimuli such as phorbol 12-myristate-13-acetate (PMA) or calcium ionophore [149-152]. However, mast cells exposed to only IL-3+SCF attached to the PDO and PCL scaffolds. This proves that a combination of fibronectin, SCF and the scaffold nanostructure can elicit mast cell attachment. Consistent with Figure 2, mast cells exposed to IgE alone attached to the scaffold in greater numbers than IL-3+SCF (Figure 12b, c). It has been demonstrated that IgE primes mast cell adhesion to fibronectin using similar pathways as IgE +Ag [153].

As noted when studying proliferation in Figure 3, IgE+DNP stimulation led to the greatest number of adherent mast cells after 3 days of culture with PDO (Figure 12d) or PCL (Figure 12h). The increased number of cells is likely due both to strong adhesion and cell division. The histology analysis also revealed an important difference between the stimuli. In the presence of SCF, mast cells remained largely on the surface of the electrospun scaffold. However, in the presence of IgE+DNP, cellular infiltration dramatically improved. The cells migrated deeper into the fibrous structures of PDO and PCL scaffolds. These data suggest that FcεRI aggregation is a potent stimulus for mast cell attachment, proliferation and migration in the presence of electrospun bioresorbable graft structures.

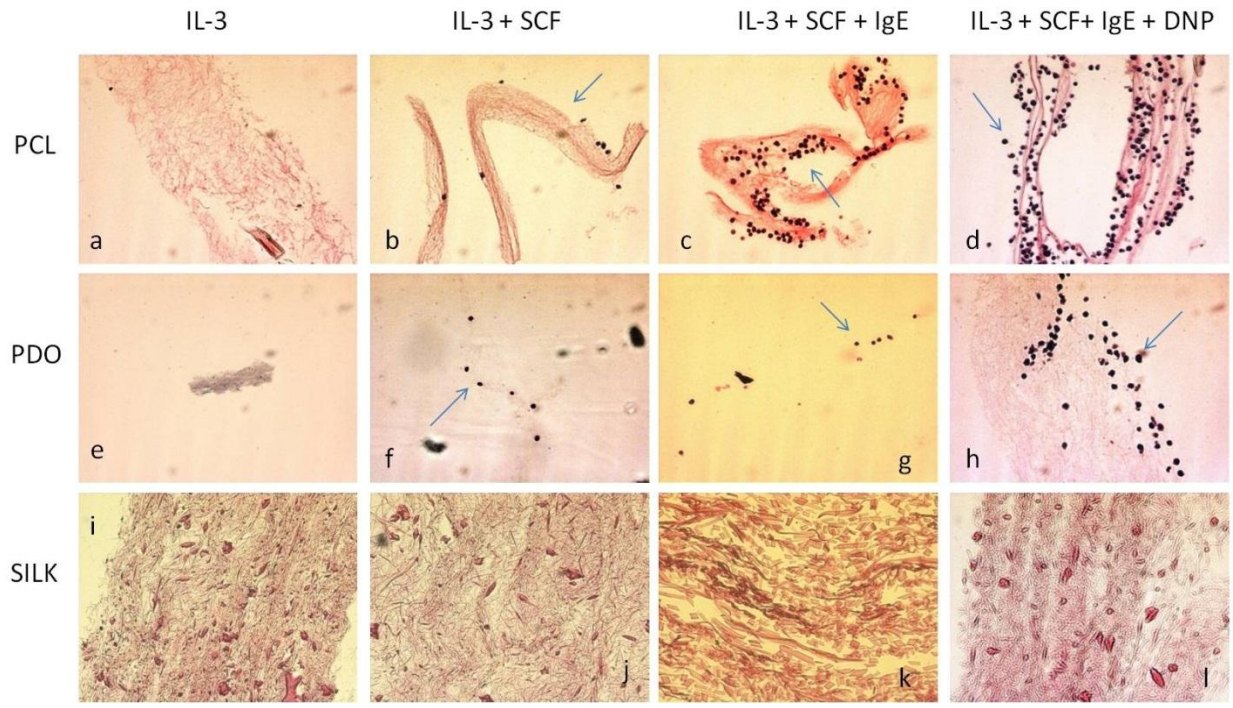

Figure 11 H&E staining of mast cell seeded PCL, PDO and silk scaffolds on day 3. The blue arrows indicate the seeded surface.

II.4.3 Mast Cell Cytokine Secretion

To assess the functionality of mast cells adhered to electrospun scaffolds, we measured cytokine secretion. Mast cells secrete an array of cytokines and chemokines. We chose to measure TNF-α (Figure 13), MIP-1α (Figure 14) and IL-13 (Figure 15), which are well known for their roles in mast cell mediated inflammation [154-165]. IL-3 alone group and silk scaffold were omitted from this study due to their poor capacity for cell adhesion and proliferation. When compared to the background (media alone), only group 4 cells (IgE + DNP) produced any cytokines on the PDO and PCL substrates. While IL-3 and SCF are strong mast cell mitogens, neither is a potent inducer of cytokine secretion as a sole stimulus. In keeping with this, IgE+DNP was the only stimulus to consistently elicit

cytokine production on PDO, PCL and TCP. More importantly, mast cells cultured on PDO or PCL showed similar cytokine responses to the control group cultured on TCP. These data indicate that mast cell adhesion to bioresorbable polymers did not hinder their functionality.

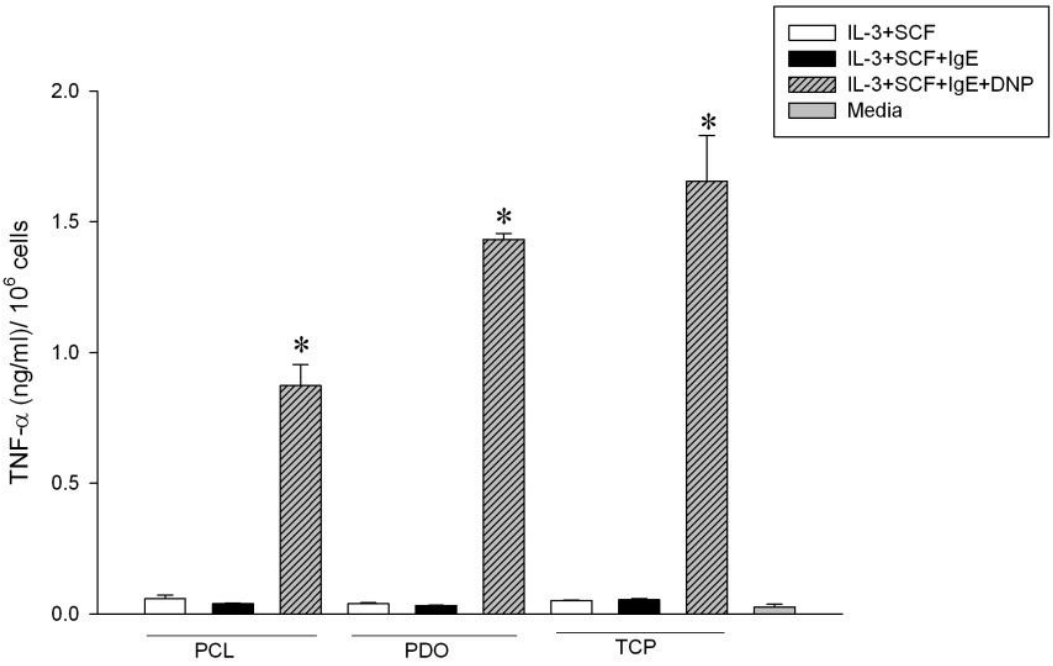

Figure 12 Production of TNF-alpha by mast cells on electrospun scaffolds. Symbol '*' indicates statistical difference from all groups for that particular material.

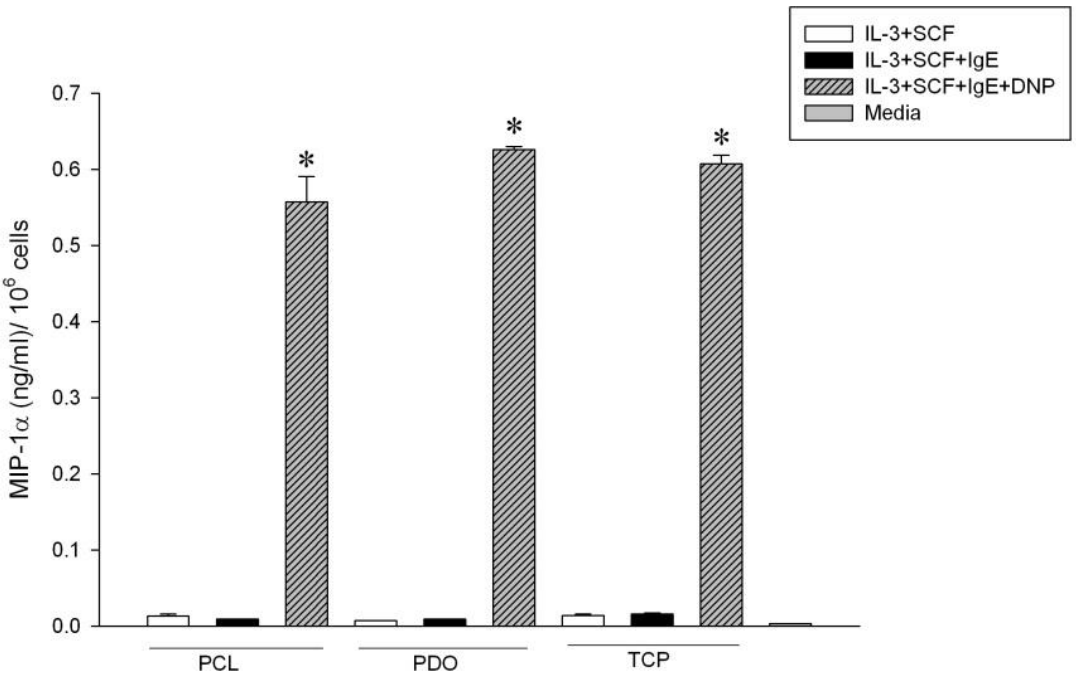

Figure 13 Production of MIP-1alpha by mast cells on electrospun scaffolds. Symbol '*' indicates statistical difference from all groups for that particular material.

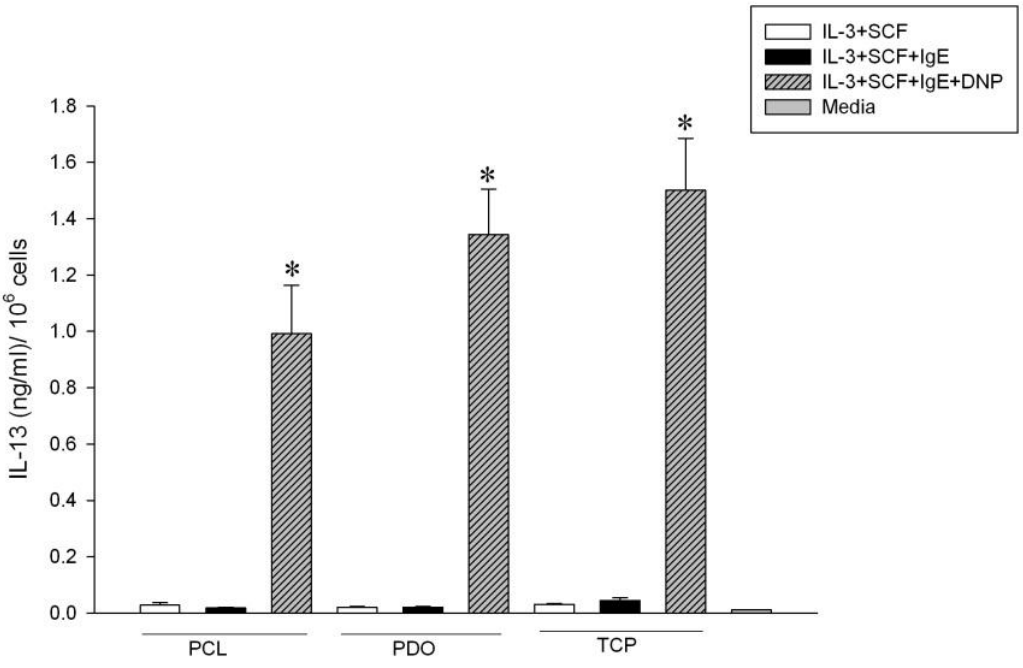

Figure 14 Quantification of IL-13 release by ELISA on day 1. Symbol '*' indicates statistical difference from all groups for that particular material.

II.5 Discussion

One of the main requirements of tissue engineered scaffolds is to provide cells with a suitable environment for cell attachment, which is the first step in the cellular growth process. The use of electrospinning for fabricating nanofibrous tissue engineering scaffolds has escalated at a dramatic rate in the recent years. Electrospinning is capable of producing fibers in micro/nanometer range, which mimic the structural dimension of the native extracellular matrix (ECM). The scaffolds produced by electrospinning possess a highly porous microstructure with interconnected pores and extremely high surface-area-to-volume ratio, which is conducive to cellular growth, attachment and organization [166]. Material interaction with the cells is guided by its physicochemical surface properties [167]. Surface modifications of the electrospun scaffolds can drastically improve the biological performance while retaining all the nanostructure features and properties [168]. He *et al.* fabricated a collagen coated poly (L-lactic acid)-co-poly(ε-caprolactone) scaffold that exhibited enhanced spreading, viability and attachment of endothelial cells (EC) [47]. It was observed in another study that fibronectin coating of polymeric substrates was required for Human Umbilical Vein Endothelial Cell (HUVEC) attachment and spreading [167]. In this study, fibronectin coating was found to be imperative for mast cell attachment and spreading on the electrospun scaffolds (data not shown). Plasma fibronectin modulates the foreign body response and fibrous encapsulation of implanted materials [169]. Cellular transmembrane integrin receptors recognize the Arginine-Glycine-Aspartic acid (RGD) sequences within fibronectin. Once integrins bind to fibronectin, they activate a cascade of intercellular signaling pathways [167, 170].

It has been documented that human mast cells attach to fibronectin and vitronectin only when stimulated by phorbol 12-myristate 13 –acetate (PMA) and or calcium ionophore [150]. In another study, it was found that following $Fc_{\varepsilon}RI$-mediated activation mast cells exhibited flattening and spreading accompanied by cell translocation on laminin, fibronectin and matrigel [149]. However, in this study mast cells adhered to fibronectin-coated electrospun scaffolds in the presence of SCF and IL-3 without any activation agents. But our data certainly did not refute the importance of mast cell activation in adhesion. In fact, we found that $Fc_{\varepsilon}RI$ aggregation augmented initial adhesion and supported proliferation on electrospun bioresorbable vascular graft materials. IgE binding to mast cells is referred to as a 'passive presensitization' step. In this study, IgE in the absence of antigen greatly augmented adhesion but did not support long-term survival and proliferation of mast cells in the absence of antigen. It is important to note that surface $Fc_{\varepsilon}RI$ on mast cells are nearly saturated in vivo. It has been reported previously that more than 80% of mast cell surface $Fc_{\varepsilon}RI$ are occupied by 7 weeks of age in mice [171]. Therefore, passive presensitization is likely to occur, and may have important effects on mast cell adhesion to grafted polymers.

Xiang *et al.* showed that the survival effect of FcεRI aggregation occurs due to the expression of the anti-apoptotic Bcl-2-family protein A1. Mast-cell survival was abolished in *A1a*−/− mast cells, and the increase in the number of mast cells that is induced by FcεRI aggregation *in vivo* was not observed in *A1a*−/− mice [172]. In Figure 3, the decline in cell numbers by day 5 suggests that in the absence of antigen, continuous exposure to IgE is required for mast cell survival. In this study, IgE was not added to the culture medium that was used to feed the cells after day 1. It has been proposed that prolonged FcεRI

aggregation is required for augmented proliferation of mast cells [173]. It has been shown that the binding of monomeric IgE to FcεRI does not induce DNA synthesis, but it renders mast cells resistant to apoptosis induced by growth factor deprivation. However, continuous presence of IgE is required for this anti-apoptotic effect [144]. It can therefore be concluded that the effects of IgE in the absence of antigen are short lived and are more prominent early on as compared to IgE+DNP, which has long-term effects on cells.

It should be noted that the MTS assay cannot efficiently quantify cells that have migrated into the three-dimensional structure of the scaffold and only provides a reliable estimation of the cell number on the surface. The polymeric materials pose unique challenges via various mechanisms including diffusion gradients and sequestering effects. Efforts are underway to validate the modified diphenylamine assay for cell quantification, recently published for use with three-dimensional polymeric scaffolds [174].

The physical properties of silk and its ability to promote endothelial cell growth and proliferation make it a promising candidate for vascular tissue engineering scaffolds. However, this study found that silk scaffold with or without fibronectin treatment was not conducive for mast cell adhesion. Our results are consistent with a study conducted by Panilaitis *et al*. showing that silk was largely inert and even inhibitory with respect to murine macrophage activation [175].

Tissue regeneration requires multiple cells and cytokines acting together in concert in a proper sequence. Mast cells stimulated with IgE+DNP on PDO and PCL scaffolds as well as TCP produced high amounts of TNF-α, MIP-1α and IL-13. It has been demonstrated that mast cell derived TNF-α is a crucial component of host defense against bacterial

infection and is involved in recruitment of leukocytes by establishing cytokine networks [158, 159]. In healing wounds, MIP-1α plays a critical role in macrophage recruitment. It has been reported that MIP-1α levels increase during the inflammatory phase, and decrease as inflammation resolves and repair proceeds. It is essential for T-cell chemotaxis to inflamed tissue and also plays a critical role in the regulation of trans-endothelial migration of monocytes, dendritic cells, and natural killer cells [163-165].

IL-13 was also produced by mast cells adherent to the polymer scaffolds. IL-13 induces expression of endothelial adhesion molecules such as vascular endothelial adhesion molecule-1 (VCAM-1) and chemokines which are required for recruitment of granulocytes and monocytes into tissues [176]. IL-13 stimulates macrophages and fibroblasts to synthesize collagen and promotes fibrosis by stimulating macrophages to produce transforming growth factor (TGF-β) [177]. These results demonstrate that mast cell cytokine synthesis can influence the biological response of various cell types that play an important part in tissue regeneration and angiogenesis. Improved knowledge of these mechanisms will allow us to control and modulate the reactions occurring at the host/implant interface.

VEGF could only be produced from mast cells when they were cultured at very high densities. Mast cells were seeded at $23x10^6$ cells/mL in a 48 well plate and stimulated with IgE (10 μg/mL) and DNP (100 ng/ml). Cell culture supernatants were collected after 24 hours and the VEGF levels were quantified using ELISA. Both TCP and PDO produced similar levels of VEGF as shown in Figure 15.

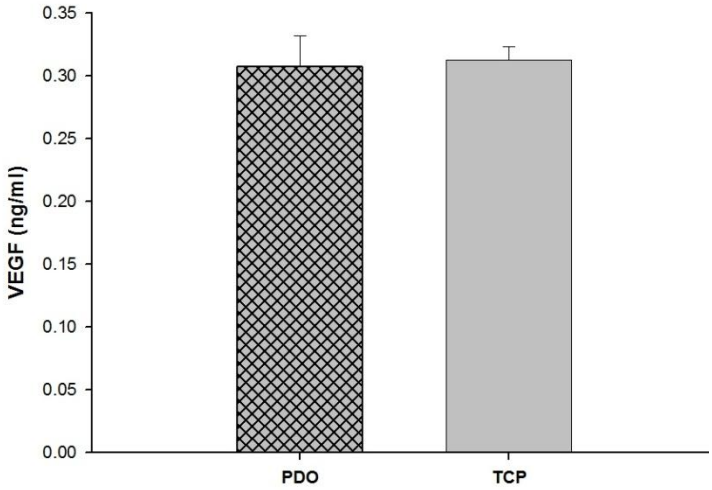

Figure 15 Production of VEGF from murine mast cells on PDO and TCP.

Although many of the differences between human and mouse mast cells appear quite subtle, caution must be observed when interpreting animal model research for use in clinical applications. Animal studies are important in assessing and screening for risks associated with the use of biomaterials in humans. They also help in determining the mechanisms of immune modulation and the cell types affected following biomaterial exposure [116, 178]. Evaluations that understand the behavior of mast cells on electrospun scaffolds at a molecular level may provide insight into the specific causes of effects observed in these studies. Such evaluations will help biomedical researchers in promoting biomaterial integration with the host tissue without any undesirable immune reactions.

II.6 Conclusion

The present study examined for the first time the cytokine expression and adhesion of mast cells on bioresorbable electrospun scaffold for potential use as a vascular graft. The study demonstrates that biomaterial exposure can affect mast cell adhesion and cytokine expression. This indicates that mast cells might play a role in the process of biomaterial integration into the host, tissue regeneration, and possibly angiogenesis. Mast cell attachment onto fibronectin coated electrospun scaffolds led to survival and proliferation, and these cells retained their IgE-induced cytokine production. Improved knowledge of mast cell responses to biomaterials will allow a better understanding of the regeneration process and modulation of both acute and chronic inflammation of implanted biomaterials.

Chapter III: Macrophage Polarization (M1/M2) in Response to Varying Dimensions of Electrospun Bioresorbable Vascular Grafts

Koyal Garg*, Nicholas A. Pullen#, John J. Ryan# and Gary L. Bowlin*

*Department of Biomedical Engineering, Virginia Commonwealth University

#Department of Biology, Virginia Commonwealth University

III.1 Abstract

Macrophages (MΦ) are innate immune cells, crucial for tissue homeostasis, presentation of foreign and self-antigens following infection/injury, pathogen clearance, inflammation resolution, angiogenesis, and wound healing. MΦ display plasticity and can acquire pro-inflammatory (M1) or angiogenic/wound healing (M2) phenotypes depending upon the environmental stimuli. It has been well demonstrated in the literature that MΦ play a key role in determining the fate of any acellular prosthetic/scaffold. In this study, we analyzed how different properties of an electrospun scaffold impact the MΦ phenotype.

Bone marrow derived murine macrophages (BMMΦs, 10^6 cells) were seeded on TCP (24 well plate) and PDO scaffolds (15 mm discs) electrospun from varying polymer concentrations (60, 100, and 140 mg/ml). Scaffold evaluation showed that large polymer concentrations led to larger fiber diameters, which in turn led to larger pore-sizes and porosity but a smaller surface area to volume ratio. After 24 hrs of culture, the cell lysates were analyzed for arginase (Arg1) and inducible nitric oxide synthase (iNOS) expression by western blot and cell culture supernatants were analyzed for nitric oxide (NO_2^-), tumor Necrosis Factor – alpha (TNF-α), interleukin-6 (IL-6), vascular endothelial growth factor (VEGF), transforming Growth Factor – beta1 (TGF-β1) and basic fibroblast growth factor (bFGF) levels.

The results indicated a correlation between Arg1 expression and increasing fiber/pore-size, indicating that the larger fiber/pore-sizes polarize towards a M2 phenotype. Also, the expression of iNOS was downregulated on the larger fiber/pore-size. The levels of NO_2^- were significantly higher on the lower fiber/pore-sizes indicating an M1

phenotype. The levels of VEGF, TGF-β1 and bFGF increased with increasing fiber/pore-sizes.

Therefore, in this study we have demonstrated that by varying the fiber diameter and the corresponding pore-size, we can modulate the macrophage phenotype. The study also shows that electrospun scaffolds of larger fiber/pore-size polarize BMMΦs towards a M2 phenotype.

III.2 Introduction

Tissue engineered biomaterials often induce an inflammatory reaction, also known as the FBR after *in vivo* implantation. Upon exposure to implanted biomaterials MΦs fuse into multinucleated giant cells called FBGCs and ultimately lead to fibrous encapsulation. However, the presence of MΦ is also essential for early remodeling processes. The phenotypic profile of macrophages as M1 or M2 following exposure to the biomaterial can dictate the downstream processes of remodeling and angiogenesis. These processes are modulated via "cross-talk" between macrophages and other cells (e.g. endothelial cells) as well as factors within the local environment. This study aims to gather insight into the macrophage activity on electrospun PDO by identifying the macrophage phenotype (M1 or M2). In general, M1s or classically activated MΦs are pro-inflammatory and microbicidal, whereas M2s or alternatively activated MΦs are immunomodulatory, reparative, and poorly microbicidal. The balance of these two phenotypes of MΦs plays a critical role in the phagocytosis of pathogens and bacteria, the clearance of apoptotic cells, and the remodeling of injured tissues. These activation states of MΦs are hypothetical ends of a spectrum. The actual MΦ phenotype is viewed as a continuum of functional states.

Recently M2s were further divided into M2a, M2b and M2c based on their different roles in tissue remodeling. M2a phenotype arises in response to IL-4 and IL-13 and these MΦ are associated with Th2 responses. The M2b phenotype is induced by immune complexes as well as agonists of TLRs or IL-1 receptors and these MΦ secrete high amounts of IL-10 but reduced IL-12. M2c phenotype is induced by IL-10 or glucocorticoids and they produce elevated levels of IL-10 and TGF-β1 and is associated with immune suppression and remodeling [3, 13]. In contrast, INF-γ or TNF-α primed MΦs are grouped as M1s. These MΦs have decreased phagocytic capability and (FcγR)II expression. M1s secrete pro-inflammatory cytokines, such as TNF-α, IL-1, IL-6, IL-12, and IL-23, possess anti-proliferative functions and induce Th1 responses. In addition, M1s are also crucial in matrix destruction and tissue reorganization at injured tissues via the production of a variety of enzymes such as MMPs, collagenase, elastase and hyaluronidase. This allows M1s to quickly migrate through injured tissues to clear pathogens and debris [3]. Mosser *et al.* suggested a spectrum of MΦ phenotypes and characterized MΦ populations based on three fundamental homeostatic activities, including host defense, wound healing, and immune regulation. MΦ are grouped into three primary phenotypes: classically activated MΦ for microbicidal activity, wound-healing MΦ for tissue repair, and regulatory MΦ for anti-inflammatory activity [12].

MΦ phenotypes exhibit plasticity, meaning that a classically activated M1 can switch to an alternatively activated M2. Prolonged activation of M1s can lead to tissue injury. Therefore, after disinfecting and debriding the wound site, the M1s must switch over to M2s at later stages to facilitate proper tissue remodeling. In a recent study skin biopsies from human patients were obtained and gene expression was analyzed on early (Day 1-2)

and late stages (Day 4-8) of cutaneous wound healing. It was observed that the early stage included a mix of M1 and M2 markers (11 M1 genes and 7 M2 genes) whereas the late stage expressed predominately M2 markers (1 M1 gene and 9 M2 genes) [17].

Several biomaterial strategies have been used for the modulation of MΦ phenotype. It has been shown that the biologic scaffold can profoundly affect the MΦ phenotype. Uncrosslinked decellularized porcine small intestinal submucosa (SIS) induced a M2 response ($CD163^+$) and showed constructive tissue remodeling after 16 weeks in a rat model. Whereas, a carbodiimide crosslinked CuffPatch device elicited a M1 response ($CD80^+$ and $CCR7^+$) leading to chronic inflammation [179]. In another study, it was found that acellular ECM scaffolds induced a predominately M2 phenotype but cellular ECM scaffolds supported a M1 phenotype [111].

MΦ response to biomaterials is also dependent on their size. It has been shown that when foreign materials are < 10 μm, MΦ can effectively phagocytose them. The process of phagocytosis leads to the formation of membrane bound phagosomes in the cytoplasm. The phagosomes fuse with endosomes and lysosomes to form phagolysosomes, which contain proteolytic and microbicidal substances to kill, digest and degrade the internalized particles. On encountering larger foreign materials (10-100 μm) that cannot be engulfed by a single MΦ, mutltinucleated MΦs or FBGCs are formed by the fusion of multiple MΦs. These FBGCs then phagocytose and digest the foreign materials. When FBGCs encounter bulk materials that even they cannot effectively engulf, they undergo a process called “frustrated phagocytosis”. In this process MΦs release an array of substances such as

cytokines, reactive oxygen species and proteolytic enzymes in an attempt to degrade the implanted materials [1].

The impact of fiber diameter on MΦ activation and response has been extensively studied. In a recent study, MΦ (RAW 264.7 cell line) were cultured on electrospun poly(L-lactic) (PLLA) scaffolds. The impact of substrate topography of PLLA scaffold on MΦs was studied by comparing a PLLA film to electrospun aligned microfibers, aligned nanofibers, random microfibers, and random microfibers. The results showed that nanofibrous PLLA scaffolds (fiber diameter ~ 0.6 μm) minimized the inflammatory response when compared to films and microfibrous (fiber diameter ~ 1.6 μm) scaffolds. Histological evaluation demonstrated a higher number of FBGCs on the PLLA film than on the micro- and nanofibrous scaffolds. The fiber alignment didn't seem to have an effect on the *in vitro* MΦ activation and secretion of proinflammatory molecules [180]. In another study, single polypropylene fibers of diameters ranging from 2.1 to 26.7 μm were implanted in the subcutaneous dorsum of Sprague-Dawley rats. Results at 5 weeks showed reduced MΦ density and fibrous capsule thickness for small diameter fibers in the range of 2.1 to 6 μm [181].

The influence of pore-size on the MΦ response has also been explored in several studies. Results have shown that pore dimensions of at least 10 μm are needed to allow connective tissue ingrowth and to avoid global tissue encapsulation [182]. In another study it was shown that a pore size range of 0.8-8.0 μm can facilitate neo-vascularization 80-100 fold compared to samples with pores 0.1-0.8 μm or between 8-15 μm [101]. Dr. Ratner and co-workers fabricated poly (2-hydroxyethyl methacrylate-co-methacrylic acid) (pHEMA-

co-MAA) hydrogel scaffolds with parallel channels by polymer fiber templating. The cardiac implantation of these hydrogels with pore diameters of 30-40 μm showed maximum vascularization and minimal fibrotic response and an increase in the number of M2 phenotype MΦs [183].

In this study, bone marrow derived primary MΦs (BMMΦ) have been used instead of commercially available cell lines (RAW 264.7, J774A.1 or IC-21). This was done because the MΦ cell lines are not equivalent in maturity or activation potential to primary MΦs. A study done by Chamberlain *et al.* showed that cytokine expression at the protein level varied greatly between primary MΦs and immortalized cell lines, with primary MΦs initiating stronger and more diverse responses than the cell lines [184].

III.3 Materials and Methods

III.3.1 Electrospinning of PDO Polymer

PDO (Ethicon Inc.) was dissolved in 1,1,1,3,3,3-hexafluoro-2-propanol (TCI America) in concentrations of 60, 100 and 140 mg/ml. These solutions were then loaded into a Becton Dickinson syringe (5.0 ml) with an 18 gauge blunt tip needle and placed in a KD scientific syringe pump to be dispensed at a rate of 6 ml/hr. Solutions were then electrospun onto a flat rotating stainless steel mandrel (2.5 cm wide × 10.2 cm long × 0.3 cm thick) to produce a flat sheet. All electrospinning was performed at an applied voltage of 23 kV, while the mandrel was rotated at a rate of 500 rpm and placed 12 cm away from the needle tip. The fiber diameter of the electrospun scaffold was measured by Image J. The pore-size, porosity and surface area to volume ratio of the scaffolds was measured using a method described by Soliman *et al*. [102]. Briefly, 10

mm disks of the electrospun scaffolds were weighed and subsequently immersed in ethanol overnight with slight mechanical agitation. This was done to allow the ethanol to penetrate into the scaffold pores. The surface of the samples was then blotted dry on a filter paper and weighed once more to determine the mass of the ethanol present within the scaffold. Measurements were made on five sample disks of each scaffold type. The density of ethanol is 0.789 g/mL and the density of PDO is 1.34 g/mL.

The porosity (ε) was calculated as:

$$\varepsilon = \frac{V_{ETH}}{V_{ETH} + V_{PDO}}$$

V_{ETH} is the volume of the intruded ethanol and was calculated as the ratio between the observed mass change after intrusion and ρ_{ETH}. V_{PDO} is the volume of PDO fibers and was calculated as the ratio between the dry scaffold mass before intrusion and the density of PDO (ρ_{PDO}). The pore-radius was calculated from the following equation:

$$r = \frac{\omega}{\ln\left(\frac{1}{\varepsilon}\right)}$$

where ω is the fiber diameter and ε is the scaffold porosity. The surface area to volume ratio of the scaffolds was calculated using the formulas given by Boland *et al.* [137].

$$\text{Surface area to volume ratio} = \frac{2*\pi*r_f*L}{V_{PDO}}$$

$$L = \frac{M_{PDO}}{\rho_{PDO}*\pi*r^2}$$

where L is the equivalent fiber length, r_f is the average fiber radius.

III.3.2 Endotoxin Content

The endotoxin content of the electrospun polydioxanone (PDO) was determined by the Limulus Amebocyte Lysate (LAL) kinetic chromogenic assay (Endochrome-K™, Charles River) following manufacturer's protocol. Briefly, 6 mm disks of PDO were incubated in endotoxin-free distilled water at 37^0C for 24 h. Absorbed endotoxin was determined after incubation of the PDO disks in endotoxin-free distilled water at 37^0C for 60 min with constant shaking. Afterwards, samples (water) were collected under sterile conditions and transferred to endotoxin-free tubes. Endotoxin levels were quantified using the LAL kinetic chromogenic assay at 450 nm [25].

III.3.3 Macrophage Isolation and Cytokine Secretion

Bone marrow derived murine macrophages (BMMΦs) interaction with electrospun PDO (100 mg/ml, 10 mm discs) and tissue culture plastic (TCP) was evaluated by seeding 500,000 cells in a 48 well plate with or without lipopolysaccharide (LPS, Sigma-Aldrich L6529) (100 ng/ml). The supernatants were collected after 24 hrs to quantify pro-inflammatory mediators (TNF-α, IL-6, Nitrite ($N0_2^-$)) and wound-healing mediators (VEGF, TGF-β1 and bFGF) by ELISA. The C57BL/6 mouse strain was used as a source of bone marrow. Following standard protocol in Dr. Ryan's lab, the mice were euthanized and the bone marrow was isolated from the femurs/tibias. To deplete the adherent stromal cells, the harvested bone marrow was cultured overnight in complete RPMI (with 1% penicillin and streptomycin, L-glutamine, HEPES, sodium pyruvate, 10% FBS, and 30 ng/ml recombinant murine MΦ-colony stimulating factor (rmM-CSF)). Non-adherent cells were collected, red blood cells lysed, remaining non-adherent mononuclear cells plated, and cultured for 7 days in the presence of rmM-CSF. Phenotype uniformity (naïve MΦ (M0) vs.

monocytes) was verified by flow cytometry with our results showing this protocol to achieve a >96% MAC (CD68+) population. After maturation the BMMΦ were divided into three different groups and stimulated for 48 hrs in the presence of either IL-4 and IL-13 to polarize BMMΦ to a M2 phenotype or INF-γ to polarize the BMMΦ to a M1 phenotype. The INF-γ treated BMMΦ were then rinsed with media and treated with LPS for additional 18 hrs. Untreated BMMΦs were used as the naïve group (M0s). The morphology of polarized MΦs on TCP is shown in Figure 16. Extensive pseudopodia were observed in M1s compared to M0s and M2s. In contrast, M2s appeared more rounded. Stimulation with IL-4 and IL-13 produced a mild proliferative effect whereas, stimulation with INF-γ led to an apoptotic effect.

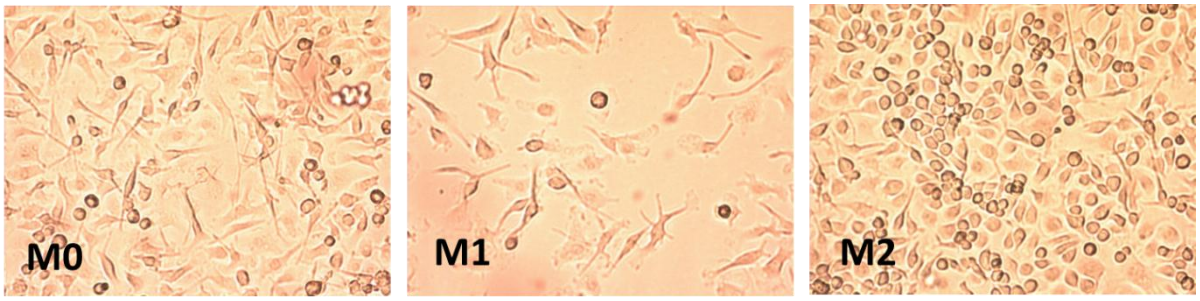

M0	M1 (Negative Control)	M2 (Positive Control)
Naïve (unstimulated BMMϕ).	M1 phenotype BMMϕ stimulated with 20 ng/ml of INF-γ for 48 hours, rinsed and stimulated with LPS for 18 hours.	M2 phenotype BMMϕ stimulated with 20 ng/ml of both IL-4 and IL-13 for 48 hours.

Figure 16 BMMΦ polarization into M1 and M2 phenotypes on TCP.

III.3.4 Arginase and iNOS Expression

BMMΦs (10^6 cells) were seeded on TCP (24 well plate) and PDO scaffolds (15 mm discs) made from varying polymer concentrations (60, 100, and 140 mg/ml). After 24 hrs, the cell lysates were analyzed for arginase (Arg1) and inducible nitric oxide synthase (iNOS) expression by western blot. Cell seeded scaffolds were picked up from the well plate and transferred to a micro-centrifuge tube. The scaffolds were rinsed with PBS and lysed on ice in 50 µl of lysis buffer consisting of 10mM Tris-Cl, 150mM NaCl, 1mM EDTA, 1% Triton X-100, 0.5% sodium dexoycholate, 1mM phenylmethyl sulphonylfluoride (PMSF) and complete protease inhibitor cocktail tablet. The extracts were vortexed vigorously for 3 times at 5 min intervals. The lysates were collected and transferred to a fresh micro-centrifuge tube. The lysates were centrifuged and the supernatants were obtained and stored at -20°C until needed. Protein concentration was determined by the Bradford method using BioRad's protein assay reagent. Protein lysates were completely denatured by boiling in Lammeli sample buffer for 10 mins and subjected to SDS-PAGE. The proteins separated in the gel were transferred to a nitrocellulose membrane. The membrane was blocked with 5% nonfat dry milk in Tris –buffered saline containing 1% Tween 20 (TBST). The membrane was then washed four times with TBST and incubated in the primary antibody solution (containing 5% BSA) overnight at 4°C. The membrane was washed again four times in TBST and incubated in HRP-conjugated secondary IgG antibody-diluted solution (in 5% non-fat dry milk) for 1h at room temperature. After the membrane is thoroughly washed with TBST four times, chemiluminescense was detected using the ECL western blotting detection reagent. The antibodies used in this study are Arginase I (Abcam, ab91279, dilution 1:3000) and iNOS (Abcam, ab15323, dilution 1:2500).

III.3.4 Comparison of fiber diameter vs. pore-size in BMMΦ phenotype modulation

In order to investigate which property of the PDO scaffolds plays a more important role in BMMΦ phenotype modulation, the 60 mg/ml PDO scaffolds were made more porous and the 140 mg/ml PDO scaffolds were made less porous without significantly changing their fiber diameter. The 60 mg/ml PDO scaffold was made more porous using a method described by McClure *et al.*, called air-flow impedance electrospinning. PDO (60 mg/ml) was loaded into a 3 mL plastic Becton Dickinson syringe with an 18 gauge tip needle and dispensed at a rate of 6 ml/h. The needle tip was subjected to +25kV with an air gap distance of 20 cm between the needle and the mandrel. Perforated mandrel contained 0.75 mm diameter holes laterally spaced 2.0 mm center to center distance, while the center to center longitudnal distance was 1.50 mm. The perforated mandrel was subjected to an air pressure of 100 kPa. On one end of the perforated mandrel, a lure lock was fitted and taped to the perforated mandrel using electrical tape. On the other end, a 3 mm diameter solid mandrel was inserted into the perforated mandrel and taped in place. The setup is depicted in Figure 17 [109].

The 140 mg/ml PDO scaffold was made less porous by compressing the scaffolds. Briefly, PDO scaffold of 140 mg/ml was cut into flat rectangular sheets carefully avoiding any raised edges. The sheets were then placed in between two flat stainless steel blocks. This assembly was compressed to 5000 psi using a mechanical hydraulic press (Carver, Inc. Wabash, IN) and the pressure was held for one minute. This method of compression collapsed the pores in the scaffold. This led to a decrease in the pore-size of the scaffold from 14 μm to 9 μm without severely impacting the fiber diameter.

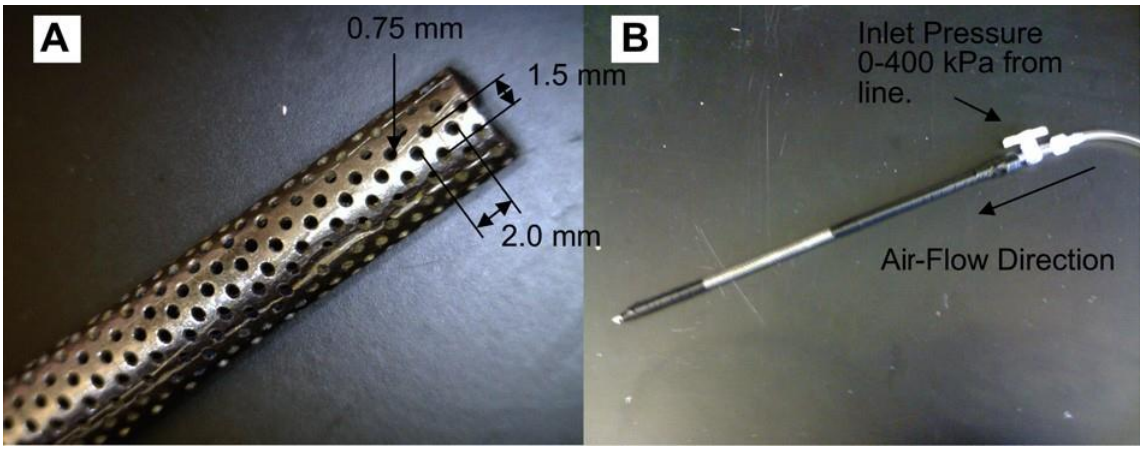

Figure 17 (A) Perforated mandrel used for electrospinning, (B) mandrel set up with air line connected [109].

BMMΦs (10^6) were seeded on 12 mm disks of 60 mg/ml PDO scaffolds electrospun on solid and air-flow impedance impedance mandrels as well as on regular and compressed 140 mg/ml PDO scaffolds , in a 48 well plate. The BMMΦs were seeded on these scaffolds as pre-polarized M2s as described previously. Cell culture lysates were collected after 24 hours and analyzed for Arg1 expression.

III.3.5 Statistical Analysis

Data expressed in this chapter is in the format of means ± standard deviation. Each experiment was done in triplicates and was reproduced at least twice. All statistical analysis of the data was based on a Kruskal-Wallis one-way analysis of variance on ranks and a Tukey-Kramer pairwise multiple comparison procedure (α=0.05) performed with JMP®IN 8 statistical software (SAS Institute). $P<0.05$ was considered significantly different.

III.4 Results

Iii.4.1 Electrospun PDO Properties

It was observed that by increasing the polymer concentration of PDO, electrospun scaffolds of varying properties are obtained (Figure 18). Increasing the polymer concentration led to a linear increase in the fiber diameters, pore-sizes and porosity but decreased the surface area to volume ratio. The statistical differences were only observed in the case of 60 mg/ml and 140 mg/ml scaffolds. The properties of 100 mg/ml and 140 mg/ml scaffolds were not statistically different from one another. It was also noted that the 60 mg/ml scaffold showed beaded fibers but this was not observed with 100 and 140 mg/ml scaffolds that showed smooth continuous fibers. It should also be noted that above 140 mg/ml, the polymer solution becomes too viscous and the scaffolds cannot be reproducibly electrospun leading to inconsistency in data.

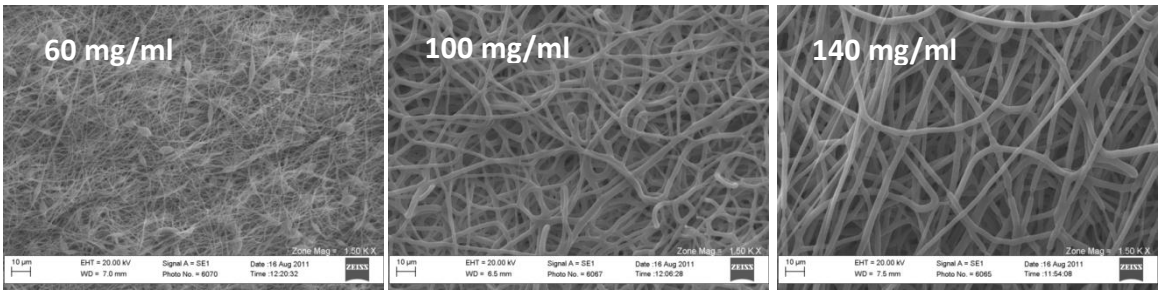

Concentration (mg/ml)	Pore Radius (μm)	Fiber Diameter (μm)	Surface Area to Volume Ratio (m^2/cm^3)	Porosity (%)
60	0.96 ± 0.09	0.35 ± 0.2	11.4	69.4 ± 2.33
100	10.57 ± 0.72	2.2 ± 0.1	1.8	81.16 ± 1.13
140	14.73 ± 0.62	2.8 ± 0.5	1.4	82.67 ± 0.703

Figure 18 Properties of PDO scaffolds electrospun from different concentrations.

III.4.2 Endotoxin Content

Before proceeding with any experiments, we made sure that our PDO scaffolds were not contaminated with bacteria. Since the most common source of bacterial contamination is endotoxin, we determined its levels in our scaffolds. The values for endotoxin content ranged from 0.03 – 0.09 EU/ml. Therefore, the highest endotoxin level for any scaffold was at least 12,000 times lower than the lowest amount used to activate BMMΦs (100 ng/ml of LPS corresponding to 1100 EU/ml) and well below the acceptable U.S. Pharmacopeia standard for clinical applications (<0.25 EU/ml). This study indicated that the PDO materials used in this study were endotoxin free.

III.4.3 Histological Evaluation

The histological evaluation (H&E staining) of PDO scaffolds showed greater BMMΦ (M0s and M2s) infiltration into the fibrous structures of larger fiber/pore-size scaffold (Figure 19). BMMΦ infiltration was quantified using Image J. As expected, the results showed that with increasing fiber/pore-sizes, BMMΦ infiltration of the scaffold cross-sectional area for M0s and M2s increased linearly. The M0s and M2s in the case of small fiber/pore-size PDO (60 mg/ml) scaffold were found concentrated at the surface. The BMMΦ infiltration was statistically higher in the large fiber/pore-size scaffold (140 mg/ml) when compared to the 60 mg/ml scaffold. However, an unexpected result was observed in BMMΦ of the M1 phenotype. In the case of M1s, greater infiltration was observed on the 60 mg/ml. This observation might be attributed to the release of MMPs and other matrix degrading proteolytic enzymes (such as collagenase, elastase and hylauronidase) secreted by the M1 phenotype macrophages [3]. It is known that M1s make their way into tissue by

degrading and destroying it in an attempt to clear the tissue of pathogens and debris. Therefore, prolonged activation of M1s in the absence of M2s leads to tissue injury.

III.4.4 Arginase and iNOS Expression

The results indicated a correlation between Arg1 expression and increasing fiber/pore-sizes in all BMMΦ groups (M0, M1 and M2) on Day 1 (Figure 20). The expression of iNOS decreased with increasing fiber/pore-sizes. Three pieces of data emerge from these results: (1) These results indicate that the larger fiber/pore-sizes (140 mg/ml PDO scaffold, 14 μm pore-size) polarize towards an M2 phenotype in naïve BMMΦ (M0s). (2) The larger fiber/pore-sizes are able to induce statistically higher Arg1 expression and downregulate iNOS in M1 pre-polarized BMMΦ (3) The pre-polarized M2 BMMΦs induce statistically higher Arg1 expression on the large fiber/pore-sizes on Day 1.

On Day 3, it was observed that M0s were unable to maintain Arg1 expression (Figure 21). However, M1 and M2s were able to maintain Arg1 expression. Just like day 1, the larger fiber/pore-sizes induced statistically higher Arg1 by M1s on Day 3 as well. The Arg1 expression level by M2s was maintained on the large fiber/pore-size. It was also observed that the M2s on the small fiber/pore-size PDO increased their Arg1 production on Day 3 compared to Day 1. The expression of iNOS was totally abolished by Day 3 on all fiber/pore-sizes of PDO. In the previous study, we have demonstrated that larger fiber/pore-sizes allow increased M0 and M2 phenotype BMMΦ infiltration of the scaffold, when compared to smaller fiber/pore-sizes.

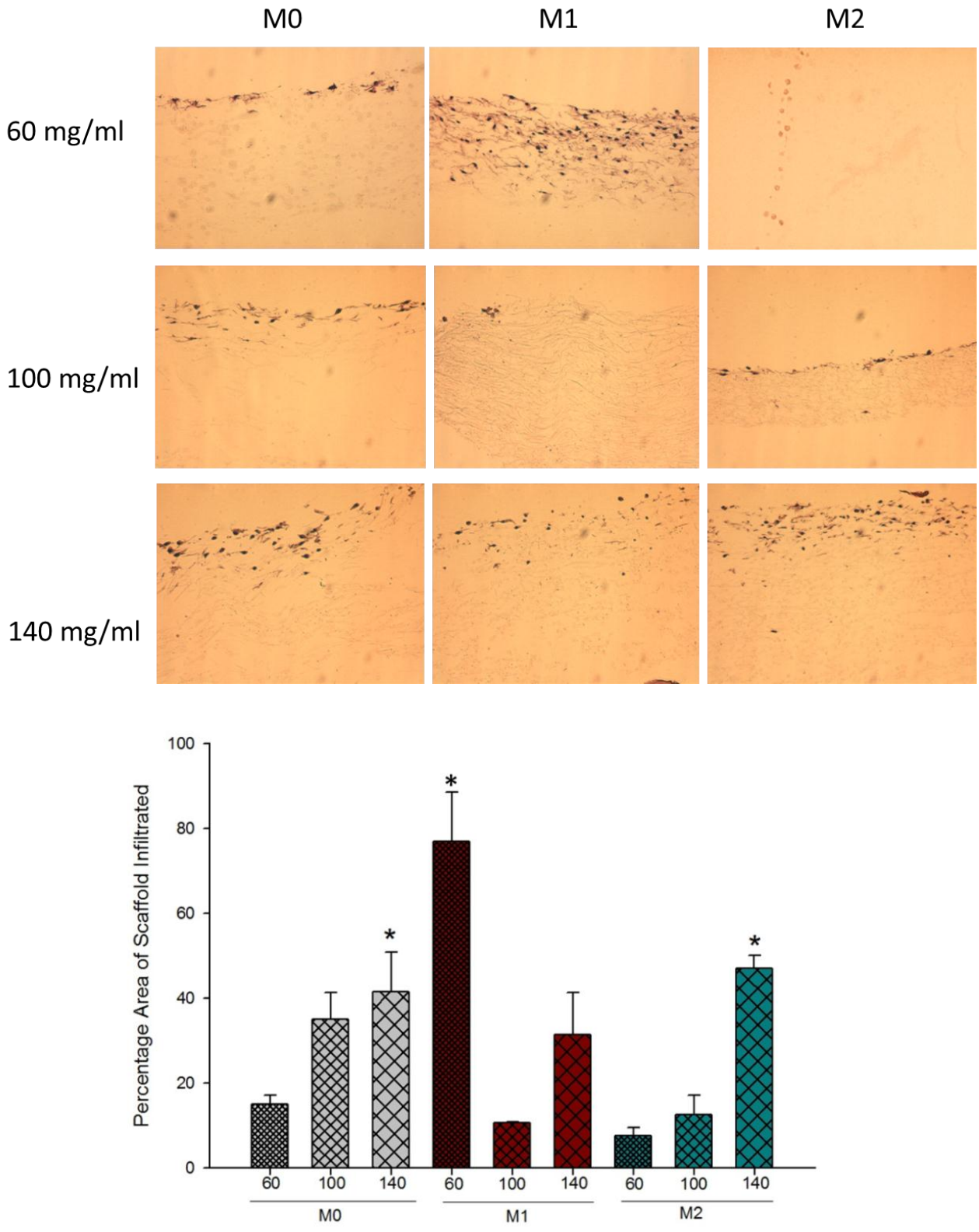

Figure 19 Histological evaluation of BMMΦ infiltration into the fibrous structures of PDO.

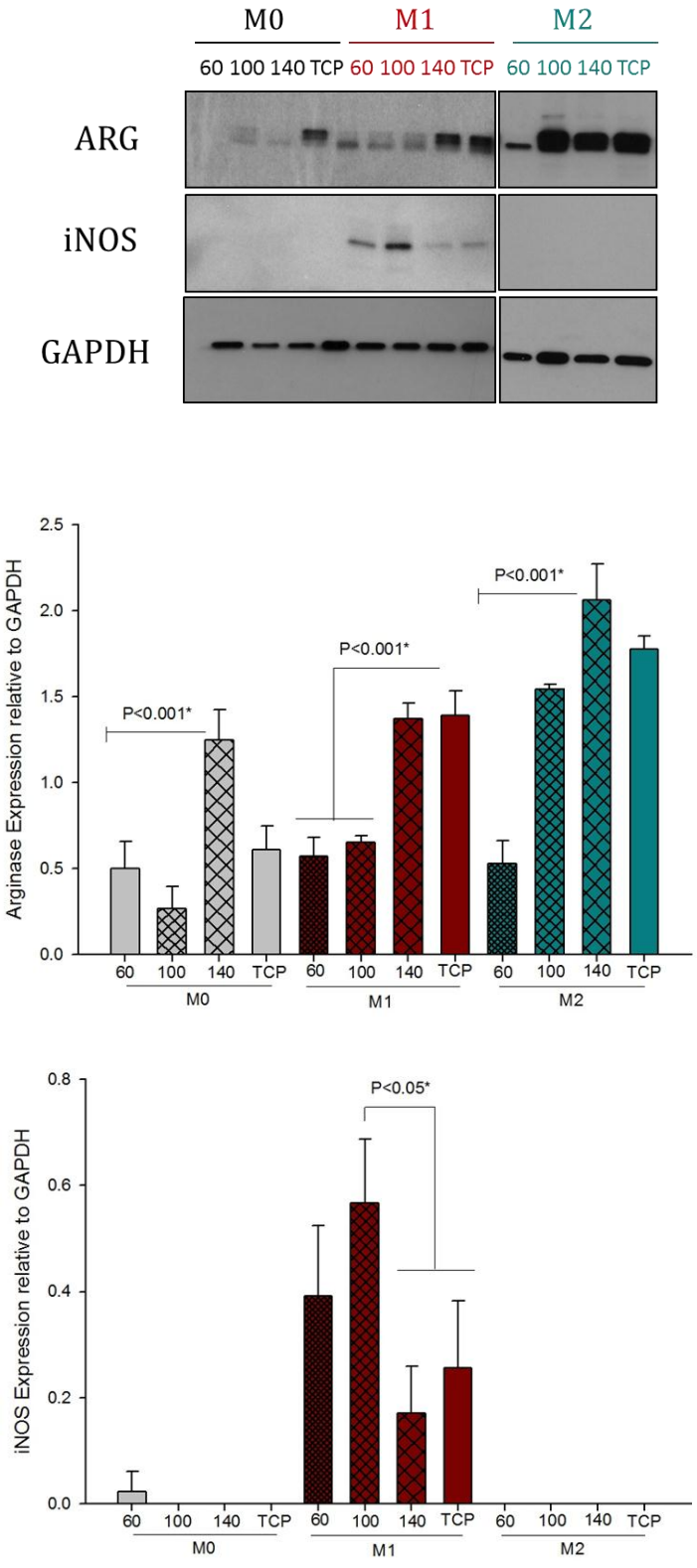

Figure 20 Arginase and iNOS expression by BMMΦs on Day 1.

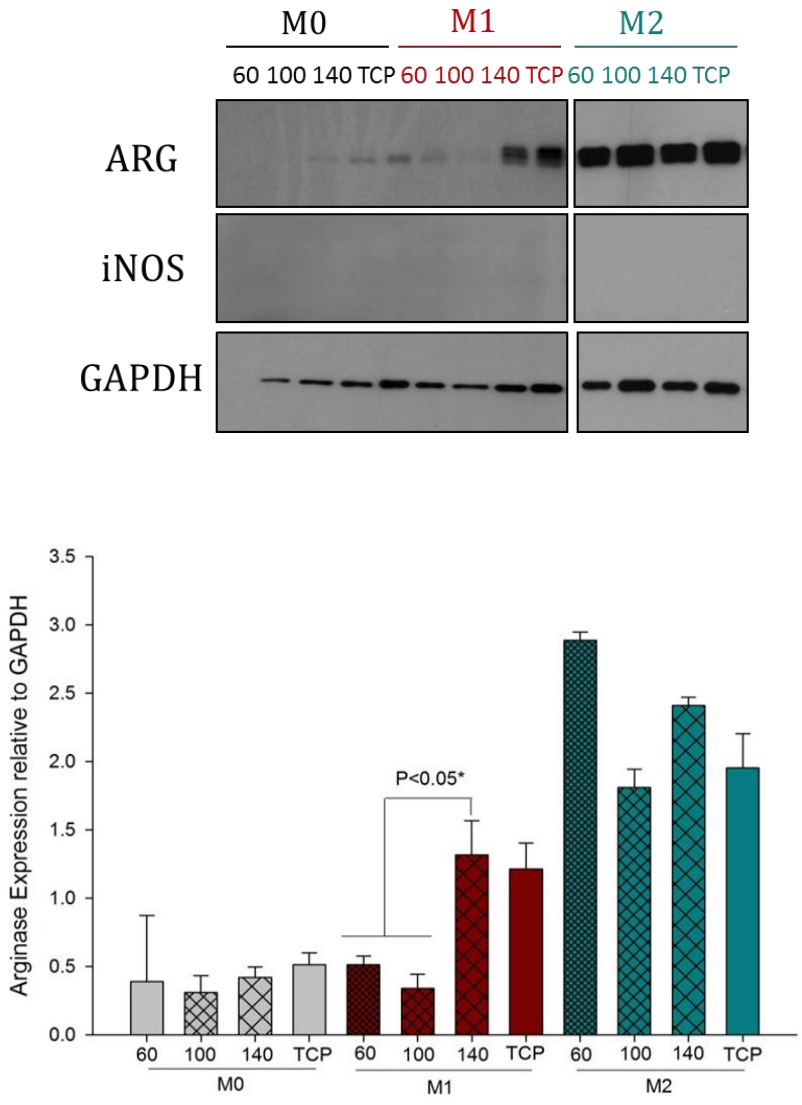

Figure 21 Arginase and iNOS Expression Analysis on Day 3.

Additionally, the ease of migration through the bigger pore-size material combined with their orientation in the 3D space of the scaffold nanostructure may have a role to play in the observed shift of BMMΦ towards a M2 phenotype. In contrast, the BMMΦ in case of the 100 mg/ml scaffold are spatially confined. In case of the 60 mg/ml scaffold, the BMMΦ are concentrated at the surface likely undergoing frustrated phagocytosis. This may have a role to play in pushing the BMMΦs towards a M1 phenotype on the 60 mg/ml and 100 mg/ml scaffold. The M1s invade deeper into the 60 mg/ml scaffold but they probably do it by causing tissue injury through MMPs. This could be the reason why these M1s are unable to shift to an M2 phenotype.

III.4.5 BMMΦ Mediator Secretion

The production of cytokines and growth factors characteristic of both M1 and M2 phenotypes were quantified on Day 1 and 3. The level of Nitrite (NO_2^-, M1 phenotype) production was measured by the Griess Assay (Promega). All ELISA kits were purchased from Peprotech except for bFGF (Abcam) and TGF-β1 (R&D systems). The levels of TNF-α, IL-6 (indicative of M1 phenoype) and growth factors associated with the M2 phenotype (VEGF, bFGF, TGF-β1) were measured by ELISA. The levels of all cytokines and growth factors were normalized to the total protein content. The results showed that PDO is a potent activator of BMMΦs, characterized by the secretion of both pro-inflammatory (M1) and wound healing (M2) mediators.

The production of Nitrite (NO_2^-) is shown in Figure 22. Nitrite is a product of Arginine metabolism by iNOS. The levels of nitrite are often used in the literature as a measure of iNOS activity. As seen in Figure 22, the highest levels of nitrite were produced by M1s on Day 1. The levels were found to be much lower on Day 3 compared to Day 1. The

level of nitrite was downregulated in M1s cultured on the larger fiber/pore-size PDO on both Day 1 and Day 3.

The levels of TNF-α are shown in Figure 23. The highest levels of TNF-α were produced from the M1 phenotype BMMΦ (~ 300 times greater compared to M0s and M2s). The levels of TNF-α were not found to be significantly different between PDO scaffolds of different fiber/pore-sizes. The levels were decreased on Day 3 and trended lower on the 140 mg/ml scaffold while still remaining statistically not significant compared to the 60 mg/ml scaffold.

The quantification of IL-6 cytokine is shown in Figure 24. The levels of IL-6 were also produced in highest quantities by M1 phenotype BMMΦs. Just like TNF-α, the levels of IL-6 could not be downregulated by the large fiber/pore-size PDO. The levels remained fairly constant across different fiber/pore-sizes on both Day 1 and 3.

The levels of VEGF by BMMΦ are shown in Figure 25. Similar levels of VEGF were produced from M1 and M2 BMMΦs and were found to be higher than M0s. In the case of M0s, the production of VEGF was significantly higher on the larger fiber/pore-size PDO. Continuing to look at M0s, it was observed that compared to Day 1, the level of VEGF on the 60 mg/ml scaffold were much lower on Day 3 indicating that the 60 mg/ml scaffold is unable to maintain the expression of VEGF. In contrast, the level of VEGF on the 140 mg/ml scaffold increased on Day 3 compared to Day 1 indicating sustained expression of VEGF on the 140 mg/ml scaffold. In the case of M1s and M2s, no differences with respect to fiber/pore-sizes were noted.

The cell culture supernatants were acid-activated as per manufacturer's instructions prior to the TGF-β1 ELISA. Comparable levels of TGF-β1 were produced by all three BMMΦ

phenotypes; M0s, M1s and M2s. The TGF-β1 expression was maintained until Day 3. The levels of TGF-β1 increased with increasing fiber/pore-sizes in M0s, M1s and M2s. The production of TGF-β1 was statistically higher on the 140 mg/ml scaffold compared to the 60 mg/ml scaffold on Day 1 in the case of M0s and on both Day 1 and 3 in the case of M1s and M2s.

The quantification of bFGF is shown in Figure 27. Just like the two other angiogenic growth factors (VEGF and TGF-β1), bFGF was also produced in comparable amounts by BMMΦ of all three phenotypes; M0s, M1s and M2s. The production of bFGF was statistically higher on the 140 mg/ml scaffold compared to the 60 mg/ml scaffold on Day 1 in the case of M0s and M1s and on Day 3 in the case of M2s.

The expression of two chemokines: Macrophage inflammatory factor -1 alpha (MIP-1α) (Figure 28) and Macrophage chemotactic protein (MCP-1) (Figure 29) was also analyzed by ELISA. The levels of MIP-1α were much higher in M0s compared to M1s and M2s. The production of MIP-1α was statistically higher on the larger fiber/pore-size scaffold (140 mg/ml) compared to the 60 mg/ml scaffold in the case of M0s, M1s and M2s. The levels of MCP-1 were statistically higher on the 140 mg/ml PDO scaffold compared to the 60 mg/ml scaffold in the case of M1s on Day 1.

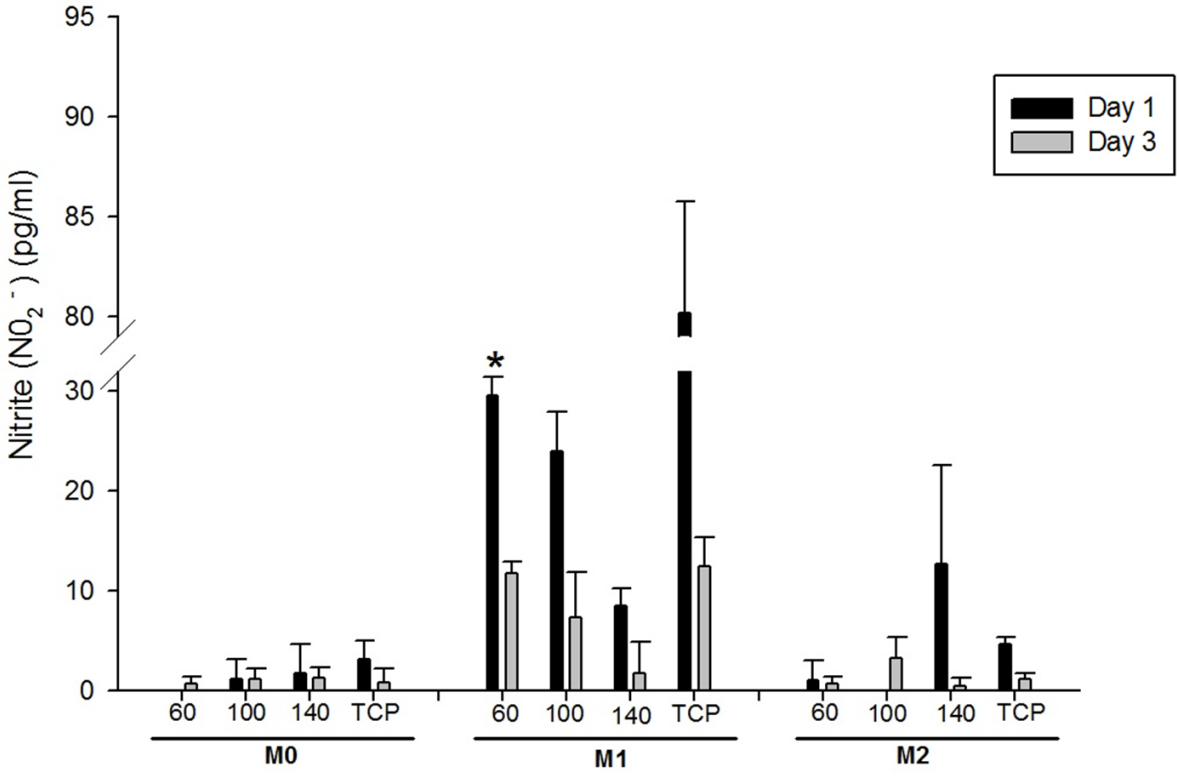

Figure 22 Expression of Nitrite by BMMΦs indicating an M1 phenotype. The asterisk '*' indicates a statistical difference between the 60 mg/ml and the 140 mg/ml scaffold.

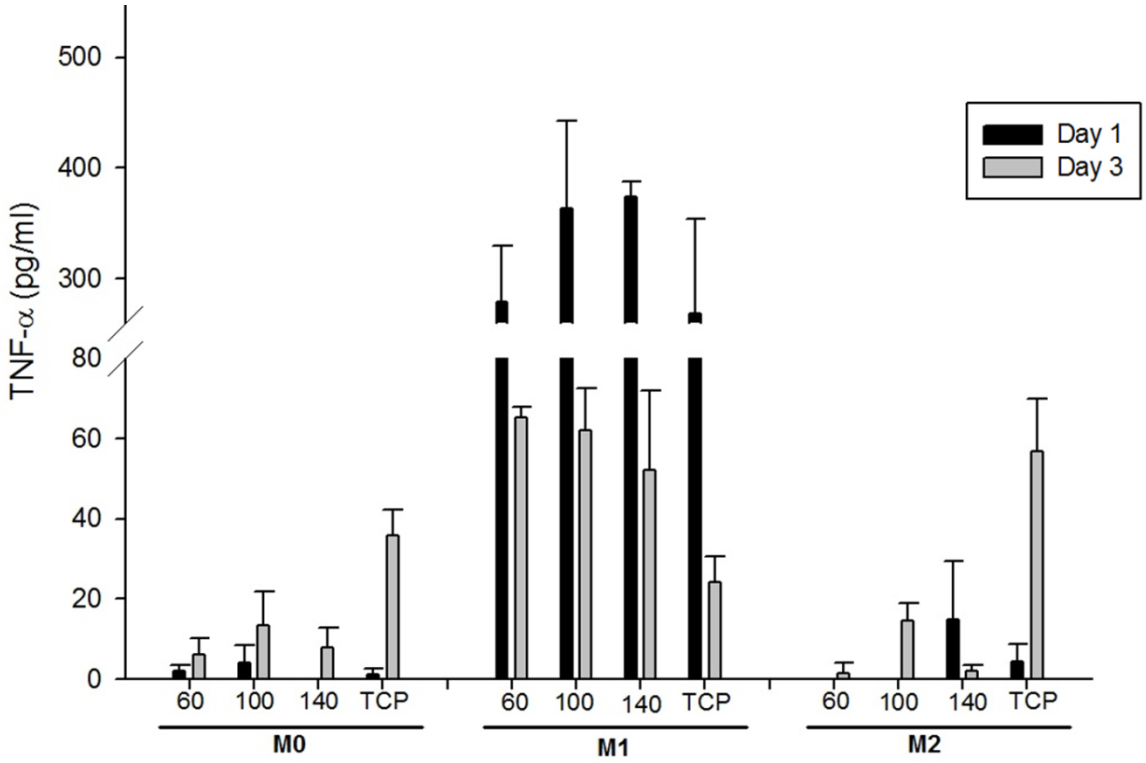

Figure 23 Expression of TNF-alpha by BMMΦs indicating a M1 phenotype.

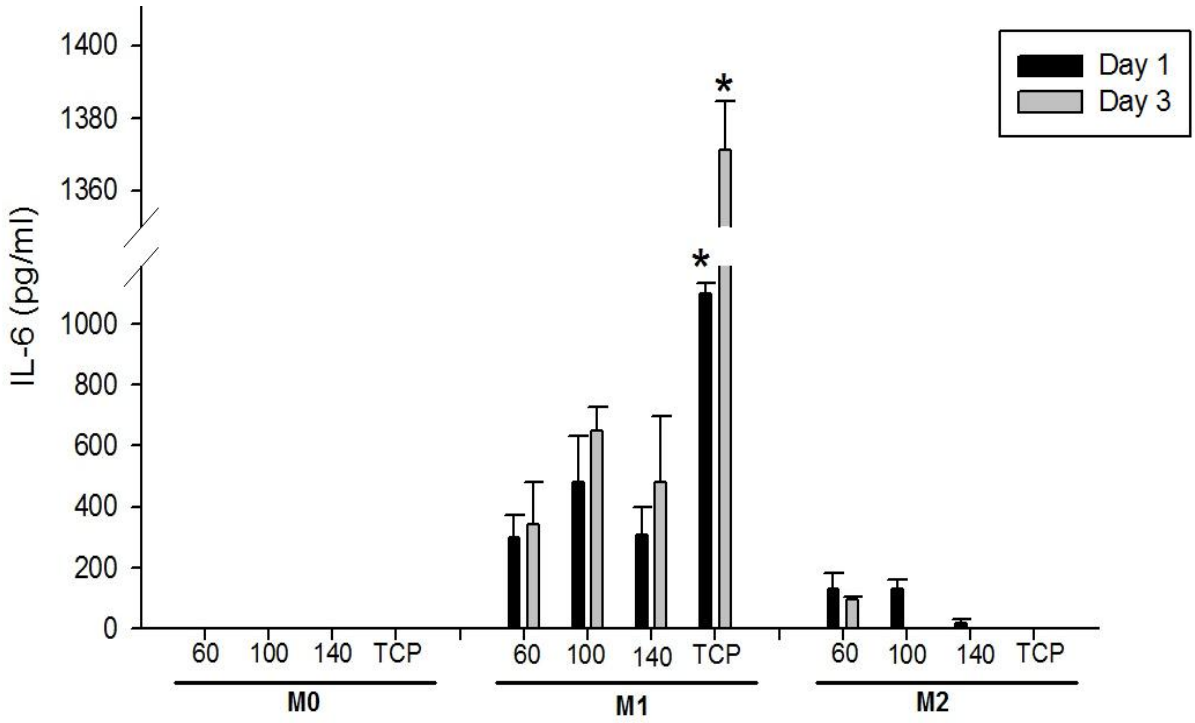

Figure 24 Production of IL-6 by macrophages. The asterisk '*' indicates a statistical difference between the 60 mg/ml and the 140 mg/ml scaffold.

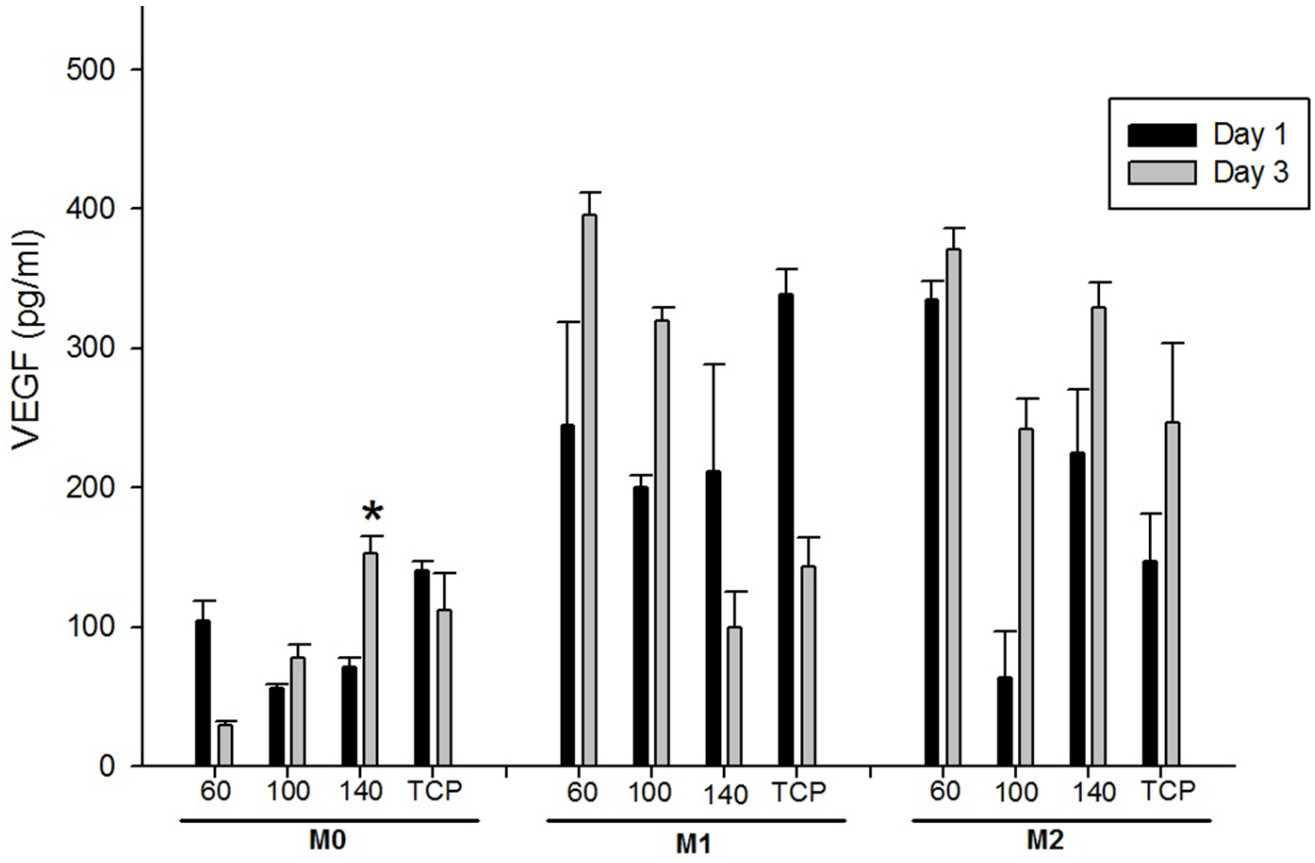

Figure 25 Expression of VEGF by BMMΦs indicating a M2 phenotype. The asterisk '*' indicates a statistical difference between the 60 mg/ml and the 140 mg/ml scaffold.

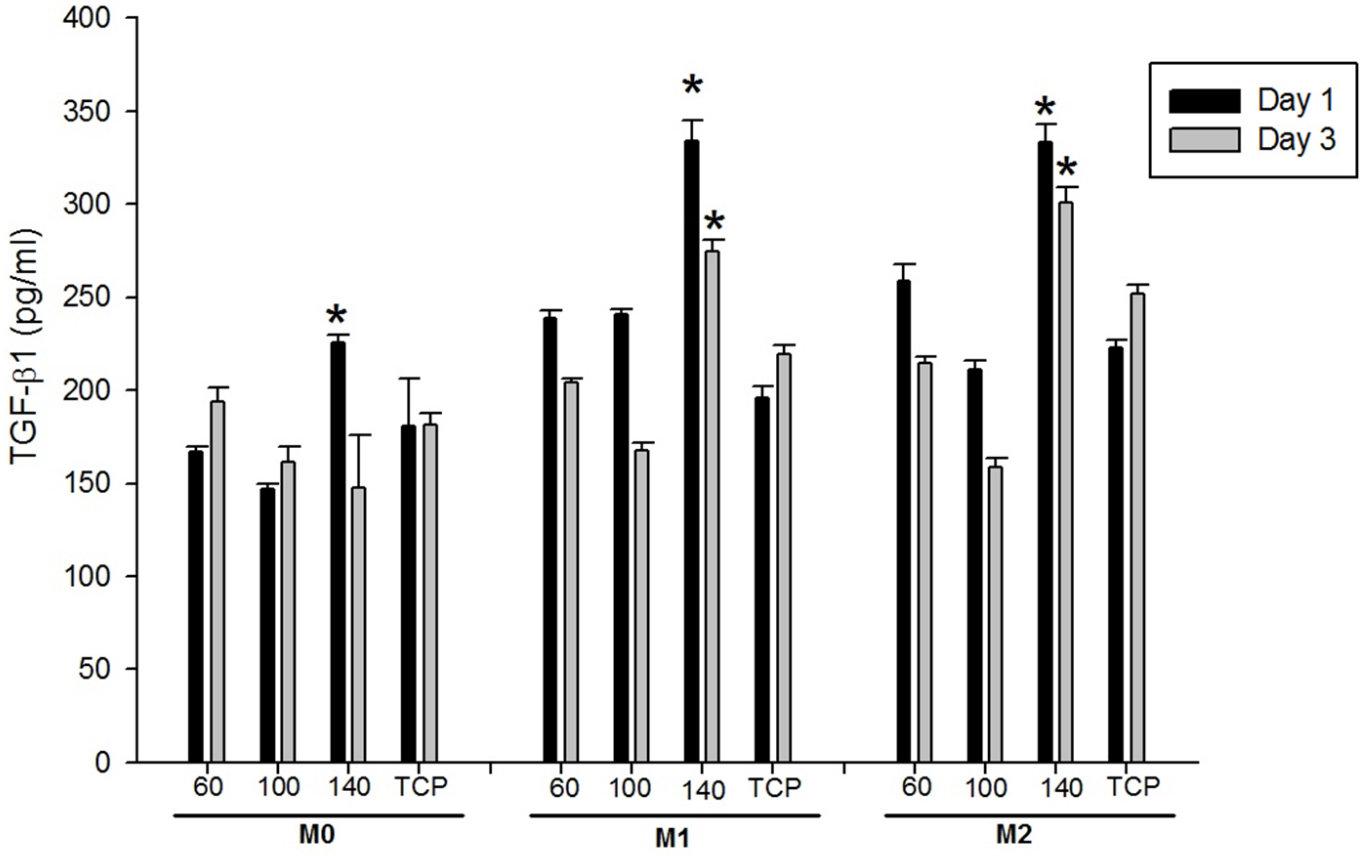

Figure 26 Production of TGF-beta1 by BMMΦs indicating a M2 phenotype. The asterisk '*' indicates a statistical difference between the 60 mg/ml and the 140 mg/ml scaffold.

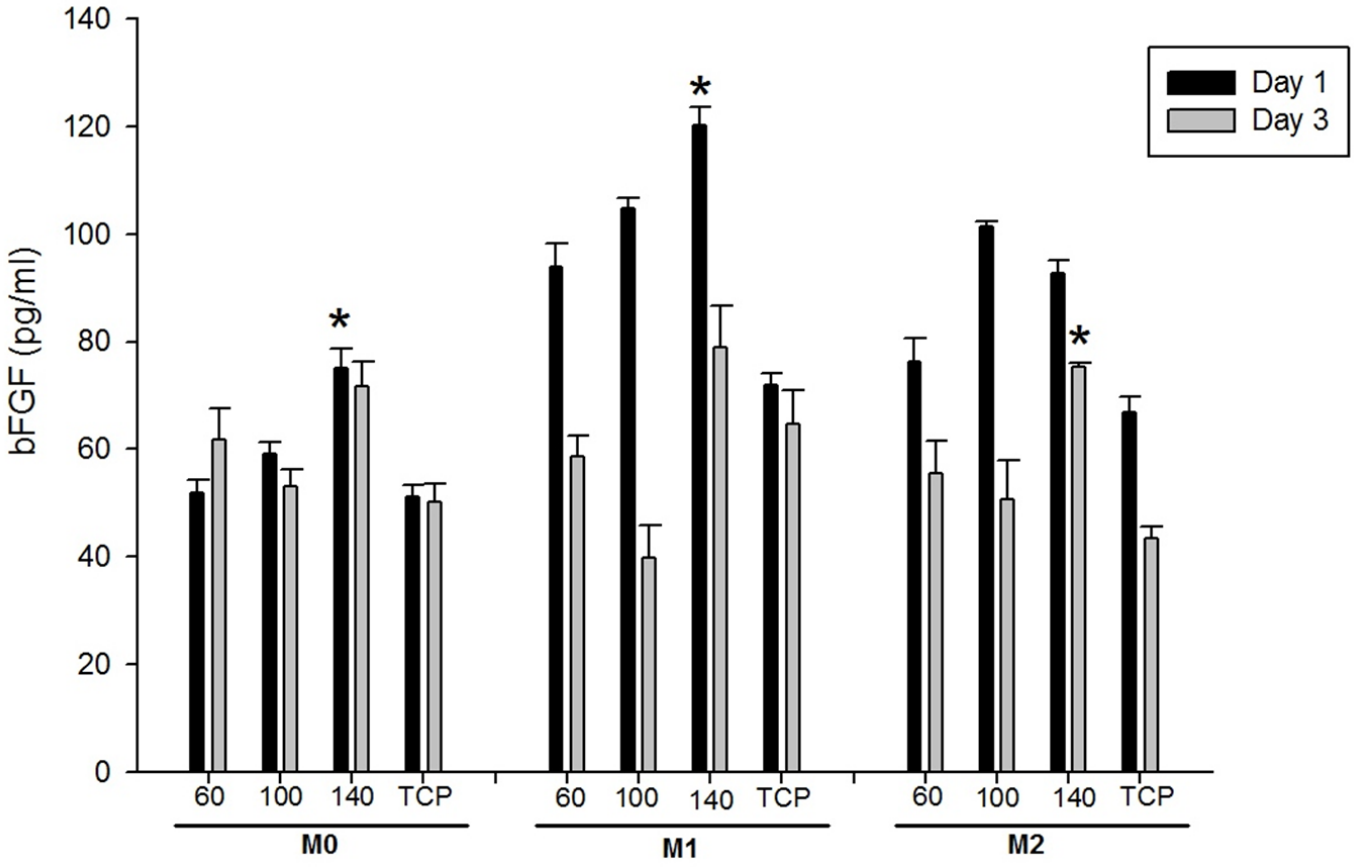

Figure 27 Expression of bFGF by BMMΦs indicating a M2 phenotype. The asterisk '*' indicates a statistical difference between the 60 mg/ml and the 140 mg/ml scaffold.

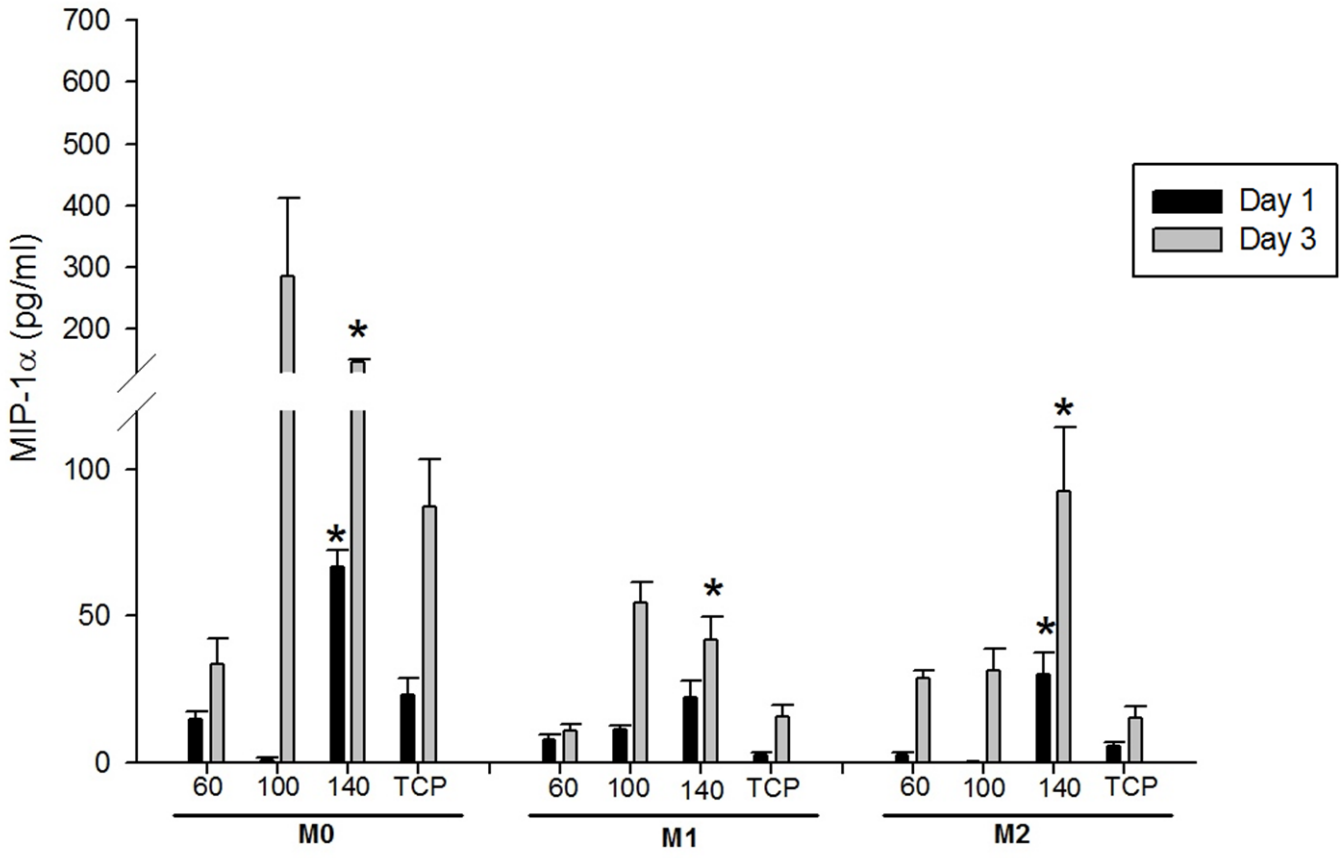

Figure 28 Production of MIP-1alpha by BMMΦs indicating either a M1 or M2 phenotype. The asterisk '*' indicates a statistical difference between the 60 mg/ml and the 140 mg/ml scaffold.

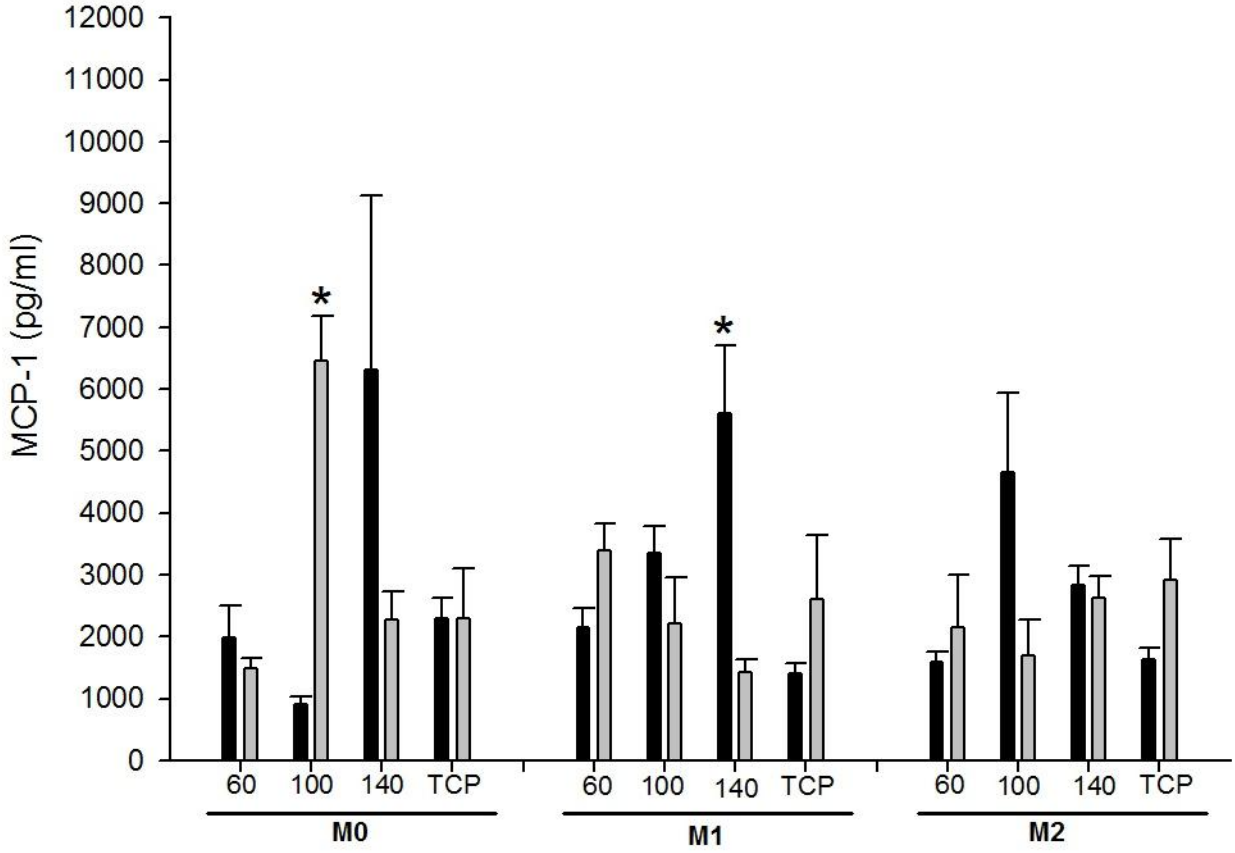

Figure 29 Production of MCP-1 by BMMΦs indicating either a M1 or M2 phenotype. The asterisk '*' indicates a statistical difference between the 60 mg/ml and the 140 mg/ml scaffold.

III.4.6 Comparison of fiber diameter vs. pore-size in BMMΦ phenotype modulation

During the electrospinning process, as fibers are deposited onto the perforated mandrel, pressurized air emanating from the mandrel perforations is introduced into the developing fibrous structure causing the fibers near the mandrel perforations to be less dense, creating regions of increased scaffold porosity. In contrast, fibers deposited on solid, non-perforated sections of the mandrel (e.g. located between and adjacent to the perforations) are, in comparison, densely packed. The scaffold thus contains regions in which the fibers are porous and regions in which the fibers are densely packed, all within a single contiguous, seamless structure prepared during a single deposition event, thus not requiring multiple deposition steps and/or processing steps [109]. The properties of scaffolds created on solid vs. perforated mandrels are shown in Figure 30. The air-flow impedance method created a statistically significant increase in the pore-size and porosity of the scaffold but did not impact the fiber-diameter and the surface area to volume ratio.

BMMΦ were seeded on the 60 mg/ml PDO scaffolds (12 mm disks) created by traditional and air-flow impedance electrospinning methods at a density of 10^6 cells/well in a 48 well plate as pre-polarized M2s as described previously. The cell lysates were collected after 24 hours and analyzed by western blot for Arg1 expression. The analysis is shown in Figure 31. Compared to the solid mandrel, the air flow mandrel showed higher expression of Arg1 on M2s. The result corroborates our theory that bigger pore-size leads to a M2 phenotype.

The 140 mg/ml PDO scaffold that was compressed had a pore-size of 9 μm compared to the normal 140 mg/ml PDO scaffold, which had a pore-size of 14 μm. The

overall porosity of the compressed scaffold also decreased significantly. The method of compression did not fuse the fibers but did flatten them out to some extent. This led to a slight increase in the overall fiber diameter as shown in Figure 32. The Arg1 expression by M2s was reduced on the compressed 140 mg/ml scaffold compared to the normal 140 mg/ml scaffold. This result shows that pore-size is a more crucial regulator of Arg1 expression. However, since the results were not significantly different from each other, it might indicate a role for the fiber-diameter in the modulation of Arg1 expression as well.

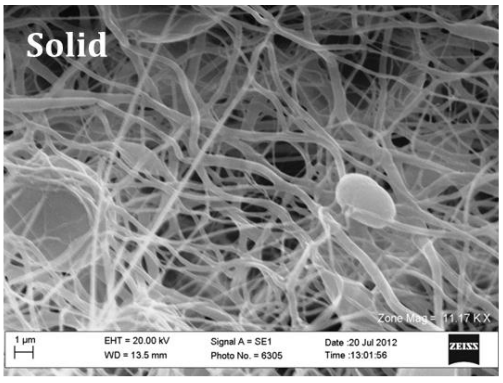

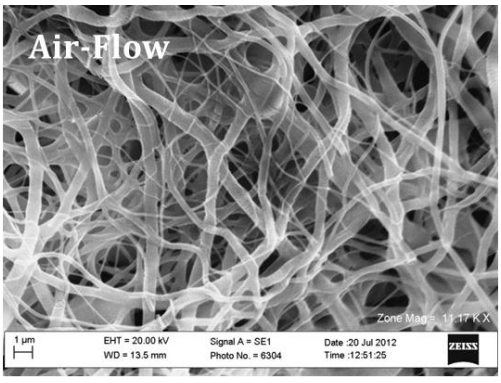

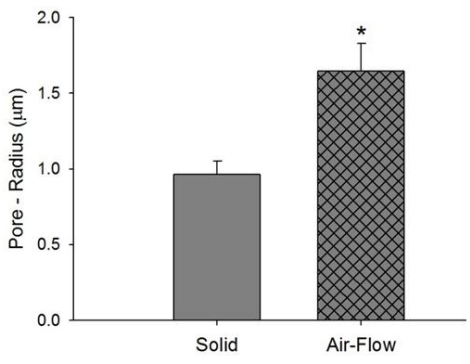

60 mg/ml scaffold	Fiber Diameter (µm)	Porosity (%)	Surface area to volume ratio
Solid Mandrel	0.35 ± 0.126	69.3 ± 2.3	11.43
Air- Flow Mandrel	0.354 ± 0.146	80.4 ± 1.95	11.3

Figure 30 Comparison of 60 mg/ml PDO scaffolds electrospun on the solid vs. air flow impedance mandrel. The asterisk '*' indicates a statistical difference between the 60 mg/ml and the 140 mg/ml scaffold.

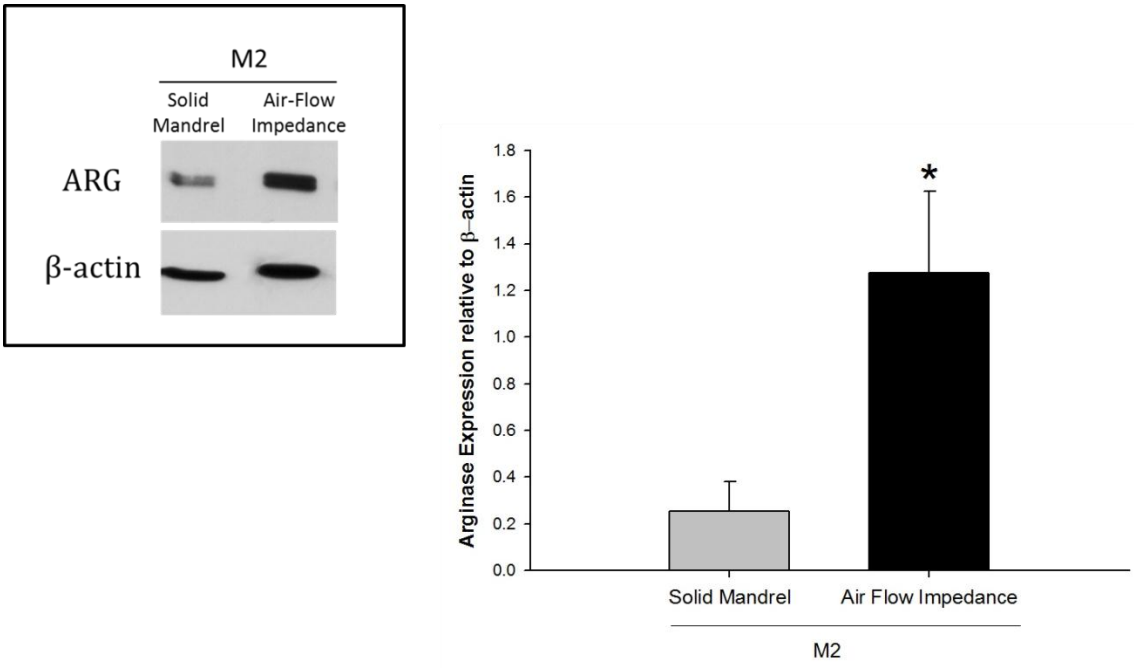

Figure 31 Arginase expression by M2s on 60 mg/ml scaffold electrospun on solid vs. air flow impedance mandrel. The asterisk '*' indicates a statistical difference between the 60 mg/ml and the 140 mg/ml scaffold.

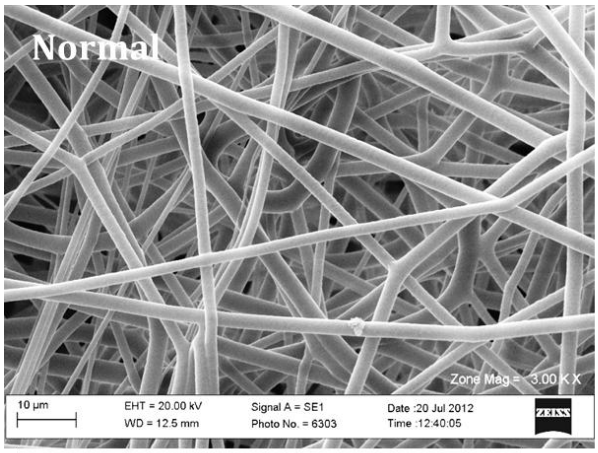

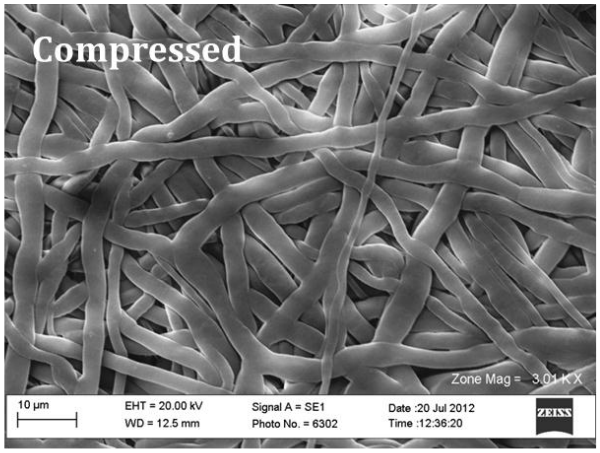

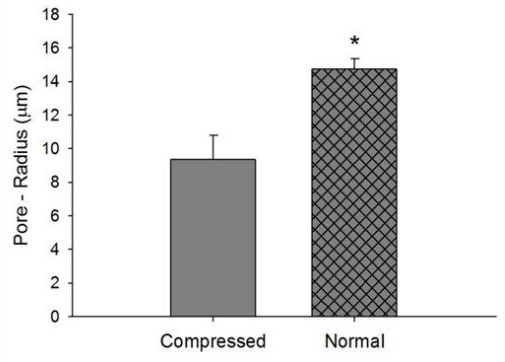

140 mg/ml scaffold	Fiber Diameter (µm)	Porosity (%)	Surface area to volume ratio
Normal	2.8 ± 0.5	82.67 ± 0.7	1.428
Compressed	2.92 ± 1.04	75.52 ± 2.98	1.54

Figure 32 Comparison of Normal vs. Compressed 140 mg/ml PDO scaffold. The asterisk '*' indicates a statistical difference between the 60 mg/ml and the 140 mg/ml scaffold.

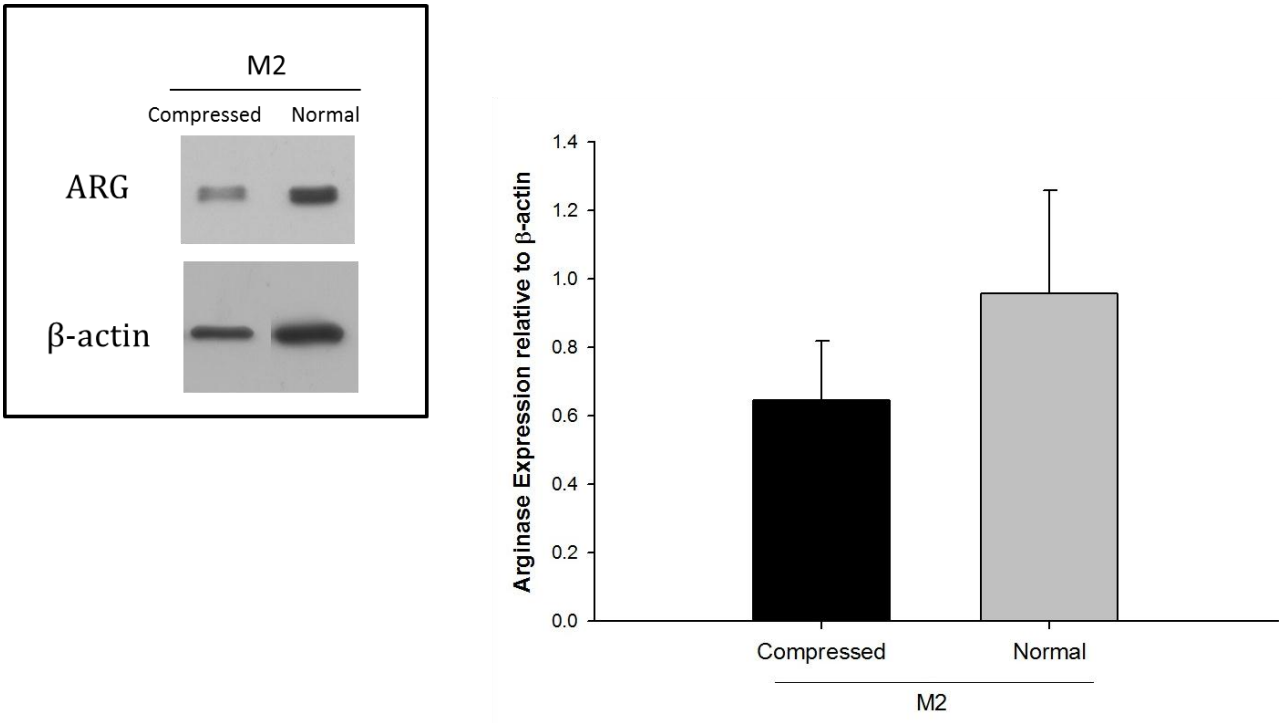

Figure 33 Expression of Arg1 by M2s on normal and compressed 140 mg/ml PDO scaffolds.

III.5 Discussion

The present study examined the effects of fiber/pore-size of a scaffold on MΦ polarization. The study also examined the relationship between MΦ polarization. The results of this study demonstrate that increase in the fiber/pore-size shifts the MΦ phenotype to a more M2, tissue regenerative phenotype *in vitro*. This shift to an M2 phenotype has been demonstrated in this study by increased Arg1, TGF-β1, VEGF, bFGF expression and decreased iNOS and $N0_2^-$ expression.

The activation states of MΦ are hypothetical ends of a spectrum. The actual MΦ phenotype is viewed as a continuum of functional states. In the literature M2s have been classified into 3 main groups: M2a, M2b and M2c. M2a phenotype is induced by IL-4 and IL-13 and they produce high amounts of anti-inflammatory cytokines and enzymes such as Arg1, FIZZ1 and RELM-1α. The M2b phenotype is induced by immune complexes as well as agonists of TLRs or IL-1 receptors and these MΦ secrete high amounts of IL-10 but reduced IL-12. M2c phenotype is induced by IL-10 or glucocorticoids and they produce elevated levels of IL-10 and TGF-β1. We wanted to select an M2 phenotype that can function most effectively at tissue remodelling and angiogenesis. The production of VEGF by BMMΦ on TCP in response to IL-4 combined with IL-10 and IL-13 is shown in Figure 34. IL-4 was chosen as an M2 phenotype inducer because it is known to activate MΦ to produce arginase, fibronectin and other matrix proteins such as βIG-H3 and facilitates tissue remodelling and organization. The highest amount of VEGF was produced by BMMΦ after treatment with both IL-4 and IL-13. Th2 cytokines, IL-4 and IL-13 are structurally similar and share a functional signalling receptor chain. It has been shown in a previous study that VEGF enhances IL-13 expression in the airways, suggesting a positive feedback loop with

VEGF enhancing Th2 sensitization and inflammation and IL-13 subsequently enhancing VEGF production [185].

The production of MCP-1 and MIP-1α was significantly higher by M0s on 140 mg/ml scaffold when compared to M1s and M2s. Whether these chemokines fall under the M1 or the M2 phenotype category is not clearly known in the literature. Several studies have associated MCP-1 with Th2 or M2 macrophage phenotype responses [17, 186, 187]. It has been shown by Varin *et al.* that IL-4 inhibits MCP-1 [188]. Whereas, Martinez and Gordon documented that IL-4 induces MCP-1 [9]. Several studies have also classified MIP-1α as pro-inflammatory [180, 189]. In another study it was documented that MIP-1α is involved in chemotaxis and recruitment of monocytes and leukocytes during the initial inflammatory response, followed by a transition towards pro-wound healing activity [190]. Mantovani *et al.* and Schutte *et al.* classified both MIP-1α and MCP-1 as indicators of M1 macrophage phenotype [13, 191]. It has been shown that MCP-1 recruits fibroblasts, MΦs, endothelial cells and smooth muscle cells *in vitro* in cell migration assays and *in vivo* in murine carotid aneurysms. The same study also showed that MCP-1 mediated vascular inflammatory repair occurs via a MIP-1α and MIP-2 dependent pathway. Blocking MIP-1α and MIP-2 caused a significant decrease in MCP-1 mediated intra-aneurysmal tissue healing [192]. It has also been shown that MCP-1 can stimulate IL-4 production and MCP-1 deficient mice are unable to mount Th2 responses [186]. There is also evidence for an essential pathogenic and inflammatory role for MCP-1, in which it is required for the accumulation of MΦ. In another study, wound healing in MIP-1α and MCP-1 knockout mice was examined. It was found that wound re-epithelialization, angiogenesis and collagen synthesis in MIP-1α deficient mice was nearly identical to the WT controls. In contrast,

MCP-1 deficient mice displayed significantly delayed wound re-epithelialization, angiogenesis and collagen synthesis. Surprisingly, no change in the number of wound MΦ was observed in the MCP-1 deficient mice, suggesting that monocyte recruitment into the wounds is independent of this chemokine [164]. In the light of this evidence, we would classify these chemokines at the cross-roads between M1s and M2s.

The morphology of naïve (M0) and polarized MΦs (M1 and M2) on electrospun PDO (100 mg/ml) is shown in Figure 35. It was observed that both M0s and M2s were spread out and interacting with fibers. In contrast to M0s and M2s, that had acquired a flattened shape on the scaffold, the M1s assumed a more rounded morphology. This rounded morphology could be due to the propensity for M1s to invade the matrix to destroy pathogens and debris. The rounded morphology probably enables them to squeeze through the pores in the scaffold and migrate into its structure.

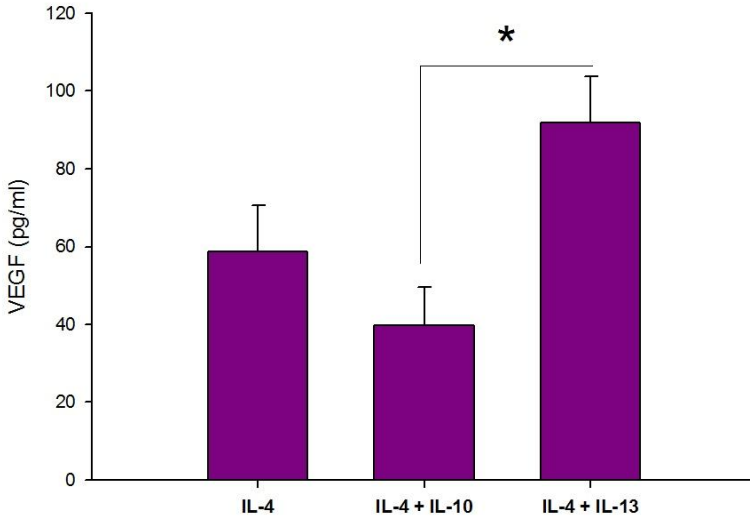

Figure 34 Production of VEGF from M2/Th2 associated cytokines. The asterisk '*' indicates a statistical difference.

There were several limitations in the present study. A limited number of cytokines and surface markers were utilized for the characterization of the M1/M2 profile of the BMMΦ. It is also recognized that species variations do exist. The markers chosen in this study (iNOS and Arg1) have been widely used as markers of M1 and M2 polarization in several studies. Care must be taken when extrapolating these studies to human MΦs. In contrast to murine MΦs, which can simply be identified by their ability to produce NO, human monocyte-derived MΦs do not generate NO in response to classical activating stimuli. Therefore, human MΦs must be identified by other criteria, including the upregulation of surface molecules such as major histocompatibility complex (MHC) Class II, co-stimulatory molecule CD86 and opsonic receptors [e.g., FcRIII (CD16)], enhanced ability to kill and degrade intracellular microorganism and the elevated capability to process and present antigens [3].

The 60 mg/ml scaffolds and 140 mg/ml scaffolds differ remarkably in both pore-size and fiber diameter. The results show that BMMΦ are polarized towards a more M2-like phenotype on the 140 mg/ml scaffold. However, it is not known whether this result is because of the fiber diameter or the pore-size. To investigate this we made our 60 mg/ml scaffold more porous by electrospinning it using the air-flow impedance method. Using this method the fiber diameter stayed the same but the pore-size and the overall porosity of the scaffold improved. The results showed higher Arg1 expression in M2s on the 60 mg/ml scaffold created by the air-flow impedance method compared to the 60 mg/ml scaffold created on the solid mandrel created by traditional electrospinning. This result indicates

that pore-size might be playing a greater role compared to fiber diameter in BMMΦ phenotype modulation.

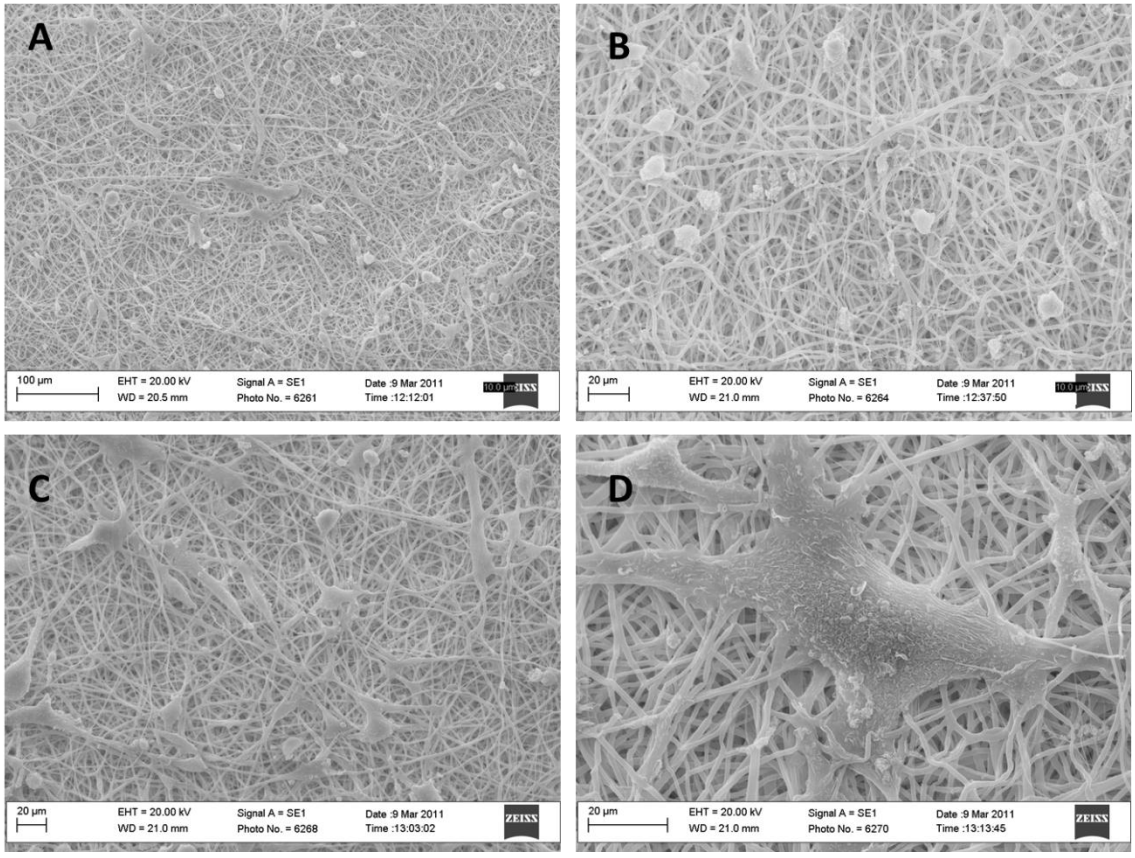

Figure 35 BMMΦ morphology on electrospun PDO (100 mg/ml). (A) M0s (B) M1s (C) M2s (D) zoomed in view of a M2.

The 140 mg/ml PDO scaffold was made less porous by compressing it using a hydraulic press. The Arg1 expression by M2s was reduced on the compressed 140 mg/ml scaffold compared to the normal 140 mg/ml scaffold. This result also showed that pore-size is a more crucial regulator of Arg1 expression and BMMΦ phenotype modulation.

III.6 Conclusion

In this study we have demonstrated that by varying the fiber diameter and the corresponding pore-size, we can modulate the BMMΦ phenotype. Electrospun PDO scaffolds of larger fiber/pore-sizes upregulated Arg1 expression and downregulated iNOS and nitrite expression in BMMΦ. In contrast, electrospun PDO scaffolds of smaller fiber/pore-sizes upregulated iNOS and nitrite expression but not Arg1. The production of angiogenic growth factors such as VEGF, TGF-β1 and bFGF from BMMΦ was also greater on the larger fiber/pore-size PDO scaffolds. These results indicate that fiber/pore-size can influence the phenotype of BMMΦ and that larger fiber/pore-size is capable of polarizing BMMΦ towards a M2 phenotype. It was also observed that differences in fiber/pore-size of materials cannot modulate the expression of pro-inflammatory cytokines such as TNF-α and IL-6. The results showed higher Arg1 expression in M2s on the 60 mg/ml scaffold created by the air-flow impedance method compared to the 60 mg/ml scaffold created on the solid mandrel created by traditional electrospinning. The Arg1 expression was reduced on the compressed 140 mg/ml PDO scaffold compared to the normal 140 mg/ml scaffold. This result indicates that pore-size might be playing a greater role compared to fiber diameter in BMMΦ phenotype modulation.

Chapter IV: Angiogenic Responses of Macrophage Phenotypes (M1/M2) to Varying Dimensions of Electrospun Bioresorbable Vascular Grafts

Koyal Garg*, Nicholas A. Pullen#, Carole A. Oskeritzian£, John J. Ryan# and Gary L. Bowlin*

*Department of Biomedical Engineering, Virginia Commonwealth University

#Department of Biology, Virginia Commonwealth University

€Department of Biochemistry and Molecular Biology, Virginia Commonwealth University

€Present Address: Department of Pathology, Microbiology and Immunology, University of South Carolina, School of Medicine

IV.1 Abstract

In order to assess the angiogenic potential of BMMΦs cultured on PDO scaffolds, a previously described 3D angiogenesis bead assay was performed using conditioned media from the BMMΦ:PDO interaction [110]. Cytodex beads were coated with mouse endothelial cells and embedded in collagen gels in a 24 well plate. The supernatants from BMMΦs (M0, M1 and M2) cultured on 12 mm disks on 60, 100 and 140 mg/ml PDO scaffolds were added on top of the collagen gels. The endothelial cells were allowed to form sprouts in the collagen gels for a period of 6 days. VEGF (20 ng/ml) was used as positive control in the study. The results of the 3D angiogenesis bead assay showed that the conditioned media from BMMΦ of M0 and M2 phenotypes cultured on the bigger fiber/pore-size PDO scaffold (140 mg/ml) induced significantly larger average length of sprout. The conditioned media from BMMΦ of M0, M1, and M2 phenotypes cultured on the bigger fiber/pore-size PDO scaffold induced significantly higher percentage density of sprouts. These results demonstrate that the M2 phenotype BMMΦs cultured on the larger fiber/pore-size PDO scaffold are functional and are capable of supporting angiogenesis in the right microenvironment. The study further confirms that the naïve (M0s) and pre-polarized M1 BMMΦs behave like M2s in phenotype (shown by arginase and angiogenic growth factor expression in Chapter III) and function when cultured on the 140 mg/ml scaffold.

IV.2 Introduction

Angiogenesis is associated with degradation and reformation of the vascular basement membrane (VBM). In response to growth factors and matrix metalloproteinases (MMPs), the VBM undergoes degradative and structural changes. This transition from

mature VBM to provisional matrix promotes the proliferation and migration of vascular endothelial cells. Growth factors, such as vascular endothelial growth factor (VEGF), basic fibroblast growth factor (bFGF) and platelet-derived growth factor (PDGF), are released from the VBM, and are also produced by tumour cells, fibroblasts and immune cells. This induces formation of an intermediate, and then a new (mature) VBM. Endothelial cells assemble as solid cords that eventually acquire a lumen. Together with the vascular endothelial cells and pericytes, the VBM mediates formation of a new blood vessel [28].

Endothelial cell differentiation (i.e. lumen or tube formation) can be studied *in vitro* both in two dimensions and in three dimensions. Endothelial cells cultured on plates coated with matrix proteins such as Matrigel (a matrix scaffold that incorporates extracellular matrix and basement membrane proteins), collagen, or fibrin can be induced to differentiate and lend themselves to a common model of *in vitro* angiogenesis [193]. However, it has been shown in several studies that in order to mimic the *in vivo* features of both cell morphological phenotype and gene expression profile, 3D culturing models should be used [194, 195]. In this angiogenesis study, we used a 3D collagen gel as a matrix to facilitate sprouting from endothelial cells. It has been shown in previous studies that matrix stiffness has an inverse relationship with angiogenesis. Less rigid matrices (such as fibrin or matrigel) promote better blood vessel formation *in vitro* compared to stiffer matrices such as collagen. We observed that plain cRPMI media with 10% FBS was capable of inducing sprouts from endothelial cell coated beads in a fibrin gel. This was not observed in the case of collagen gels. In order to avoid background issues with fibrin gels, we decided to pursue this assay with collagen gels. Also, the main aim of this study is to design a vascular graft. We are mainly interested in applying the understanding and control of

angiogenic processes to promoting vascular healing after arterial injury. Collagen is an abundant protein of the native blood vessel and so using collagen gels for this angiogenesis study is a better model for our overall aim of designing a vascular graft compared to fibrin [196-198].

IV.3 Materials and Methods

IV.3.1 Three Dimensional (3D) Angiogenesis Assay

In order to assess the angiogenic potential of these M2 polarized BMMΦs, a 3D angiogenesis bead assay was performed following the method described by Chen *et al*. [110] using conditioned media from the non-stimulated BMMΦ:PDO interaction. The BMMΦ were isolated from the bone marrow of C57BL/6 mice as described in chapter III. The BMMΦ were seeded on 15 mm disks of PDO scaffolds electrospun at 60, 100 and 140 mg/ml in a 24 well plate at a density of a 10^6 cells/ml. The cell culture supernatants were collected on Day 1 and 3. The dry Cytodex 3 microcarriers (Sigma Aldrich) were hydrated and autoclaved. Approximately 6 million mouse endothelial cells (ECs, ATCC) from a confluent T175 flask (passage 5) were mixed with Cytodex beads (~9000) in 25 ml of Endothelial growth media (DMEM high glucose with 10% FBS, 1% P/S) media in a 50 ml centrifuge tube. This mixture of EC and beads was incubated at 5% CO2 and 37°C for 4-5 hours. The centrifuge tube was agitated every 30 mins to avoid clumping of the bead-cell suspension and to ensure uniform coating. The mixture was then removed from the centrifuge tube and placed in a T-25 flask. The mixture in the T-25 flask was then incubated overnight to allow the cells that were not attached to the beads to attach to the flask. The next morning the beads were washed in Ca^{2+} and Mg^{2+} free PBS. The

media and the beads from the T-25 flask were transferred to a sterilized 50 ml centrifuge tube. The beads were then allowed to settle to the bottom of the centrifuge tube. As soon as the beads had settled, it was important to remove the medium quickly before the floating debris settled. After the medium was removed, 10 ml of Ca^{2+} and Mg^{2+} free PBS was gently added into the centrifuge tube to repeat the wash procedure. A collagen solution was prepared by combining eight volumes of cold collagen type I (3 mg/ml, Sigma-Aldrich) with one volume of 10x PBS and one volume of sodium hydroxide (0.1N). The EC coated beads were suspended in this collagen solution and added to a 24 well plate (500 µL/well). The plates were incubated at 37°C and 5% CO_2 for 15 min to allow collagen gel formation. The EC coated beads were cultured in 500 µL of either BMMΦ: PDO conditioned media, EGM with 3% FBS (negative control) or EGM with 20 ng/ml VEGF (positive control).

IV.3.2 Quantification of Angiogenesis

Each well containing the EC coated bead was digitally photographed under inverted microscopy at Day 6. A special grid (Figure 36) made by dividing a circle with radially oriented lines around 360 degrees with 10 degree intervals was used to quantify the percentage density of sprouts. This grid has been used in a previous study to quantify the migration of sprouts in the 3D matrix [199]. The digital photographs were transparently overlaid with the grid in Adobe Photoshop. The number of grid spaces with sprouts are counted and divided with the total number of grid spaces. The length of the sprout was calculated using the Image J software (NIH). The length of sprout was measured from the surface of the bead using the segmented line tool in the Image J software. A sprout was defined as a structure originating from the microcarrier

bead surface that was > 45 μm in length.

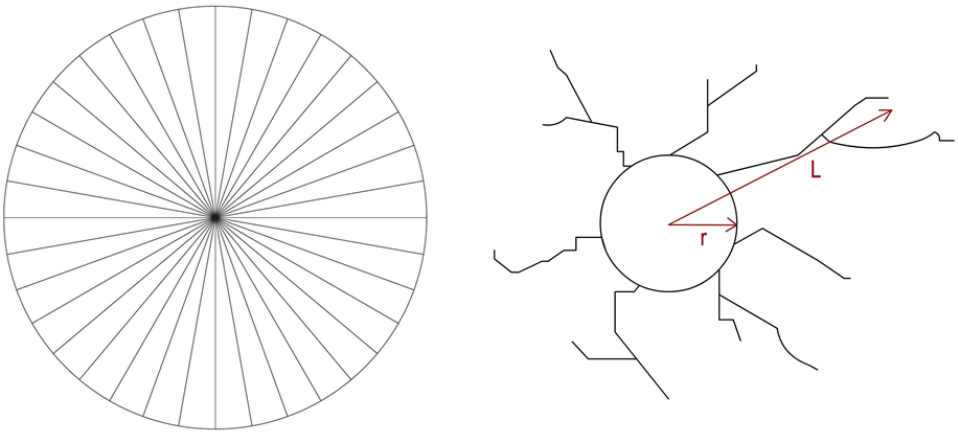

Figure 36 Grid for quantification of angiogenesis (left) and diagram showing how the length of sprout was calculated.

IV.3.3 Statistical Analysis

Data expressed in this chapter is in the format of means ± standard deviation. Each experiment was done in triplicates and was reproduced at least twice. All statistical analysis of the data was based on a Kruskal-Wallis one-way analysis of variance on ranks and a Tukey-Kramer pairwise multiple comparison procedure (α=0.05) performed with JMP®IN 8 statistical software (SAS Institute).

IV.4 Results

The results of the 3D bead assay are shown in Figure 37. A representative image of each condition done in triplicate is shown. In all cases (M0s, M1s and M2s), the images showed greater sprouting from the conditioned media from BMMΦ cultured on the larger fiber/pore-size PDO. Angiogenesis was measured by quantification of the average sprout length and the percentage density (Figure 38). The average sprout length induced by M0s on the larger fiber/pore-size (140 mg/ml) was statistically higher when compared to

smaller fiber/pore-sizes (100 mg/ml and 60 mg/ml PDO scaffolds). No sprouting was observed from the conditioned media of M0s cultured on the 60 mg/ml scaffold. The sprout length in the case of M0s cultured on the 140 mg/ml scaffold was statistically higher than all other samples tested except for the M2s cultured on the 140 mg/ml scaffold. This result shows that a naïve BMMΦ (M0) cultured on the 140 mg/ml scaffold is as angiogenic as a pre-polarized M2. The sprout lengths induced by M1s were not different across different fiber/pore-sizes. In the case of M2s, the sprout length induced by the conditioned media from 140 mg/ml scaffold was statistically higher compared to the 60 mg/ml scaffold. Overall it was observed that M0s induced a ~200 fold higher and M2s induced a ~2 fold higher length of sprout from the 140 mg/ml compared to the 60 mg/ml PDO scaffolds.

The quantification of the percentage density of sprouts is shown in Figure 34 (bottom). It was observed that significantly higher density of sprouts was induced by BMMΦs (M0s, M1s and M2s) cultured on the larger fiber/pore-sizes. Compared to the 60 mg/ml scaffolds, the 140 mg/ml scaffolds induced a 94 fold higher density of sprouts from M0s, 7 fold higher density of sprouts from M1s and 17 fold higher density of sprouts from M2s. Therefore, these studies show that the larger fiber/pore-size PDO scaffold has greater potential for BMMΦ mediated angiogenesis compared to the 60 mg/ml scaffold.

The positive control used in this assay was 20 ng/ml VEGF. It should be noted that BMMΦ conditioned media (especially in the case of 140 mg/ml scaffold) produced greater average length of sprouts and higher percentage density of sprouts compared to the positive control. This can be attributed to the fact that BMMΦ conditioned media contains a lot of growth factors besides VEGF (such as TGF-β1 and bFGF) which also play very crucial roles in the process of angiogenesis. Therefore, it is not surprising that their combined

effects produced greater sprouting in terms of sprout length and density. The histograms for all the measurements of the sprout lengths are shown in Figure 39. These histograms were generated using MATLAB® R2011a. The *dfittool* of MATLAB® was used to fit a 'gamma' distribution to the data. It can be clearly seen that the 140 mg/ml has the highest sprout length across all the groups of BMMΦ tested (i.e. M0, M1 and M2).

IV.5 Conclusion

The assay showed the potential for PDO scaffolds to support MΦ mediated angiogenesis. The conditioned media from BMMΦ:PDO interaction was capable of inducing sprouts in the 3D angiogenesis assay. It was observed that the BMMΦ of M0, M1 and M2 phenotypes cultured on the PDO scaffolds with bigger fiber/pore-size induced higher percentage density of sprouts. However, the conditioned media from BMMΦ of only M0 and M2 phenotypes cultured on the bigger fiber/pore-size PDO scaffold (140 mg/ml) induced significantly larger average length of sprout. Overall, the study confirms that the BMMΦs of M2 phenotype are functional and support angiogenesis and that the naïve BMMΦs acquire a functional M2-like phenotype when in contact with the bigger fiber/pore-size scaffold.

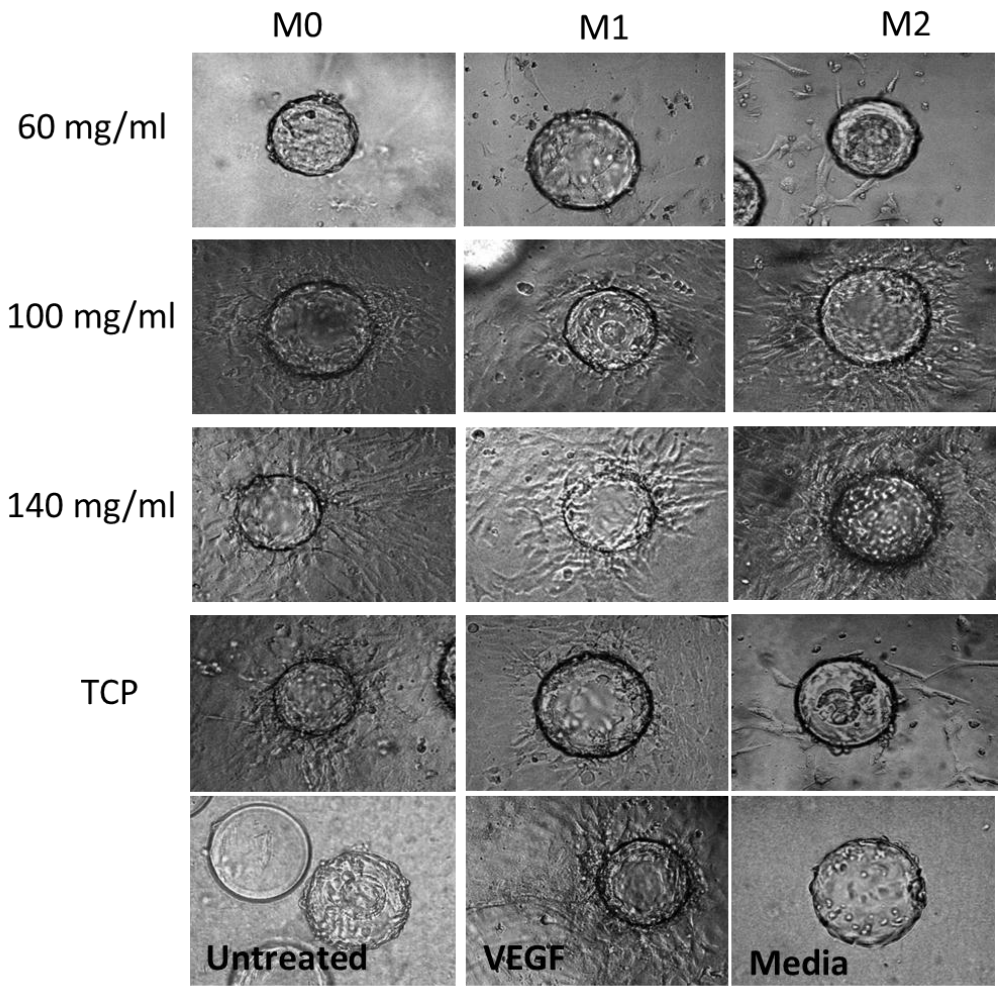

Figure 37 Sprouting from endothelial cell coated beads in response to conditioned media from BMMΦ and PDO interaction (magnification 10x).

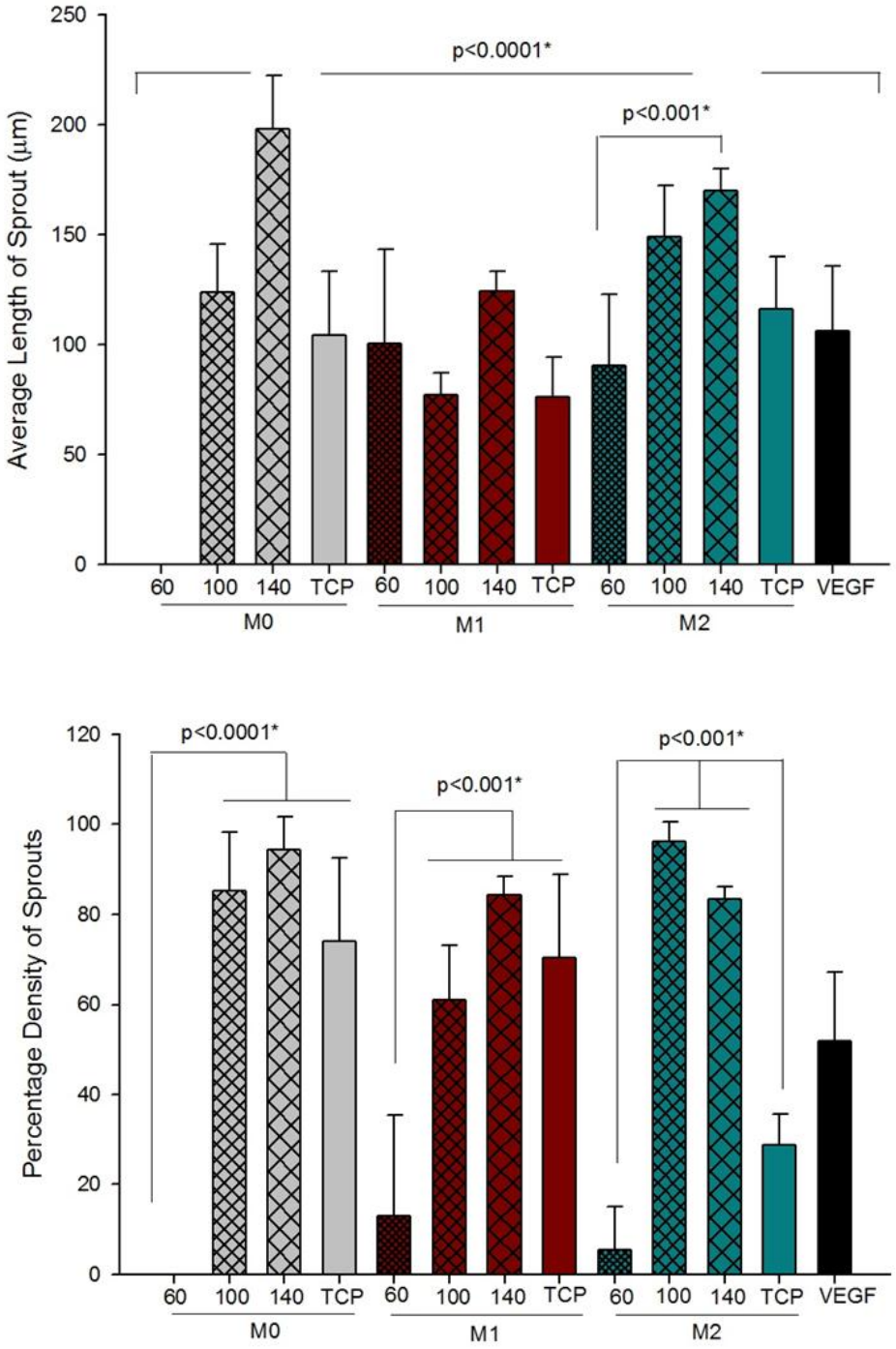

Figure 38 (Top) Quantified Average length of sprouts from the BMMΦ conditioned media.

(Bottom) Quantified Percentage density of sprouts from BMMΦ conditioned media.

M0

M1

M2

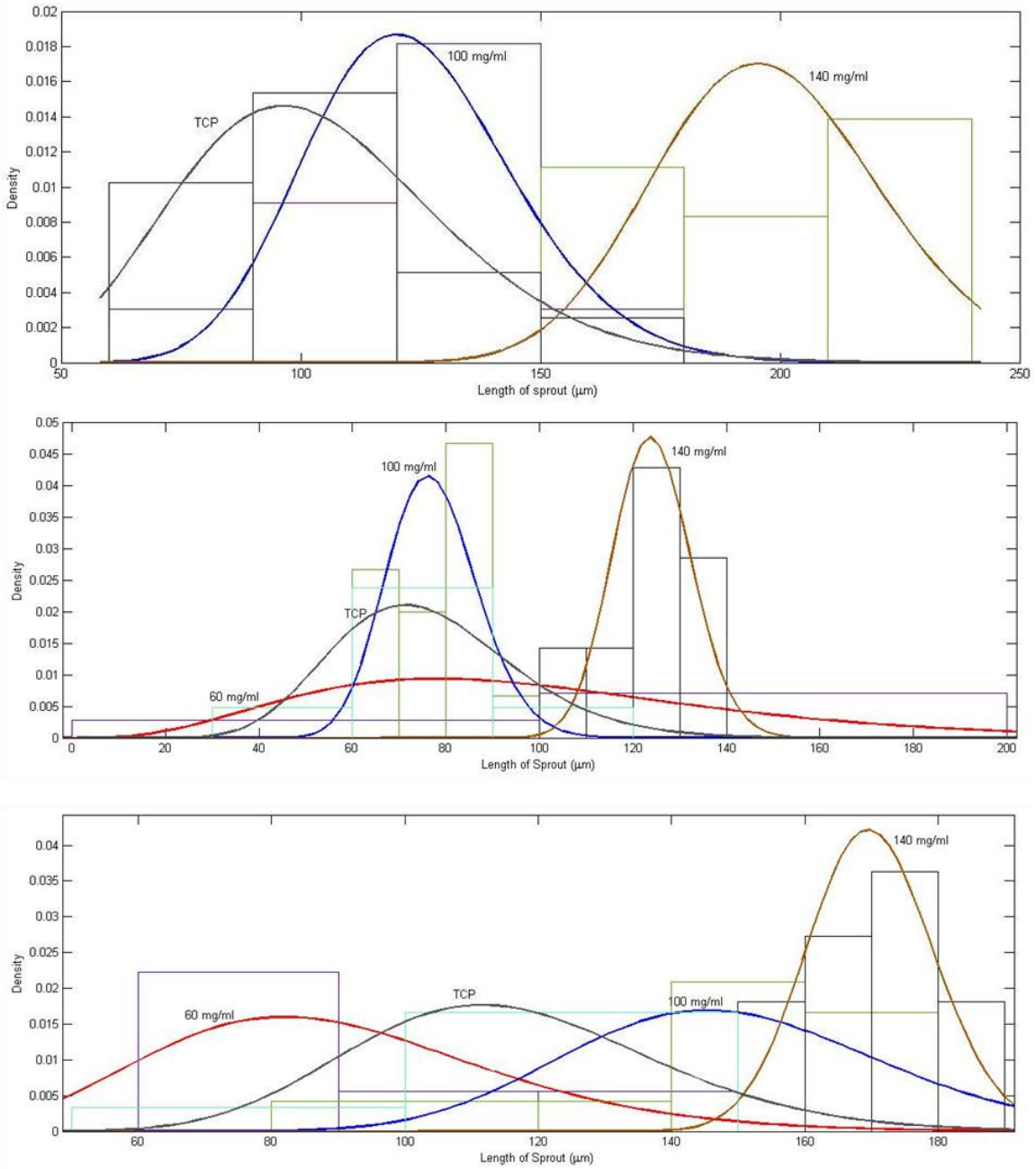

Figure 39 Density histograms of the measured sprout lengths.

Chapter V: Signaling Mechanisms of Macrophage Phenotypes (M1/M2) on Varying Dimensions of Electrospun Bioresorbable Vascular Grafts

Koyal Garg*, Nicholas A. Pullen#, John J. Ryan# and Gary L. Bowlin*

*Department of Biomedical Engineering, Virginia Commonwealth University

#Department of Biology, Virginia Commonwealth University

V.1 Abstract

Toll-like receptors (TLRs) have been well recognized for their pivotal role in the detection of pathogen associated molecular patterns (PAMPs). Twelve TLRs, each detecting a distinct set of PAMPs, have been identified in mammals. TLR signaling is mostly MyD88 dependent except for TLR3 signaling, which requires a TRIF adaptor. In the previous chapters, we have shown that BMMΦs acquire different phenotypes on small vs. large fiber/pore-size materials. In this study we sought to investigate if they signal these responses via different mechanisms. We decided to assess TLR4 and MyD88 as potential candidates. BMMΦs were isolated from TLR 4 and MyD88 knock-out mice and compared to BMMΦs from WT mice. BMMΦs were cultured on 60 mg/ml and 140 mg/ml PDO scaffolds in three different conditions: M0s (naïve), M1 (classically activated) and M2 (alternatively activated). The Arginase and iNOS expression of WT and TLR4 or MyD88 knockout mice was compared by western blot. No significant differences between 60 mg/ml and 140 mg/ml scaffolds were observed in the case of TLR4 deficient and WT BMMΦs. However, severely impaired iNOS and Arginase expression was observed in the case of MyD88 deficient M1 BMMΦs on the 140 mg/ml scaffold. This result indicates a potential role for MyD88 in regulating the signaling mechanisms for BMMΦs of M1 phenotype on the large vs. small fiber/pore-size PDO scaffold.

V.2 Introduction

The mammalian TLRs are germline-encoded receptors expressed by the cells of the innate immune system. They recognize specific patterns of microbial components that are conserved among pathogens, but are not found in mammals. These patterns

characteristically expressed by bacteria, viruses and fungi are known as PAMPs. TLR interactions trigger the expression of proinflammatory cytokines as well as the functional maturation of antigen presenting cells of the innate immune system [21].

TLR family consists of 12 members (TLR1-TLR12) and each TLR has been shown to recognize specific components of pathogens (Figure 40). TLR1–TLR7 and TLR9 have been characterized to recognize microbial components. TLR2 is essential for the recognition of microbial lipopeptides. TLR1 and TLR6 associate with TLR2, and discriminate subtle differences between triacyl- and diacyl lipopeptides, respectively. TLR4 recognizes LPS. TLR9 is the CpG DNA receptor, whereas TLR3 is implicated in the recognition of viral dsRNA. TLR5 is a receptor for flagellin. Thus, the TLR family discriminates between specific patterns of microbial components. Different TLRs use different combinations of adaptor proteins to determine downstream signaling. The majority of TLR's signal through an adapter protein called MyD88, which couples the TLR to downstream signaling kinases, eventually leading to the activation of NFκB by translocation from the cytoplasm to the nucleus. However, MyD88 independent signaling pathways do exist for TLR3 and TLR4. TLR4 possesses two options for signal transduction, either to signal through MyD88 or through TIR domain containing adapter inducing interferon-beta (TRIF), while TLR3 can signal only through TRIF [22].

TLR4 is an important sensor for LPS. LPS stimulation of mammalian cells occurs through a series of interactions with several proteins including LPS binding protein (LBP), CD14, MD-2 and TLR4. LBP functions as a soluble shuttle protein that directly binds to LPS and facilitates its association between LPS and CD14. The transfer of LPS to the TLR4/MD-2 receptor complex is facilitated by CD14. Upon LPS recognition, TLR4 undergoes

oligomerization and recruits TIR (toll-interleukin-1 receptor) domains. There are five TIR domain containing adaptor proteins: MyD88 (myeloid differentiation primary response gene 88), TIRAP (TIR domain containing adaptor protein, also known as Mal, MyD88-adapter-like), TRIF (TIR domain-containing adaptor inducing IFN-β), TRAM (TRIF-related adaptor molecule) and SARM (sterile α and HEAT- Armadillo motifs-containing protein). TLR4 signaling has been divided into MyD88 dependent and MyD88-independent (TRIF-dependent) pathways (Figure 41). MyD88 contains a death domain (DD), which can recruit other DD-containing molecules through homotypic interactions. Upon LPS stimulation, MyD88 recruits and activates IL-1 receptor associated kinase 4 (IRAK-4). IRAK-4 is responsible for the subsequent recruitment, activation and degradation of IRAK-1. Another adaptor protein TRAF6 (TNF receptor associated factor 6), is critical for the MyD88 dependent pathway downstream of IRAK4 and IRAK1. TRAF 6 activates TAK1 (transforming growth factor-β-activated kinase 1). TAK1 then activates downstream IKK (inhibitor of κ light chain gene enhancer in B cells (IκB) kinase) and MAPK (mitogen-activated protein kinase) pathways. IKK complex phosphorylates IκB proteins. This phosphorylation leads to the degradation of IκB proteins and subsequent translocation of the transcription factor NFκB, which controls the expression of proinflammatory cytokines, in addition to other immune related genes. The MyD88-dependent pathway can also activate p38 and c-Jun N-terminal kinase (JNK), leading to AP-1 activation followed by transcription of genes involved in regulation of cell proliferation, morphogenesis, apoptosis, and differentiation.

TLR4 can also signal via a MyD88-independent pathway to stimulate the production of the antiviral protein interferon (IFN)-β. TLR4 can recruit another TIR-domain-

containing adaptor called TRIF. Like MyD88, activated TRIF can bind to TRAF-6 to activate NFκB. Unlike MyD88, TRIF can also bind to kinases called IκKε and TBK1. These kinases activate transcription factors called IRFs (interferon regulatory factors) that are involved in stimulating IFN-β transcription. Thus, the adaptor TRIF enables TLR4 signaling to induce production of IFN-β in addition to activation of NFκB [23].

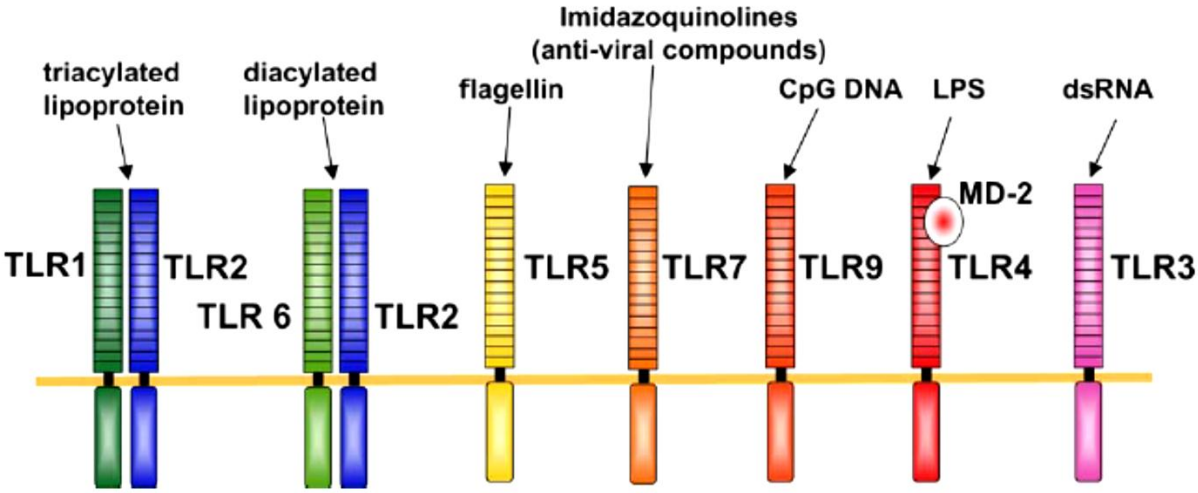

Figure 40 TLRs and their ligands [200].

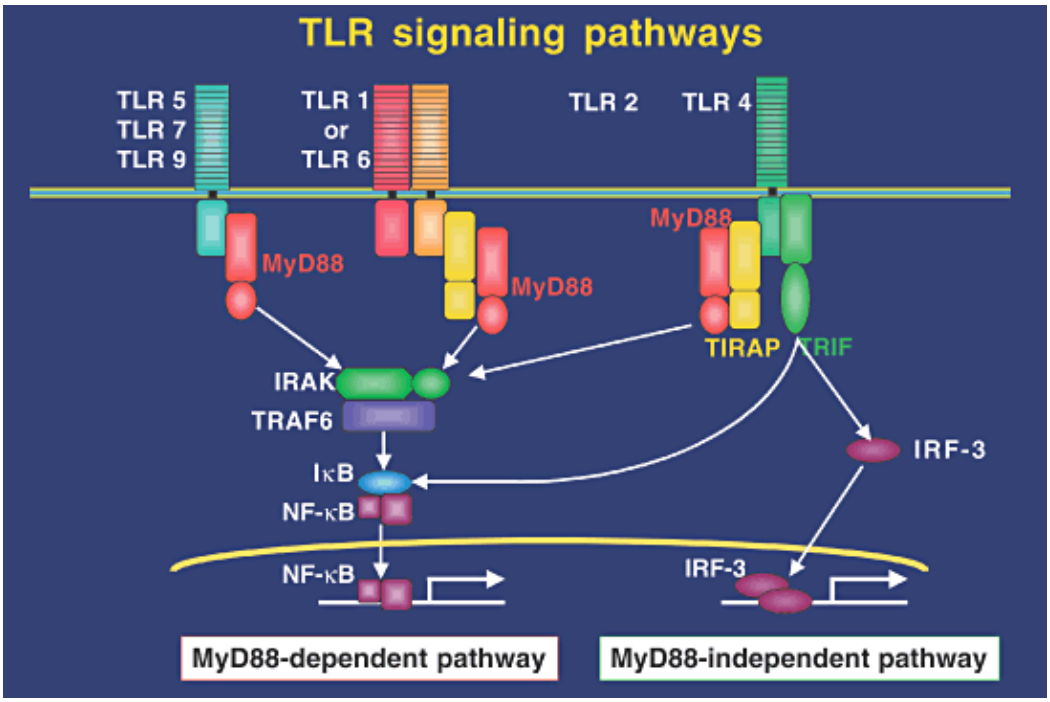

Figure 41 TLR4 Signaling pathways: MyD88 dependent and independent pathways [201].

V.3 Materials and Methods

The involvement of TLR4 was studied by isolating BMMΦ from the bone marrow of both Balb/c wild type and TLR4 knockout (KO) mice (Jackson Laboratories). To investigate the role of MyD88 in this phenotypic switch, BMMΦs were isolated from the bone marrow of both B6.129 wild type and MyD88 knockout (KO) mice (Jackson Laboratories). Following standard protocol in Dr. Ryan's lab, the mice were euthanized and the bone marrow was isolated from the femurs/tibias. To deplete the adherent stromal cells, the harvested bone marrow was cultured overnight in complete RPMI (with 1% penicillin and streptomycin, L-glutamine, HEPES, sodium pyruvate, 10% FBS, and 30 ng/ml recombinant murine MΦ-colony stimulating factor (rmM-CSF)). Non-adherent cells will be collected, red blood cells lysed, remaining non-adherent mononuclear cells plated, and cultured for 7 days in the

presence of rmM-CSF. Phenotype uniformity (naïve MΦ (M0) vs. monocytes) was verified by flow cytometry with our results showing this protocol to achieve a >96% MAC (CD68+) population. After maturation the BMMΦ were divided into three different groups and stimulated for 48 hrs in the presence of either IL-4 and IL-13 to polarize BMMΦ to a M2 phenotype or INF-γ to polarize the BMMΦ to a M1 phenotype. The INF-γ treated BMMΦ were then rinsed with media and treated with LPS for additional 18 hrs. Untreated BMMΦs were used as the naïve group (M0s). The BMMΦ were cultured on PDO (10^6 /disc) and TCP for 24 hrs and their Arg1 and iNOS expression was analyzed by western blot. PDO scaffolds electrospun at 60 mg/ml and 140 mg/ml were used in this study since they showed markedly different induction of BMMΦ phenotypes in the previous studies. Data expressed in this chapter is in the format of means ± standard error of mean. Each experiment was done in triplicates and was reproduced at least twice. All statistical analysis of the data was based on a Kruskal-Wallis one-way analysis of variance on ranks and a Tukey-Kramer pairwise multiple comparison procedure (α=0.05) performed with JMP®IN 8 statistical software (SAS Institute).

V.4 Results

In the absence of TLR4, no significant changes in iNOS or Arginase expression were observed in the case of large vs. small fiber/pore-size materials (Figure 42). This observation can be explained by the overlap and redundancy in function of the TLRs and also in their ability to elicit responses by forming receptor complexes with other TLRs.

The MyD88 knockout and wild-type (WT) M0s and M2s expressed similar levels of Arg1 and iNOS. The only difference was observed in the case of M1s cultured on the 140

mg/ml scaffold (Figure 43). The MyD88 knockout M1s showed severely impaired ability to express both Arg1 and iNOS on the 140 mg/ml scaffold when compared to the WT M1s. No differences were observed in MyD88 knockout and WT M1s cultured on the 60 mg/ml scaffold. This indicates that scaffolds with large and small fiber/pore-sizes signal differently in the case of M1s. This result also shows that MyD88 is a key component involved in the BMMΦ and 140 mg/ml scaffold interaction and signalling. It should also be noted that in this particular experiment we were unable to turn off iNOS with the larger fiber/pore-size scaffold. This could be due to the difference in the background of the mice used. It should be noted that both the MyD88 knockout and the WT mice were of the B6x129 background.

In support of MyD88-dependent monocyte motility, Cote *et al.* [202] have demonstrated that in MyD88$^{-/-}$ mice exposed to the toxin 1-Methyl-4-phenyl-1,2,3,6-tetrahydropyridine (MPTP), infiltration of monocytes/MΦ to the CNS was significantly lower as compared with WT mice. In another study it has been shown that MΦ isolated from MyD88 deficient mice did not migrate to hydrogen peroxide treated fibroblasts in a transwell model compared to the WT MΦ [203]. Fibroblasts were treated with hydrogen peroxide to put them in a state of oxidative stress. The authors also showed that monocytes placed over stressed fibroblasts demonstrated a rounded shape with cells protruding into the pores in contrast to a more flattened morphology of control cells (i.e., placed over media or mock treated cells). In contrast, monocytes placed over stressed fibroblasts and treated with MyD88 inhibitory peptide acquired a more rounded shape. These data suggest that soluble factors released from oxidized cells can influence monocyte motility and can selectively attract them in a MyD88-dependent manner [203]. It has also been reported

that LPS-mediated Src induction led to increased FAK activation and cell migration in MΦs, and which was iNOS-dependent [204]. We believe that autrocrine signals acting on M1 phenotype BMMΦs after LPS stimulation might be influencing their motility and migration capacity. We have shown in chapter III that BMMΦ migration into the large pore electrospun scaffold (140 mg/ml) can influence and shift the phenotype of pre-polarized M1s to M2. Therefore, we believe that this impaired ability of MyD88 deficient BMMΦ to migrate into the fibrous structure of 140 mg/ml scaffold leads to an impaired ability to turn into M2s (as demonstrated by decreased Arginase production).

We have also observed that BMMΦ from C57BL/6, B6x129 and Balb/c mice induce varying levels of Arg1 and iNOS expression in BMMΦ. It is known that C57BL/6 mice are pro-Th1 whereas Balb/c and 129/Sv are pro-Th2. It has been reported that the outcome of myocardial infarct healing in mice strongly depends upon the genetic background. It was shown in that 129/Sv mice display an augmented inflammatory response after myocardial infarction compared with other mouse strains such as Balb/c or C57BL/6 [205]. It has also been documented that 129/Sv mice have high levels of circulating IgE and increased expression of IgE receptor (FcεRI) and greater sensitivity to anaphylaxis when compared to C57BL/6 mice [206]. These inherent differences in the genetic background of mice might explain the observed results.

V.5 Conclusion

The result of this study indicates a potential role for MyD88 in regulating the signaling mechanisms for BMMΦs of M1 phenotype on the large vs. small fiber/pore-size PDO scaffold. No significant differences between 60 mg/ml and 140 mg/ml scaffolds were observed in the case of TLR4 deficient and WT BMMΦs. The redundancy in function of TLRs and also their ability to signal by forming receptor complexes with other TLRs could explain this result. On the other hand, severely impaired iNOS and Arginase expression was observed in the case of MyD88 deficient M1 BMMΦs on the 140 mg/ml scaffold. We believe that reduced mobility of MΦs in the absence of MyD88 leads to impaired migration into the scaffold. This impaired migration doesn't allow them to shift their phenotype to M2s (shown by impaired Arginase expression).

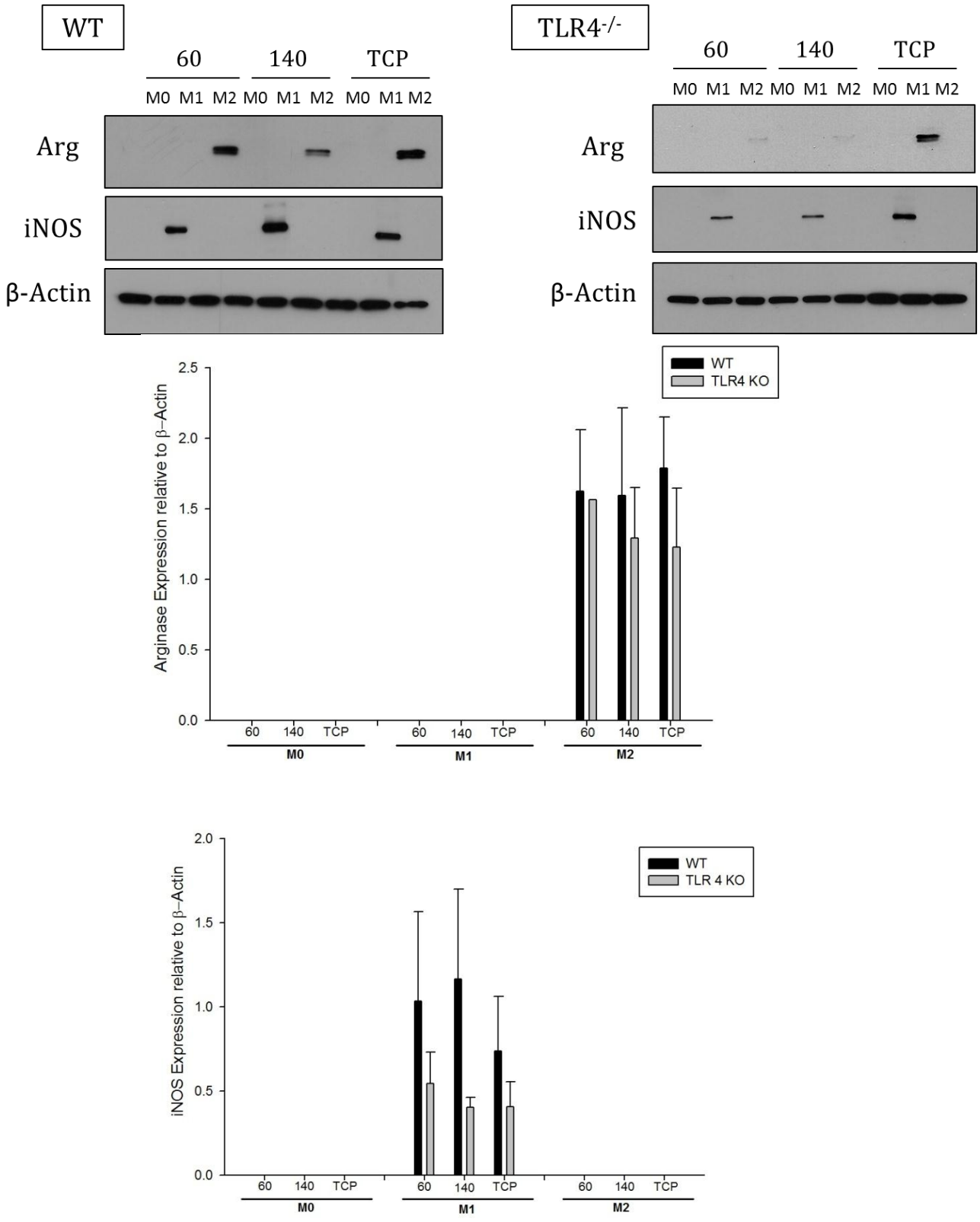

Figure 42 Involvement of TLR4 in BMMΦ signaling.

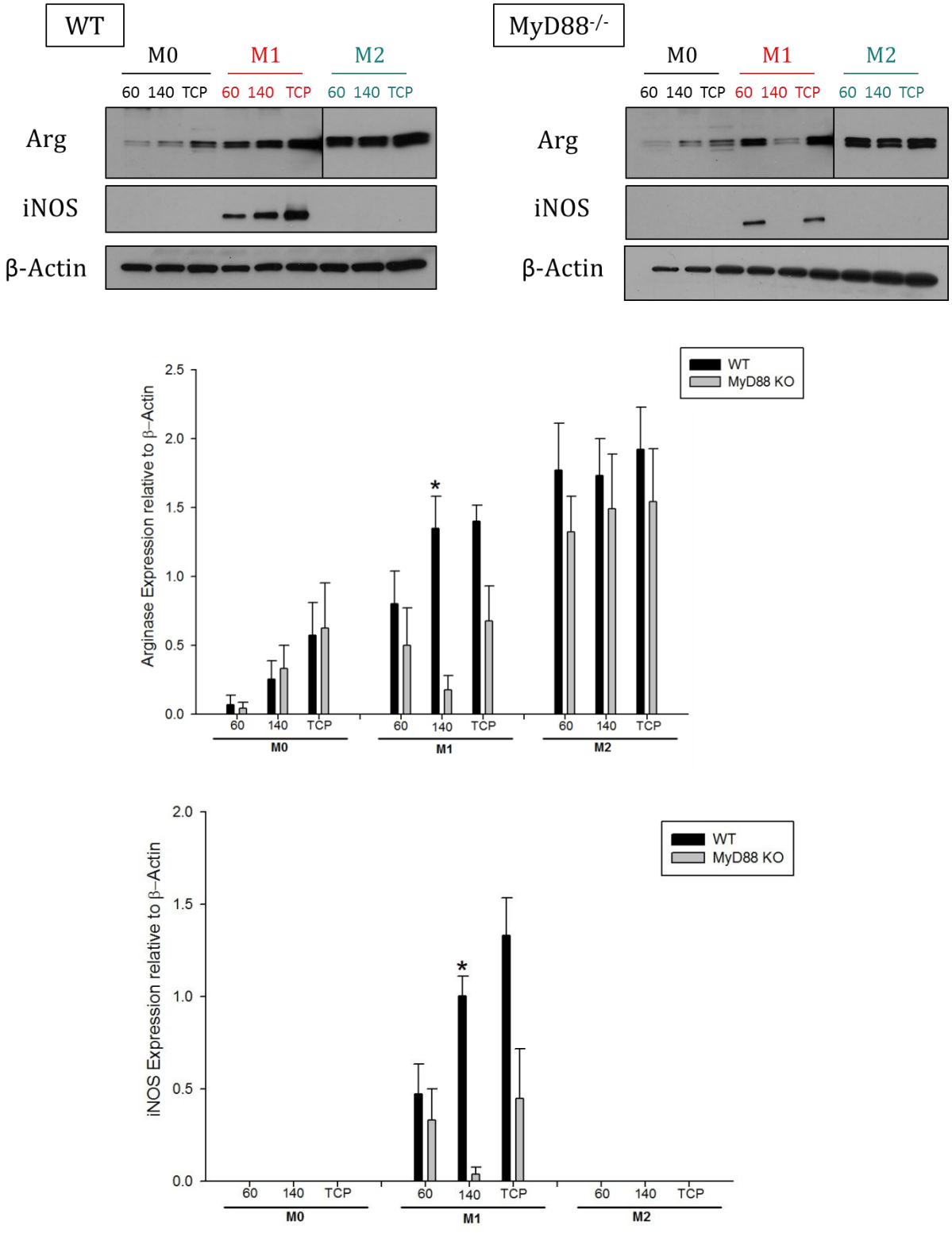

Figure 43 Role of MyD88 in BMMΦ signaling. The asterisk '*' indicates a statistical difference between the WT and MyD88 KO BMMΦ on the 140 mg/ml scaffold.

Chapter VI: *In Vivo* Evaluation of Electrospun Bioresorbable Vascular Grafts of Varying Dimensions.

Koyal Garg*, Nicholas A. Pullen#, Carole A. Oskeritzian£, John J. Ryan# and Gary L. Bowlin*

*Department of Biomedical Engineering, Virginia Commonwealth University

#Department of Biology, Virginia Commonwealth University

€Department of Biochemistry and Molecular Biology, Virginia Commonwealth University

€Present Address: Department of Pathology, Microbiology and Immunology, University of South Carolina, School of Medicine

VI.1 Abstract

Using the Directed in vivo angiogenesis assay (DIVAA), we have attempted to quantify *in vivo* angiogenesis and MΦ phenotypes in response to PDO electrospun scaffolds (composed of small and large fiber/pore-size). This assay typically consists of subcutaneous implantation of semiclosed silicone cylinders (angioreactors) into nude mice. Angioreactors are filled with only 20 µl of Trevigen's basement membrane extract (BME) premixed with or without angiogenic factors. Vascularization within angioreactors is quantified by the intravenous injection of fluorescein isothiocyanate (FITC)-dextran before their recovery, followed by spectrofluorimetry. This assay was modified to examine the angiogenic response of PDO. Tubes of 1 mm internal diameter were fabricated from 60 mg/ml and 140 mg/ml concentrations and cut to length (9.2 mm) for insertion into the angioreactors. The PDO tubes were then filled with BME and implanted into the dorsal flanks of nude mice in quadruplicate. BME mixed with PBS was used as the negative control and BME mixed with VEGF/FGF-2 was used as the positive control in this assay. The results of spectrofluorimetry showed statistically higher signal intensity for the 140 mg/ml scaffold compared to the 60 mg/ml scaffold. However, problems of high background were observed in this assay with the use of materials such as PDO. We hypothesize that the reason for the observed high background is the formation of complexes between dextran and adsorbed plasma proteins on the surface of the PDO. More studies are needed to optimize this assay for use with biomaterials such as PDO. The PDO tubes (60 mg/ml and 140 mg/ml) were also analyzed by H&E staining. The cross-sections of these tubes showed greater cell recruitment and infiltration into the fibrous structures of the 140 mg/ml tube compared to the 60 mg/ml tube. This result is in agreement with the *in vitro* result of

BMMΦ infiltrating deeper into the structures of the 140 mg/ml scaffold compared to the 60 mg/ml scaffold. The scaffolds were also analyzed by immunostaining for iNOS (indicative of M1 phenotype of MΦs). The results showed statistically higher ratios of iNOS positive:negative areas on the 60 mg/ml scaffold compared to the 140 mg/ml scaffold. Overall, these studies indicate that 140 mg/ml scaffold supports greater cell recruitment and cell infiltration *in vivo* but a smaller ratio of iNOS positive:negative areas compared to the 60 mg/ml scaffold, which supports a predominately M1 MΦ phenotype.

VI.2 Introduction

In vitro angiogenesis assays, based on endothelial cell cultures or tissue explants (e.g. aortic ring assays), focus on isolated endothelial cell functions such as proliferation, migration or invasion and fail to examine the coordination of cell functions required for a successful angiogenic response. In contrast, *in vivo* angiogenesis assays examine the entire spectrum of molecular and cellular processes, with the endpoint being formation of new, functional blood vessels. Previous angiogenesis assays have been helpful in developing our understanding of the angiogenic process, but have been difficult to objectively quantify [207-209]. Trevigen's directed *in vivo* angiogenesis assay (DIVAA™), is the first *in vivo* system for the study of angiogenesis that provides quantitative and reproducible results [210]. Typically in this assay, implant grade silicone cylinders closed at one end called angioreactors are filled with 20 μL of Trevigen's basement membrane extract (BME) premixed with or without angiogenesis modulating factors. These angioreactors were then implanted subcutaneously in the dorsal flanks of nude mice. If the angioreactor is filled with angiogenic factors, vascular endothelial cells migrate into and proliferate in the BME

to form vessels in the angioreactor. This assay is a modification of the Matrigel plug assay. The main improvement is in the design of the angioreactor that prevents errors due to the absorption of the BME by the mouse. Additionally, the technique also allows material contained in the assay to be recovered for additional biochemical, cellular, genetic or histological testing. The BME used in this study is basically an extract of the basement membrane proteins from the murine Englebreth-Holm-Swarm tumor (also known as Matrigel). Due to the presence of low concentrations of endogenous growth factors in Matrigel alone, there have been reports of minimal angiogenic responses to Matrigel alone.

VI.3 Materials and Methods

VI.3.1 Quantification of DIVAA by Measuring FITC-Dextran Intensity

Growth factor reduced BME (rBME) was thawed at 4^0C, on ice, overnight prior to assay. rBME was kept on ice until gelling. Pipette tips, angioreactors, AngioRack™, and angiogenesis modulating factors were all pre-chilled at 4^0C, and rBME was kept on ice. Working on ice, angiogenic factors were added to one tube (200 µL) of rBME. Each tube of rBME (200 µl) was used to fill 8 angioreactors. FGF-2 (1.8 µg)/VEGF (600 ng) and 1 µl of heparin solution was added per 200 µL of rBME to be used as positive control angioreactors. Sterile PBS (11 µL) was added per 200 µL rBME to be used for the negative control angioreactors. The PDO tubes were fabricated on a 1 mm diameter mandrel (wall thickness = 300 µm) from 60 mg/ml and 140 mg/ml concentrations and cut to length (9.2 mm) for insertion after ethanol disinfection and UV light sterilization (30 mins) into angioreactors. The dimensions of the angioreactor and the PDO tube are shown in Figure 44. Angioreactors were kept chilled on ice prior to filling. rBME (20 µl) was added to each

angioreactor using an insulin syringe. Bubbles if any were eliminated by centrifuging 250 x g for 5 minutes at 4^0C. The angioreactors were then subcutaneously implanted into the dorsal flanks of athymic nude mice. Four angioreactors, one of each condition (negative control, positive control, 60 mg/ml PDO tube, 140 mg/ml PDO tube) were implanted in each mouse, two on each side of the dorsal midline. Ten days after the implantation the angioreactors were harvested. Before collection of the angioreactors, mice received a 100 µL injection of 25 mg/ml FITC-dextran in PBS via tail vein. The rBME from the tubes was removed and digested in 200µL of dispase solution for 3 hours at 37^0C. After digestion the incubation mix was centrifuged and the fluorescence of the supernatant was measured in a 96 well plate (excitation 485 nm, emission 510 nm). A diagram of the protocol is shown in Figure 45.

VI.3.2 Histological Evaluation and Immunostaining

The PDO tubes collected from the angioreactors were immediately fixed in 10% formalin for histological analysis. iNOS staining of the samples was done by immunohistochemistry-paraffin (IHC-P). The unstained sections of the samples on the slides were heated in 10 mM sodium citrate buffer (pH 6) at 95-100^0C for 20 minutes. The heat was removed and the slides were incubated at room temperature in buffer for 20 minutes. The slides were rinsed in Tris-buffered saline containing 0.05% tween-20 (TBST) for 1 minute. Blocking of the samples was done with 100 µl of 1% bovine serum albumin (BSA) for 20-30 minutes at room temperature. The blocking solution was drained from the slides. This was followed by staining with 100 µl of primary antibody (rabbit anti-mouse iNOS, Abcam 1:50) overnight at 4^0C. The slides were washed 4 times in TBST for 5 minutes. A biotinylated goat anti-rabbit polyclonal antibody was used as the secondary antibody. A

100 µl of the secondary antibody diluted to 1:300 was used and the slides were incubated for 30 minutes at room temperature. The slides were washed again in TBST 4 times for 5 minutes. A 100 µL DAB substrate solution (freshly made just before use: 0.05% DAB - 0.015% H_2O_2 in PBS) was applied to the sections on the slides to reveal the color of the antibody staining. The color development was allowed to go on for 10-15 min until the desired color intensity was reached. The slides were washed in 300 ml PBS for 2 changes 5 min each. The slides were counterstained by immersing the slides in Hematoxylin for 1-2 mins. The slides were washed in running tap water for > 15 min. The slides were then dehydrate through 4 changes of alcohol (95%, 95%, 100% and 100%), 5 min each. The slides were cleared in 3 changes of xylene and coverslip using mounting solution. The exact same procedure was followed for the negative control slides except that they were not treated with the primary antibody.

VI.3.3 Quantification of Histology

The quantification of immunohistological stains (brown or blue) in the samples were analyzed by MATLAB® R2011a. A code on the MathWorks website called "Color segmentation by Delta E color difference" was modified to be used in this study. In the code an RGB image is converted to LAB color space. The RGB color space defines a color as the percentages of red, green, and blue hues mixed together. The LAB color space is based on one channel for luminance (L) or brightness and two color channels; *a* and *b*. The *a* axis extends from green to red and the *b* axis from blue to yellow. After the image is converted into a LAB color space, the user draws a freehand irregularly shaped region to identify a color. The Delta E (the color difference in LAB color space) is then calculated for every pixel in the image between that pixel's color and the average LAB color of the drawn region. The

user can then specify a number that says how close to that color would they like to be. The software will then find all pixels within that specified Delta E of the color of the drawn region. The extracted pixels of the matching colors are then displayed as “white” in a binary image. The number of non-zero (or white) pixels in the image are then counted and this value then serves as an intensity of the chosen color in the image.

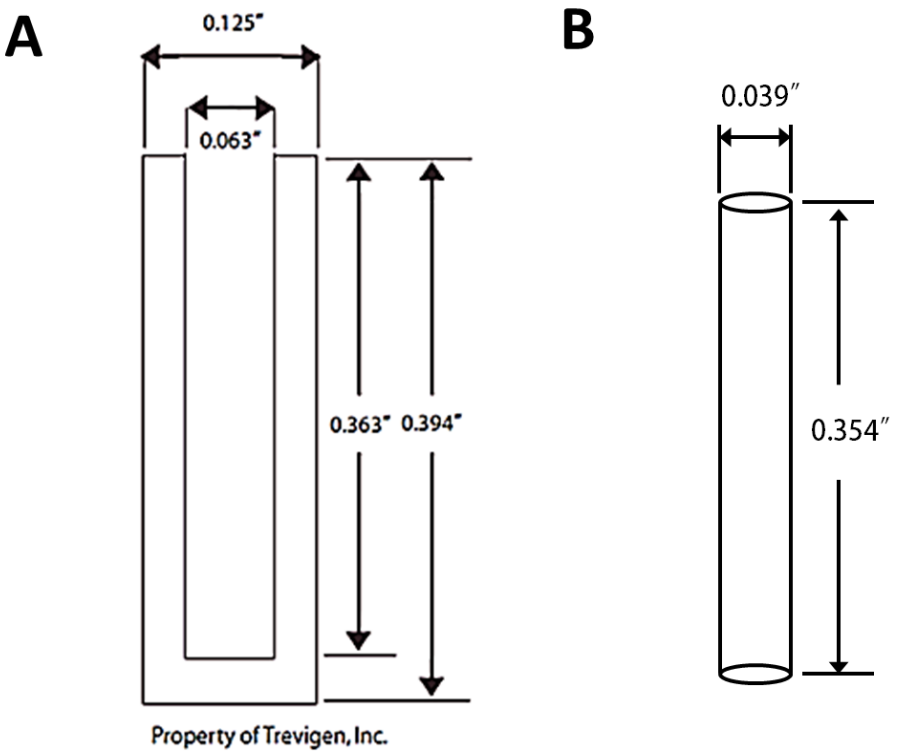

Figure 44 Dimensions of the (A) silicon angioreactor, (B) electrospun polymer tube, used in the study.

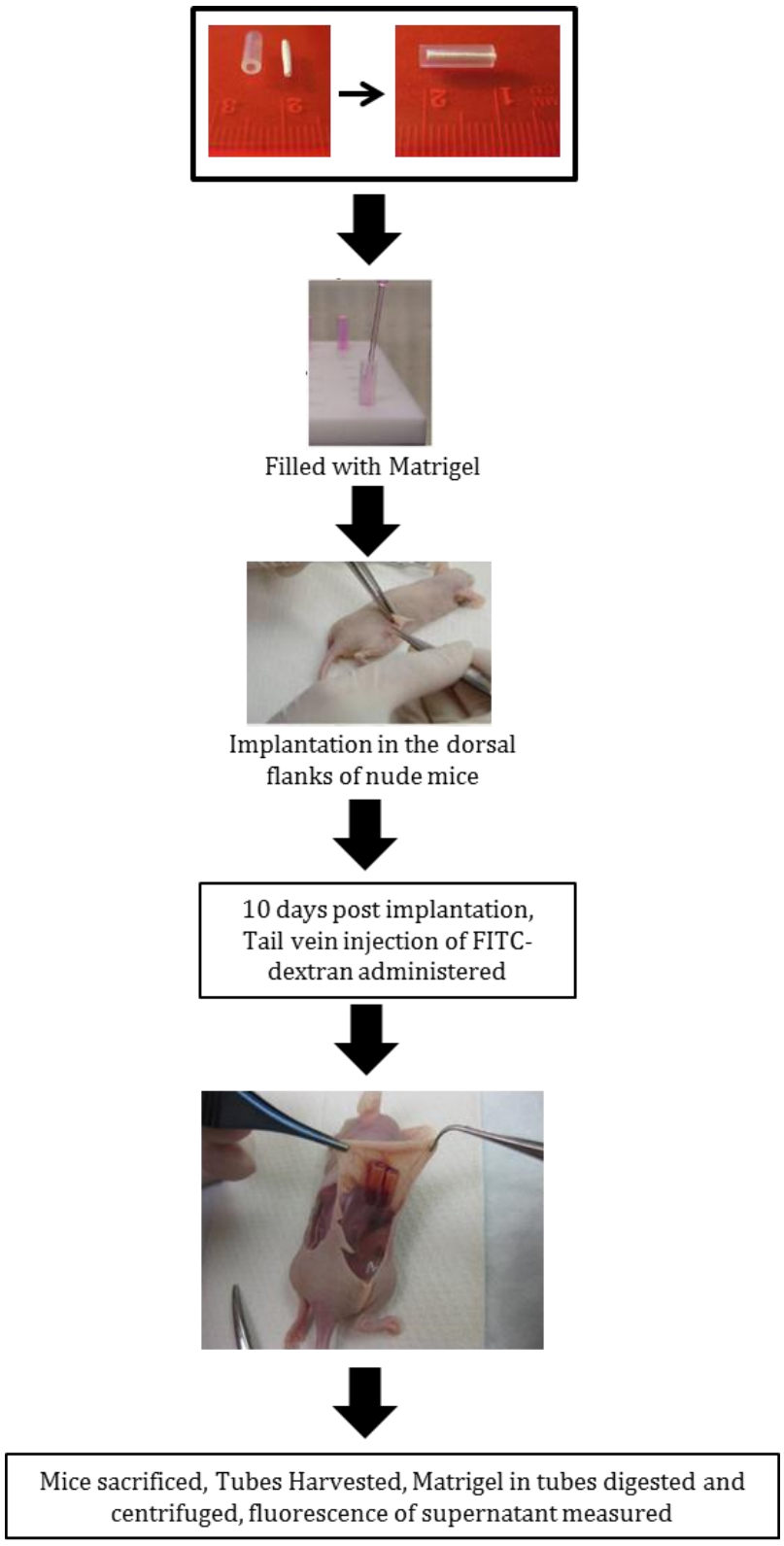

Figure 45 Diagram showing the protocol used for the modified DIVAA assay.

VI.3.4 Statistical Analysis

Data expressed in this chapter is in the format of means ± standard deviation. Each experiment was done in triplicates and was reproduced at least twice. All statistical analysis of the data was based on a Kruskal-Wallis one-way analysis of variance on ranks and a Tukey-Kramer pairwise multiple comparison procedure (α=0.05) performed with JMP®IN 8 statistical software (SAS Institute).

VI.4 Results

VI.4.1 Quantification of DIVAA by Measuring FITC-Dextran Intensity

Quantification of vascularization within the angioreactor is shown in Figure 46. Direct quantification of the angiogenic response is obtained by intravenous injection of FITC-dextran (average molecular weight, 150,000 Da) 20 mins prior to sacrificing the mice. Quantification of the fluorescence within the angioreactors reflects the internal vascular volume and is expected to correlate with the extent of angiogenic response. The results showed statistically higher signal intensity of FITC-dextran in case of the 140 mg/ml scaffold compared to all other conditions tested. Intravenous injection of the FITC-dextran is a measurement of blood volume within the angioreactor and is not necessarily a direct measure of the endothelial cell responses. Although the FITC-dextran signal intensity was greater in the positive control (containing FGF-2 and VEGF), the results showed only a 2 fold increase between the positive control and the negative control (PBS). Previous reports of the DIVAA assay have also demonstrated high background associated with the assay [210]. FITC-dextran is functionally similar to tagged RBCs. Tagged RBCs give accurate blood volume determination because even in leaky capillaries RBCs due to their shape and

size rarely leak out in the intravascular space. Also, there have been reports of dextran interacting and forming complexes with plasma proteins such as fibrinogen. It is also known that when implanted *in vivo*, biomaterials acquire a layer of protein on their surface. It is possible that the higher signal observed in the case of PDO tubes compared to the positive control is because of the interaction between dextran and the layer of protein on the PDO surface. The PDO tube electrospun at 140 mg/ml had statistically higher signal intensity for FITC-dextran compared to the 60 mg/ml PDO tube indicating greater angiogenesis on the 140 mg/ml scaffold. Due to the high background associated with the use of PDO material, this study must be confirmed by histological evaluation and CD31 staining. Furthermore, this study was only performed once. More studies are required to optimize this assay for biomaterials such as PDO.

VI.4.2 Histological Evaluation of PDO Tubes

The PDO tubes (60 mg/ml and 140 mg/ml) were also analyzed by H&E staining. The results are shown in Figure 47. The cross-sections of these tubes showed greater cell recruitment and infiltration into the fibrous structures of the 140 mg/ml tube compared to the 60 mg/ml tube. Figure 47 shows the sections analyzed from different parts of the tube. The top panel shows the open part of the tube that had direct contact with the surrounding tissue. The bottom panel shows the bottom half of the tube that was at the closed end of the silicon angioreactor. The 60 mg/ml PDO tube shows cells concentrated at the surface of the scaffold and don't migrate through the cross-section of the scaffold. In contrast, the 140 mg/ml tube showed cells infiltrating through its fibrous structure. The number of cells at the open end of the tube were quantified by MATLAB ® R2011a using the previously described method. The intensity of cells at the open end of the 140 mg/ml tube was

statistically higher compared to the 60 mg/ml tube. The quantification of cellular infiltration into the fibrous structures of the scaffolds was done using Image J. Analysis showed statistically greater depth of cellular infiltration through the cross-section of the 140 mg/ml tube compared to the 60 mg/ml tube. This result is in agreement with the *in vitro* result of BMMΦ infiltrating deeper into the structures of the 140 mg/ml scaffold compared to the 60 mg/ml scaffold.

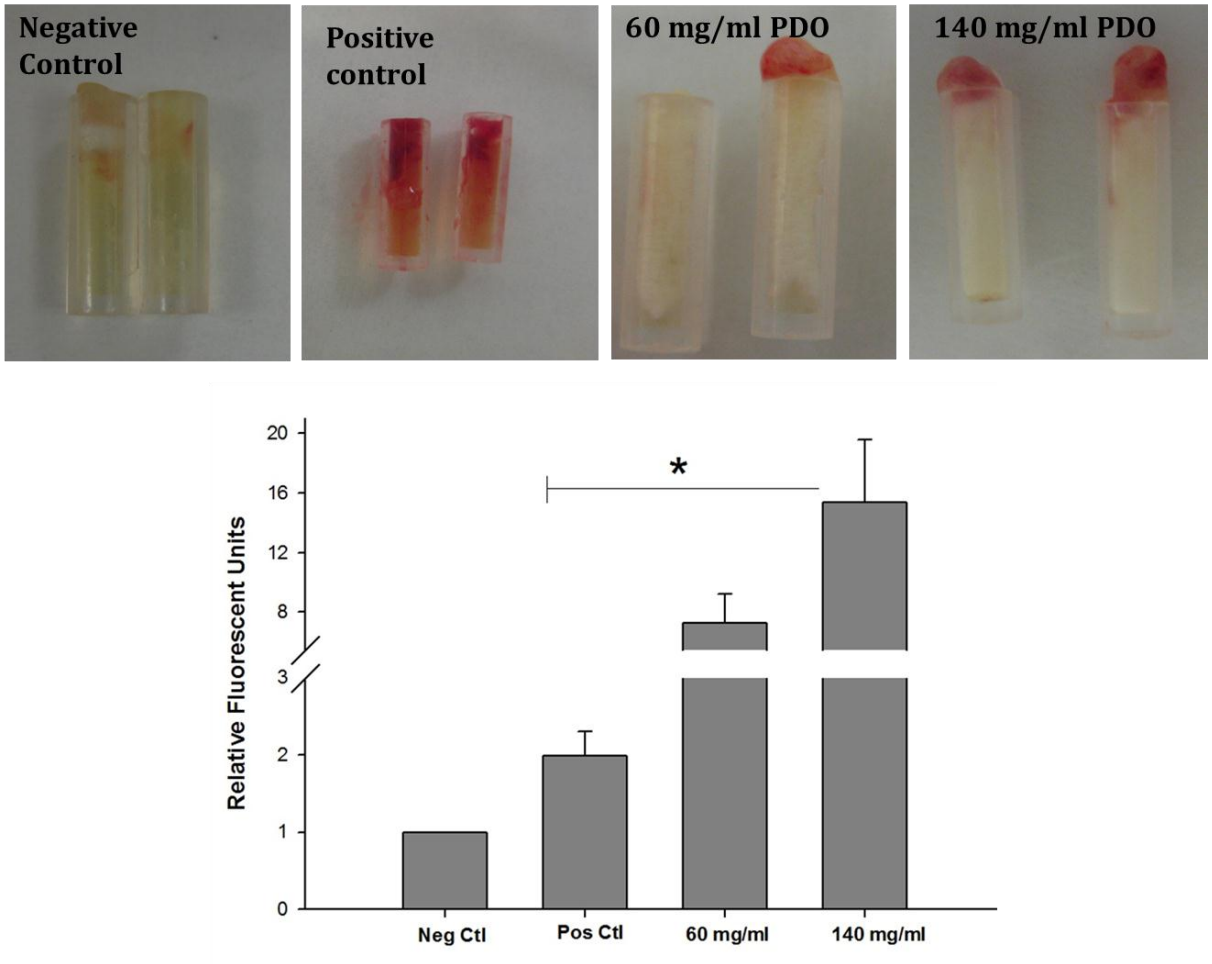

Figure 46 Evaluation of angiogenesis in DIVAATM angioreactors. The asterisk '*' indicates a statistical difference between the 140 mg/ml scaffold and all other conditions tested.

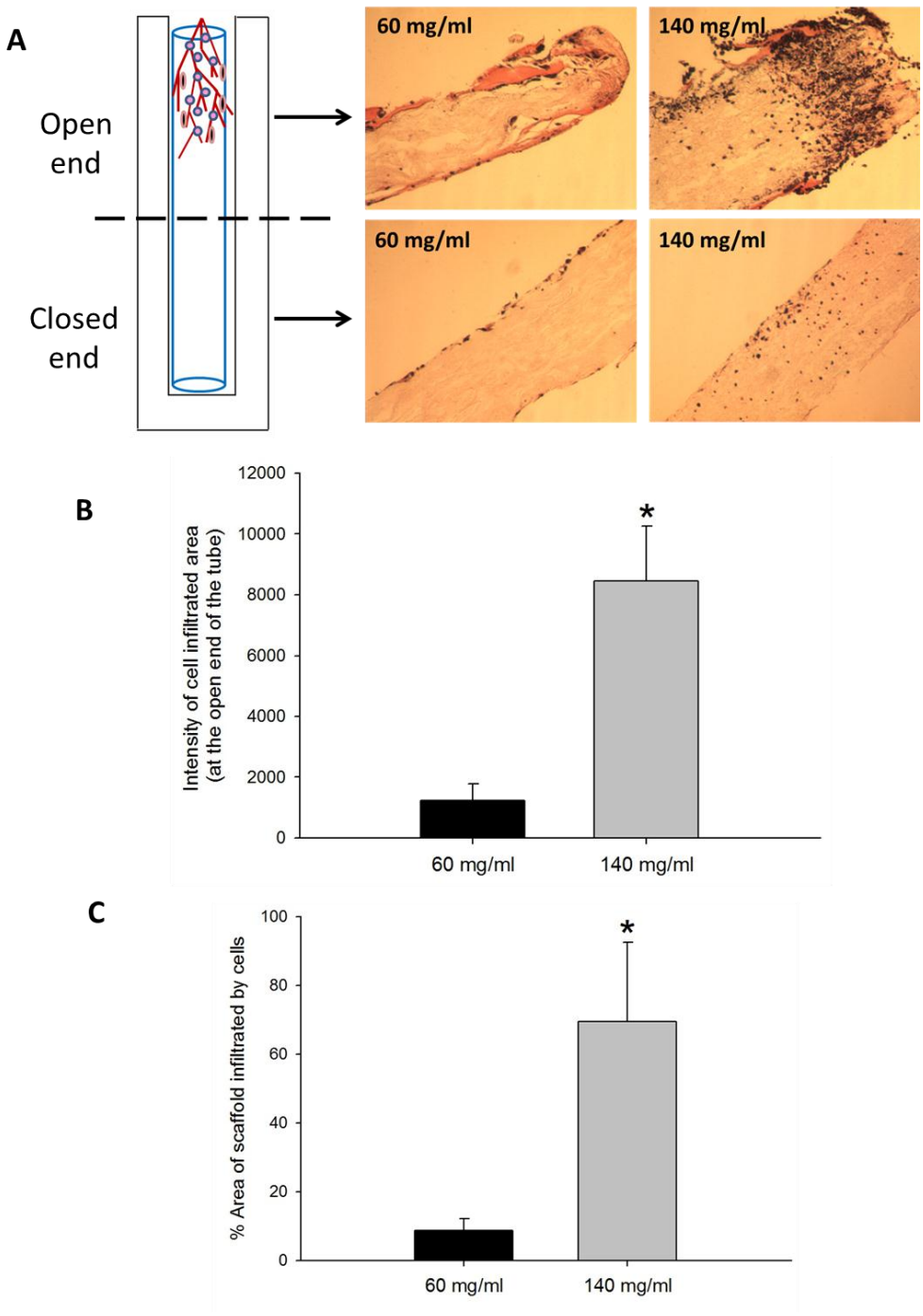

Figure 47 (A) Histological evaluation of the cross section of PDO tubes harvested from the angioreactors after 10 days of implantation in vivo (magnification 20x). (B, C) Quantification of cellular infiltration into the scaffolds. The asterisk '*' indicates a statistical difference between the 60 mg/ml and the 140 mg/ml scaffold.

VI.4.3 Immunostaining of PDO Tubes

The color segmentation method described in materials and methods was used for quantification. Briefly, each image was uploaded in MATLAB ® R2011a and the brown regions and blue regions were separated into two binary images as shown in Figure 48 and 49. The total number of white pixels was counted in the 2 binary images. The ratio of these pixel counts then served as the intensity of iNOS positive (brown) vs. iNOS negative (blue) areas for each image. Immunostaining for iNOS showed a mixed population of iNOS positive (brown) and iNOS negative (blue) cells in the 140 mg/ml scaffold. In case of 60 mg/ml scaffold majority of the recruited cells were stained positive for iNOS (Figure 50). Statistical analysis showed that 60 mg/ml scaffold had significantly higher ratio of iNOS positive: iNOS negative areas compared to the 140 mg/ml scaffold. Overall, this experiment demonstrated that the small fiber/pore-size scaffold (60 mg/ml) recruits less number of cells compared to the bigger fiber/pore-size (140 mg/ml) scaffold and the recruited cells on the 60 mg/ml scaffold are predominately of an M1 phenotype. Therefore, we have shown in a subcutaneous *in vivo* model that the 60 mg/ml scaffold supports the M1 phenotype of MΦ much strongly compared to the 140 mg/ml scaffold.

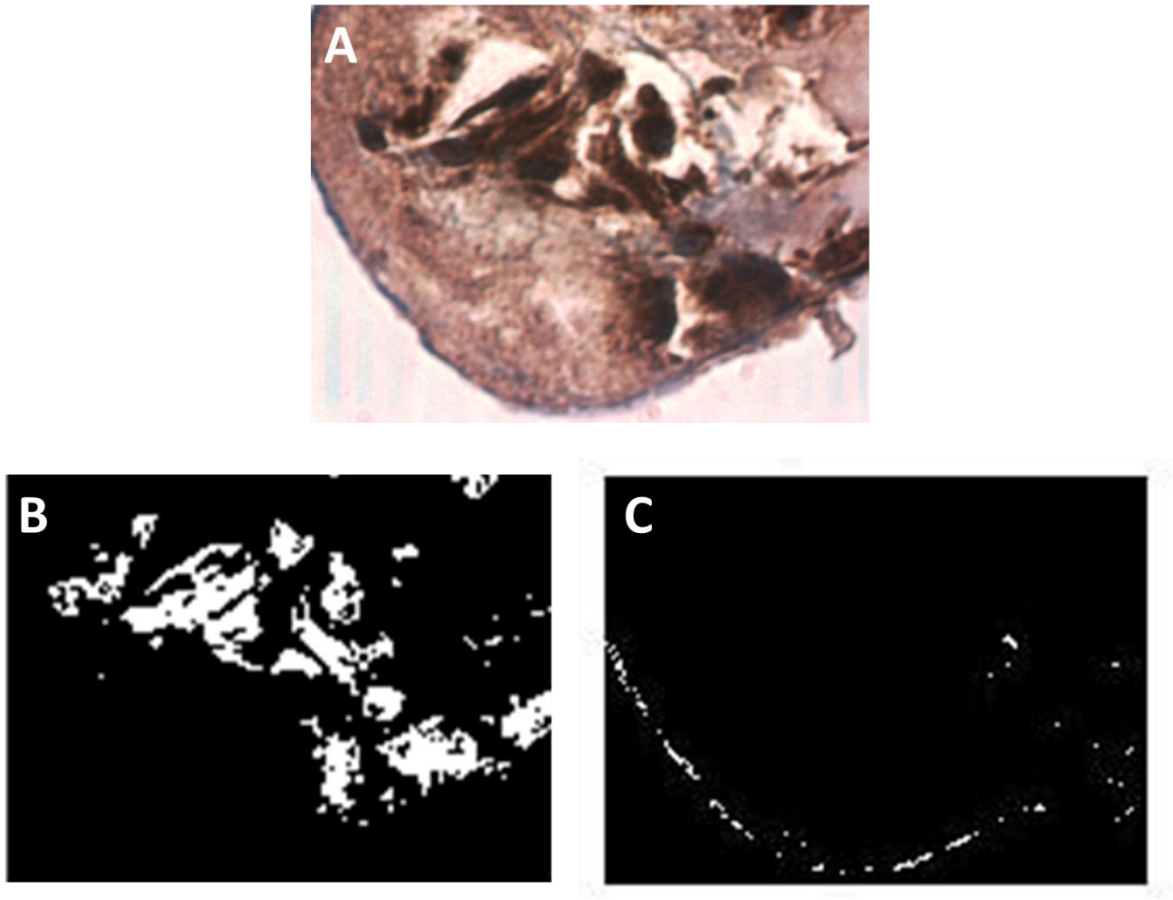

Figure 48 (A) Immunostained section of 60 mg/ml scaffold for iNOS (magnification 40x). (B) Binary image showing white pixels for all brown areas (positive for iNOS) in the original image. (C) Binary image showing white pixels for all blue areas (negative for iNOS) of the original image.

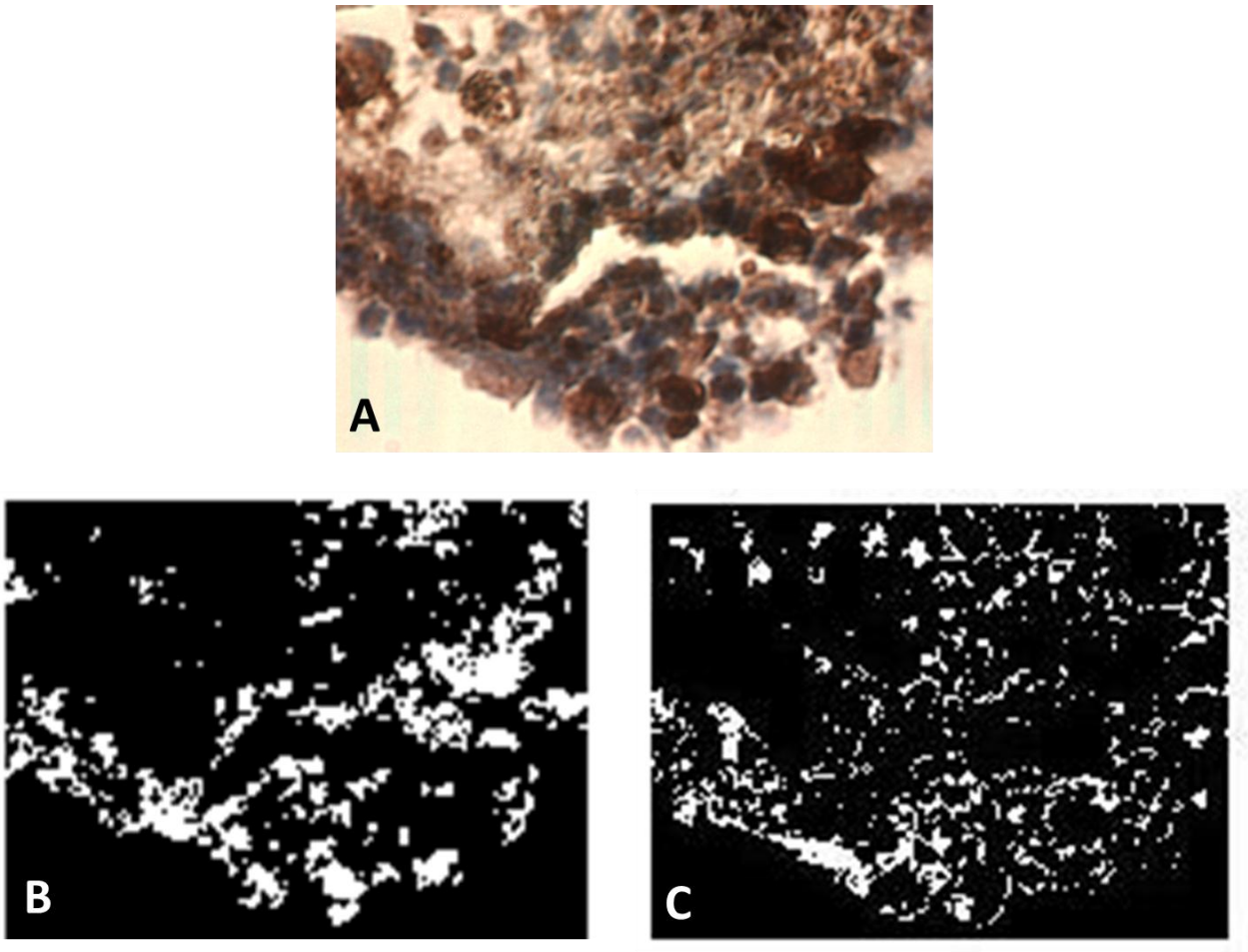

Figure 49 (A) Immunostained section of 140 mg/ml scaffold for iNOS (magnification 40x). (B) Binary image showing white pixels for all brown areas (positive for iNOS) in the original image. (C) Binary image showing white pixels for all blue areas (negative for iNOS) of the original image.

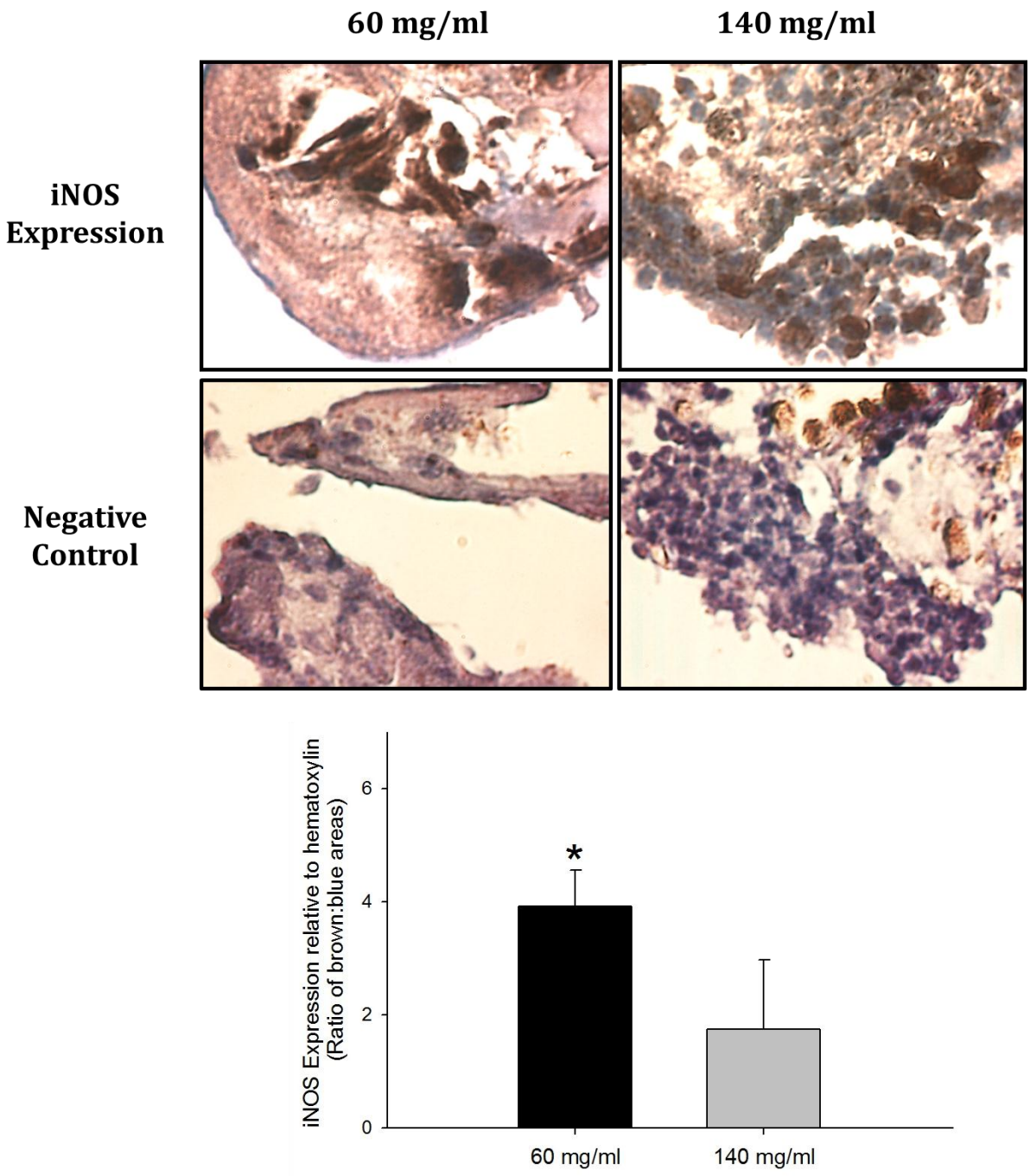

Figure 50 iNOS staining of histological samples of scaffolds from the in vivo study (magnification 40x). The asterisk '*' indicates a statistical difference between the 60 mg/ml and the 140 mg/ml scaffold.

VI.5 Conclusion

The DIVAA assay showed statistically higher FITC-dextran signal intensity for the 140 mg/ml scaffold compared to the 60 mg/ml scaffold indicating greater angiogenic response in the 140 mg/ml tube. However, problems of high background were observed in this assay with the use of electrospun PDO. The observed high background was probably due to the formation of complexes between dextran and adsorbed plasma proteins on the surface of the PDO. More studies are needed to optimize this assay for use with biomaterials such as PDO. H&E staining of the harvested PDO tubes (60 mg/ml and 140 mg/ml) was also performed. The cross-sections of these tubes showed greater cell recruitment and infiltration into the fibrous structures of the 140 mg/ml tube compared to the 60 mg/ml tube. This result corroborates the *in vitro* result of BMMΦ infiltrating deeper into the structures of the 140 mg/ml scaffold compared to the 60 mg/ml scaffold. The scaffolds were also analyzed by immunostaining for iNOS (indicative of M1 phenotype of MΦs). The results showed statistically higher ratios of iNOS positive:negative areas on the 60 mg/ml scaffold compared to the 140 mg/ml scaffold. Overall, these studies indicate that 140 mg/ml scaffold supports greater cell recruitment and cell infiltration *in vivo* but a smaller ratio of iNOS positive:negative areas compared to the 60 mg/ml scaffold, which supports a predominately M1 MΦ phenotype.

Chapter VII: Future Work and Concluding Remarks

VII.1 Summary

MΦ and mast cells are important cell types in the context of tissue remodeling and regeneration. Mast cells participate in the early stages of wound healing and modulate the acute inflammatory responses to biomaterials. Mast cells can secrete a myriad of different cytokines by the process of degranulation; the process of regulated secretion in which preformed contents stored in their granules are rapidly released by exocytosis. Some of these cytokines such as IL-4, IL-13 and TNF-α can modulate the MΦ phenotype.

In Chapter 2, the adhesion, proliferation and cytokine secretion of bone marrow derived murine mast cells (BMMC) on electrospun polydioxanone (PDO), polycaprolactone (PCL) and silk scaffolds, as well as tissue culture plastic (TCP) were investigated in the presence or absence of IL-3, SCF, IgE and IgE with a crosslinking antigen, dinitrophenol-conjugated albumin (DNP). It was previously believed that only activated BMMCs exhibit adhesion and cytokine secretion. However, this study showed non-activated BMMC adhesion to electrospun scaffolds. Silk scaffold was not found to be conducive for mast cell adhesion and cytokine secretion. Activation by IgE and DNP significantly enhanced mast cell adhesion, proliferation, migration and secretion of TNF-α, MIP-1α and IL-13. This indicates that mast cells might play a role in MΦ polarization, biomaterial integration into the host tissue, regeneration, and possibly angiogenesis.

In the next study (Chapter 3) we have demonstrated that by varying the fiber diameter and the corresponding pore-size, we can modulate the macrophage phenotype. Electrospun PDO scaffolds of larger fiber/pore-sizes upregulated Arg1 expression and downregulated iNOS and nitrite expression in BMMΦ. The production of angiogenic factors

such as VEGF, TGF-β1 and bFGF from BMMΦ was also greater on the larger fiber/pore-sizes. The expression of TNF-α and IL-6 could not be modulated by electrospun PDO of different fiber/pore-sizes.

BMMΦ mediated angiogenesis was examined using an *in vitro* bead assay in Chapter 4. It was observed that the BMMΦ of M0, M1 and M2 phenotypes cultured on the PDO scaffolds with bigger fiber/pore-size induced higher percentage density of sprouts. However, the conditioned media from BMMΦ of only M0 and M2 phenotypes cultured on the bigger fiber/pore-size PDO scaffold (140 mg/ml) induced significantly larger average length of sprout. Overall, the study confirms that the BMMΦs of M2 phenotype are functional and support angiogenesis and that the naïve BMMΦs acquire a functional M2-like phenotype when in contact with the bigger fiber/pore-size scaffold.

The role for MyD88 and TLR4 in regulating the signaling mechanisms for BMMΦs of M1/M2 phenotypes on the large vs. small fiber/pore-size PDO scaffolds was also investigated. This study is described in detail in Chapter 5. No significant differences between 60 mg/ml and 140 mg/ml scaffolds were observed in the case of TLR4 deficient and WT BMMΦs. The redundancy in function of TLRs and also their ability to signal by forming receptor complexes with other TLRs could explain this result. On the other hand, severely impaired iNOS and Arginase expression was observed in the case of MyD88 deficient M1 BMMΦs on the 140 mg/ml scaffold. We believe that reduced mobility of MΦs in the absence of MyD88 leads to impaired migration into the scaffold. This impaired migration doesn't allow them to shift their phenotype to M2s (shown by impaired Arg1

expression). Overall, this result indicates a potential role for fiber/pore-size in the signaling mechanism of BMMΦ.

A subcutaneous mouse model (described in Chapter 6) was used to evaluate the angiogenic and regenerative potential of PDO scaffolds *in vivo*. The DIVAA assay showed statistically higher FITC-dextran signal intensity for the 140 mg/ml scaffold compared to the 60 mg/ml scaffold indicating greater angiogenic response in the 140 mg/ml tube. However, problems of high background were observed in this assay with the use of electrospun PDO. The observed high background was probably due to the formation of complexes between dextran and adsorbed plasma proteins on the surface of the PDO. More studies are needed to optimize this assay for use with biomaterials such as PDO. H&E staining of the harvested PDO tubes (60 mg/ml and 140 mg/ml) was also performed. The cross-sections of these tubes showed greater cell recruitment and infiltration into the fibrous structures of the 140 mg/ml tube compared to the 60 mg/ml tube. This result corroborates the *in vitro* result of BMMΦ infiltrating deeper into the structures of the 140 mg/ml scaffold compared to the 60 mg/ml scaffold. The scaffolds were also analyzed by immunostaining for iNOS (indicative of M1 phenotype of MΦs). The results showed statistically higher ratios of iNOS positive:negative areas on the 60 mg/ml scaffold compared to the 140 mg/ml scaffold. Overall, these studies indicate that 140 mg/ml scaffold supports greater cell recruitment and cell infiltration *in vivo* but a smaller ratio of iNOS positive:negative areas compared to the 60 mg/ml scaffold, which supports a predominately M1 MΦ phenotype.

VII.2 Limitations and Future Studies

There were several limitations in the present study. A limited number of MΦ phenotype markers were used in this study. Although, iNOS and Arginase are widely accepted markers of M1 and M2 macrophages in a mouse model, care must be taken when extrapolating these studies to human MΦs. Human M1/M2 phenotype MΦs do not express iNOS or Arginase. Human MΦs are identified by other criteria, including the upregulation of surface molecules such as major histocompatibility complex (MHC) Class II, co-stimulatory molecule CD86 and opsonic receptors [e.g., FcRIII (CD16)], enhanced ability to kill and degrade intracellular microorganism and the elevated capability to process and present antigens [3].

In this dissertation, TCP is not exactly included in the studies as control but as a measure of the baseline activity of macrophages. We created films of PDO on 24 well plates. PDO films would have been the perfect 2D control for the 3D PDO scaffolds created by electrospinning. We could not successfully culture macrophages on films of PDO for 3 days. The macrophages did not survive on the PDO films past ~ 24 hours.

Future studies would include investigation into the role of NFκB as a potential mediator in the signaling mechanism of small vs. large fiber/pore-size electrospun PDO. Since NFκB is the main downstream transcription factor of both MyD88 dependent and independent signaling mechanisms, and is the main regulatory factor of pro-inflammatory cytokines, it would be interesting to investigate the outcome of NFκB inhibition. If by inhibiting NFκB, we are able to suppress M1 phenotype on the electrospun PDO, strategies could be devised to incorporate NFκB inhibitor into the fibrous structures of PDO. A

scaffold that suppresses M1 phenotype responses could prove to be more angiogenic and regenerative when implanted *in vivo*. Care must be taken when studying BMMΦ responses to NFκB activation inhibitor (Cat. No. 481406) from Calbiochem. This inhibitor is typically reconstituted in dimethyl sulfoxide (DMSO). I have found that BMMΦ treatment with DMSO induces iNOS expression. Other studies have indicated that treatment with DMSO induces increased phagocytic ability in MΦ. Alternatives to DMSO, such as ethanol can be explored to reconstitute the NFκB inhibitor. The siRNA technique could also be explored to look at the involvement of NFκB.

To identify the particular TLRs involved in MΦ interactions with electrospun scaffolds, double or triple knock out models of TLR2, 4 or 6 could be used. It has been shown that these TLRs mediate the dendritic cell interaction with biomaterials [25]. Since, DCs and BMMΦ share many similarities in lineage and function; it is possible that TLR-2, 4 and 6 might be involved in BMMΦ signaling mechanisms as well. The involvement of TLR9 can also be investigated by using siRNA technology. TLR9 could be involved since MΦs are capable of degrading the electrospun scaffolds and internalize parts of them. They can then present particles of these scaffolds as antigens to T cells and elicit immune responses to the materials.

In chapter 3, we have speculated that the increased infiltration of M1 phenotype BMMΦ into the 60 mg/ml scaffold is due to the expression of MMPs and proteolytic enzymes that degrade the electrospun matrix, facilitating the migration of BMMΦ into the scaffold. A degradation study of PDO (60 mg/ml and 140 mg/ml) must be done to confirm

this hypothesis. A quantification of the secreted MMPs and enzymes should also be done to identify the particular factors released by MΦs that degrade electrospun matrices.

This study also needs to be extended to electrospun scaffolds created by polymers other than PDO. This model of fiber/pore-size modulating MΦ phenotype needs to be validated by scaffolds of other polymers. Also, these studies have been performed in BMMΦ, which are typically considered to be relatively immature. It needs to be investigated whether these phenotypic switches can be induced in more mature MΦs such as peritoneal MΦs. Also, the differences in genetic background of mice and its influence on the phenotype of BMMΦ also needs to be explored. We have observed that BMMΦ from C57BL/6, B6x129 and Balb/c mice induce varying levels of Arg1 and iNOS expression in BMMΦ. It is known that C57BL/6 mice are pro-Th1 whereas Balb/c and 129 are pro-Th2. It has been reported that the outcome of myocardial infarct healing in mice strongly depends upon the genetic background. It was shown in the study that 129 mice display an augmented inflammatory response after myocardial infarction compared with other mouse strains such as Balb/c or C57BL/6 [205]. It has also been documented that 129 mice have high levels of circulating IgE and increased expression of IgE receptor (FcεRI) and greater sensitivity to anaphylaxis when compared to C57BL/6 mice [206].

This dissertation work primarily dealt with the involvement of mast cell and MΦ involvement in biomaterial healing. The involvement of neutrophils in the process of biomaterial healing must also be explored since they are first responders and are capable to producing several cytokines and growth factors such as TNF-α, IL-1β, IL-8, MIP-1α and

VEGF [211]. They could therefore be involved in phenotype modulation of MΦs at the implant site.

A study analyzing the regenerative or wound healing potential of BMMΦ also needs to be performed. The main focus of this thesis was the potential for angiogenesis. The M1/M2 phenotypic responses in relation to scar tissue formation and tissue remodeling have not been explored.

VII.3 Concluding Remarks

In conclusion, this study demonstrates that biomaterial architecture can influence MΦ activation to either M1 (pro-inflammatory) or M2 (anti-inflammatory/tissue regenerative). MΦ phenotype was studied as a mechanism by which biomaterial architectures promoted angiogenesis and healing. Overall, the study demonstrates that electrospun PDO scaffolds with large fiber/pore-size induce a M2 phenotype, promote angiogenesis and are more efficient at cell recruitment and infiltration *in vivo*. Majority of these recruited cells *in vivo* are of a M1 phenotype (iNOS positive) in the small fiber/pore-size scaffold whereas, the large fiber/pore-size scaffold shows a mixed population of iNOS positive and negative cells. We have also shown that the PDO scaffold of large fiber/pore-size also signals differently than the small fiber/pore-size scaffold.

Literature Cited

1. Anderson, J.M., A. Rodriguez, and D.T. Chang, *Foreign body reaction to biomaterials.* Semin Immunol, 2008. **20**(2): p. 86-100.

2. Brown, B.N., et al., *Macrophage polarization: an opportunity for improved outcomes in biomaterials and regenerative medicine.* Biomaterials. **33**(15): p. 3792-802.

3. Kou, P.M. and J.E. Babensee, *Macrophage and dendritic cell phenotypic diversity in the context of biomaterials.* J Biomed Mater Res A.

4. Anderson, J.M., *Biological Response to Materials.* Annual Review of Materials Research, 2001. **31**: p. 81-110.

5. Park, J.E. and A. Barbul, *Understanding the role of immune regulation in wound healing.* Am J Surg, 2004. **187**(5A): p. 11S-16S.

6. Sunderkotter, C., et al., *Macrophages and angiogenesis.* J Leukoc Biol, 1994. **55**(3): p. 410-22.

7. Lamagna, C., M. Aurrand-Lions, and B.A. Imhof, *Dual role of macrophages in tumor growth and angiogenesis.* J Leukoc Biol, 2006. **80**(4): p. 705-13.

8. Gordon, S., *Alternative activation of macrophages.* Nat Rev Immunol, 2003. **3**(1): p. 23-35.

9. Martinez, F.O., L. Helming, and S. Gordon, *Alternative activation of macrophages: an immunologic functional perspective.* Annu Rev Immunol, 2009. **27**: p. 451-83.

10. Martinez, F.O., et al., *Macrophage activation and polarization.* Front Biosci, 2008. **13**: p. 453-61.

11. Mosser, D.M. and X. Zhang, *Activation of murine macrophages.* Curr Protoc Immunol, 2008. **Chapter 14**: p. Unit 14 2.

12. Mosser, D.M. and J.P. Edwards, *Exploring the full spectrum of macrophage activation.* Nat Rev Immunol, 2008. **8**(12): p. 958-69.

13. Mantovani, A., et al., *The chemokine system in diverse forms of macrophage activation and polarization.* Trends Immunol, 2004. **25**(12): p. 677-86.

14. Dagtekin, G., et al., *Modulation of angiogenic functions in human macrophages by biomaterials.* Biomaterials, 2003. **24**(20): p. 3395-401.

15. Ashley, R.A., et al., *Leukocyte inflammatory response in a rat urinary bladder regeneration model using porcine small intestinal submucosa scaffold.* Tissue Eng Part A, 2009. **15**(11): p. 3241-6.

16. Biswas, S.K. and A. Mantovani, *Macrophage plasticity and interaction with lymphocyte subsets: cancer as a paradigm.* Nat Immunol. **11**(10): p. 889-96.

17. Deonarine, K., et al., *Gene expression profiling of cutaneous wound healing.* J Transl Med, 2007. **5**: p. 11.

18. Xia, Z. and J.T. Triffitt, *A review on macrophage responses to biomaterials.* Biomed Mater, 2006. **1**(1): p. R1-9.

19. Zakrzewska, M., E. Marcinkowska, and A. Wiedlocha, *FGF-1: from biology through engineering to potential medical applications.* Crit Rev Clin Lab Sci, 2008. **45**(1): p. 91-135.

20. Berton, G. and C.A. Lowell, *Integrin signalling in neutrophils and macrophages.* Cell Signal, 1999. **11**(9): p. 621-35.

21. Lu, Y.C., W.C. Yeh, and P.S. Ohashi, *LPS/TLR4 signal transduction pathway.* Cytokine, 2008. **42**(2): p. 145-51.

22. Pearl, J.I., et al., *Role of the Toll-like receptor pathway in the recognition of orthopedic implant wear-debris particles.* Biomaterials. **32**(24): p. 5535-42.

23. Murphy, K., P. Travers, and P. Walter, *Janeway's Immunobiology, 7th edition*. Immunobiology. 2008, New York: Garland Science.

24. Macedo, L., et al., *Wound healing is impaired in MyD88-deficient mice: a role for MyD88 in the regulation of wound healing by adenosine A2A receptors.* Am J Pathol, 2007. **171**(6): p. 1774-88.

25. Shokouhi, B., et al., *The role of multiple toll-like receptor signalling cascades on interactions between biomedical polymers and dendritic cells.* Biomaterials. **31**(22): p. 5759-71.

26. Carmeliet, P., *Mechanisms of angiogenesis and arteriogenesis.* Nat Med, 2000. **6**(4): p. 389-95.

27. Li, J., et al., *TGF-beta3, but not TGF-beta1, protects keratinocytes against 12-O-tetradecanoylphorbol-13-acetate-induced cell death in vitro and in vivo.* J Biol Chem, 1999. **274**(7): p. 4213-9.

28. Kalluri, R., *Basement membranes: structure, assembly and role in tumour angiogenesis.* Nat Rev Cancer, 2003. **3**(6): p. 422-33.

29. Zheng-Ming Huang, Y.-Z.Z., M. Kotaki, S. Ramakrishna, *A review on polymer nanofibers by electrospinning and their applications in nanocomposites.* Composite Science and technology, 2003(63): p. 2223-2253.

30. Zhang, Y., et al., *Electrospinning of gelatin fibers and gelatin/PCL composite fibrous scaffolds.* J Biomed Mater Res B Appl Biomater, 2005. **72**(1): p. 156-65.

31. Greiner, A. and J.H. Wendoeff, *Electrospinning: A Fascinating Method for the Preparation of Ultrathin Fibers.* Angew Chem Int Ed Engl, 2007. **46**: p. 5670-5703.

32. Ashammakhi, N., et al., *Tissue engineering: a new take-off using nanofiber-based scaffolds.* J Craniofac Surg, 2007. **18**(1): p. 3-17.

33. Burger, C., B.S. Hsiao, and B. Chu, *Nanofibrous materials and their applications.* Annual reviews in material science, 2006. **36**: p. 333-68.

34. Boland, E.D., et al., *Utilizing acid pretreatment and electrospinning to improve biocompatibility of poly(glycolic acid) for tissue engineering.* Journal of Biomedical Materials Research Part B: Applied Biomaterials, 2004. **71B**: p. 144-152.

35. Bhattarai, S.R., et al., *Novel biodegradable electrospun membrane: scaffold for tissue engineering.* Biomaterials, 2004. **25**(13): p. 2595-602.

36. Zhang, Y., et al., *Electrospinning of gelatin fibers and gelatin/PCL composite fibrous scaffolds.* Journal of Biomedical Materials Research Part B: Applied Biomaterials, 2005. **72B**: p. 156-165.

37. Lee, C.H., et al., *Nanofiber alignment and direction of mechanical strain affect the ECM production of human ACL fibroblast.* Biomaterials, 2005. **26**: p. 1261-1270.

38. Sell, S.A., et al., *Electrospinning of collagen / biopolymers for regenerative medicine and cardiovascular tissue engineering.* Advanced Drug Delivery Reviews, 2009. **In Press**.

39. Sell, S.A., et al., *The Use of Natural Polymers in Tissue Engineering: A Focus on Electrospun Extracellular Matrix Analogues.* Polymers, 2010. **2**(4): p. 522-553.

40. Kolacna, L., et al., *Biochemical and biophysical aspects of collagen nanostructure in the extracellular matrix.* Physiol Res, 2007. **56 Suppl 1**: p. S51-60.

41. Matthews, J.A., et al., *Electrospinning of Collagen Nanofibers.* Biomacromolecules,, 2002. **3**: p. 232-238.

42. Matthews, J.A., et al., *Electrospinning of collagen type II: A feasibility study.* Journal of Bioactive and Compatible Polymers, 2003. **18**: p. 125-134.

43. Barnes, C.P., et al., *Nanofiber technology: designing the next generation of tissue engineering scaffolds.* Advanced Drug Delivery Reviews., 2007. **59**: p. 1413-1433.

44. Barnes, C.P., et al., *Preliminary investigation of electrospun collagen and polydioxanone for vascular tissue engineering applications.* International Journal of Electrospun Nanofibers, 2007. **1**: p. 73-87.

45. Boccafoschi, F., et al., *Biological performances of collagen-based scaffolds for vascular tissue engineering.* Biomaterials, 2005. **26**(35): p. 7410-7.

46. Chen, Z.G., et al., *Electrospun collagen-chitosan nanofiber: a biomimetic extracellular matrix for endothelial cell and smooth muscle cell.* Acta Biomater. **6**(2): p. 372-82.

47. He, W., et al., *Fabrication of collagen-coated biodegradable polymer nanofiber mesh and its potential for endothelial cells growth.* Biomaterials, 2005. **26**(36): p. 7606-15.

48. He, W., et al., *Fabrication and endothelialization of collagen-blended biodegradable polymer nanofibers: Potential vascular graft for blood vessel tissue engineering.* Tissue Eng, 2005. **11**(9): p. 1574-1588.

49. Jeong, S.I., et al., *Tissue-engineered vascular grafts composed of marine collagen and PLGA fibers using pulsatile perfusion bioreactors.* Biomaterials, 2007. **28**: p. 1115-1122.

50. McClure, M.J., et al., *Electrospun polydioxanone, elastin, and collagen vascular scaffolds: Uniaxial cyclic distension.* Journal of Engineered Fibers and Fabrics, 2009. **4**(2): p. 18-25.

51. Tillman, B.W., et al., *The in vivo stability of electrospun polycaprolactone-collagen scaffolds in vascular reconstruction.* Biomaterials, 2009. **30**(4): p. 583-8.

52. Venugopal, J., et al., *In vitro study of smooth muscle cells on polycaprolactone and collagen nanofibrous matrices.* Cell Biol Int, 2005. **29**(10): p. 861-7.

53. Venugopal, J.R., Y.Z. Zhang, and S. Ramakrishna, *In vitro culture of human dermal fibroblasts on electrospun polycaprolactone collagen nanofibrous membrane.* Artificial Organs, 2006. **30**(6): p. 440-446.

54. Chen, P.J., G.Y. Chang, and J.K. Chen, *Electrospun collagen/chitosan nanofibrous membrane as wound dressing.* Colloids and Surfaces A: Physicochemical and Engineering Aspects, 2008. **313-314**: p. 183-188.

55. Rho, K.S., et al., *Electrospinning of collagen nanofibers: effects on the behavior of normal human keratinocytes and early-stage wound healing.* Biomaterials, 2006. **27**(8): p. 1452-61.

56. Aszodi, A., et al., *What mouse mutants teach us about extracellular matrix function.* Annu Rev Cell Dev Biol, 2006. **22**: p. 591-621.

57. Daamen, W.F., et al., *Preparation and evaluation of moleculary-defined collagen-elastin-glycosaminoglycan scaffolds for tissue engineering.* Biomaterials, 2003. **24**: p. 4001-4009.

58. Hafemann, B., et al., *Use of a collagen/elastin-membrane for the tissue engineering of dermis.* Burns, 1999. **25**(5): p. 373-384.

59. Barnes, C.P., *Design of an Electrospun Type II Collagen Scaffold for Articular Cartilage Tissue Engineering*, in *Biomedical Engineering*. 2007, Virginia Commonwealth University: Richmond, VA. p. 164.

60. Shih, Y.R., et al., *Growth of mesenchymal stem cells on electrospun type I collagen nanofibers.* Stem Cells, 2006. **24**(11): p. 2391-7.

61. Kim, H.W., J.H. Song, and H.E. Kim, *Bioactive glass nanofiber-collagen nanocomposite as a novel bone regeneration matrix.* J Biomed Mater Res A, 2006. **79**(3): p. 698-705.

62. Gentleman, E., et al., *Development of ligament-like structural organization and properties in cell-seeded collagen scaffolds in vitro.* Annals of Biomedical Engineering, 2006. **34**(5): p. 726-736.

63. Kimura, Y., et al., *Regeneration of anterior cruciate ligament by biodegradable scaffold combined with local controlled release of basic fibroblast growth factor and collagen wrapping.* Tissue Engineering Part C, 2008. **14**(1): p. 47-57.

64. Schnell, E., et al., *Guidance of glial cell migration and axonal growth on electrospun nanofibers of poly-epsilon-caprolactone and a collagen/poly-epsilon-caprolactone blend.* Biomaterials, 2007. **28**(19): p. 3012-25.

65. Berglund, J.D., R.M. Nerem, and A. Sambanis, *Incorporation of intact elastin scaffolds in tissue-engineered collagen-based vascular grafts.* Tissue Eng, 2004. **10**: p. 1526-1535.

66. Boland, E.D., et al., *Electrospinning collagen and elastin: preliminary vascular tissue engineering.* Front Biosci, 2004. **9**: p. 1422-32.

67. Buijtenhuijs, P., et al., *Tissue engineering of blood vessels: characterization of smooth-muscle cells for culturing on collagen-and-elastin-based scaffolds.* Biotechnology and Applied Biochemistry, 2004. **39**: p. 141-149.

68. Buttafoco, L., et al., *Electrospinning of collagen and elastin for tissue engineering applications.* Biomaterials, 2006. **27**(5): p. 724-734.

69. McClure, M.J., et al., *A three-layered electrospun matrix to mimic native arterial architecture using polycaprolactone, elastin, and collagen: A preliminary study.* Acta Biomater, 2010. **6**(7): p. 2422-33.

70. Boland, E.D., P.G. Espy, and G.L. Bowlin, *Tissue Engineering Scaffolds*, in *Encyclopedia of Biomaterials and Biomedical Engineering*. 2004. p. 1-7.

71. Altman, G.H., et al., *Silk matrix for tissue engineered anterior cruciate ligaments.* Biomaterials, 2002. **23**: p. 4131-4141.

72. Fan, H., et al., *Enhanced differentiation of mesenchymal stem cells co-cultured with ligament fibroblasts on gelatin/silk fibroin hybrid scaffold.* Biomaterials, 2008. **29**: p. 1017-1027.

73. Fan, H., et al., *In vivo study of anterior cruciate ligament regeneration using mesenchymal stem cells and silk scaffold.* Biomaterials, 2008. **29**: p. 3324-3337.

74. Liu, H., et al., *Modification of sericin-free silk fibers for ligament tissue engineering application.* Journal of Biomedical Materials Research Part B: Applied Biomaterials, 2006. **10**: p. 129-138.

75. Sell, S.A., *Tissue Engineering Cellularized Silk-Based Ligament Analogues*, in *Biomedical Engineering*. 2009, Virginia Commonwealth University: Richmond, VA. p. 322.

76. Sell, S.A., et al., *Preliminary investigation of airgap electrospun silk fibroin-based structures for ligament analogue engineering.* J Biomater Sci Polym Ed, 2010.

77. Seo, Y.-K., et al., *The biocompatibility of silk scaffold for tissue engineered ligaments.* Key Engineering Materials, 2007. **342**: p. 73-76.

78. Toh, S.L., et al., *Novel silk scaffolds for ligament tissue engineering applications.* Key Engineering Materials, 2006. **326-328**(1): p. 727-730.

79. McClure, M., et al., *Electrospinning-aligned and random polydioxanone-polycaprolactone-silk fibroin-blended scaffolds: geometry for a vascular matrix.* Biomedical Materials, 2009. **4**(5): p. 1-13.

80. Soffer, L., et al., *Silk-based electrospun tubular scaffolds for tissue-engineered vascular grafts.* J. Biomater. Sci. Polymer Edn., 2008. **19**(5): p. 653-664.

81. Zhang, X., C.B. Baughman, and D.L. Kaplan, *In vitro evaluation of electrospun silk fibroin scaffolds for vascular cell growth.* Biomaterials, 2008. **29**: p. 2217-2227.

82. Li, C., et al., *Electrospun silk-BMP-2 scaffolds for bone tissue engineering.* Biomaterials, 2006. **27**(16): p. 3115-24.

83. Meinel, L., et al., *Engineering bone-like tissue in vitro using human bone marrow stem cells and silk scaffolds.* J Biomed Mater Res A, 2004 Oct 1. **71**(1): p. 25-34.

84. Yeo, I.S., et al., *Collagen-based biomimetic nanofibrous scaffolds: preparation and characterization of collagen/silk fibroin bicomponent nanofibrous structures.* Biomacromolecules, 2008. **9**(4): p. 1106-16.

85. Ayres, C., et al., *Nanotechnology in tissue scaffolding / organ development for transplant.* Wiley Interdisciplinary Reviews: Nanomedicine, 2009. **In Review**.

86. Sell, S., et al., *Extracellular matrix regenerated: tissue engineering via electrospun biomimetic nanofibers.* Polymer International, 2007. **56**: p. 1349-1360.

87. Kumbar, S.G., et al., *Electrospun nanofiber scaffolds: engineering soft tissues.* Biomed Mater, 2008. **3**(3): p. 034002.

88. Kenawy, E., et al., *Release of tetracycline hydrochloride from electrospun poly(ethylene-co-vinylacetate), poly(lactic acid), and a blend.* J Control Release, 2002. **81**: p. 57-64.

89. Kim, K., et al., *Incorporation and controlled release of a hydrophilic antibiotic using poly(lactide-co-glycolide)-based electrospun nanofibrous scaffolds.* J Control Release, 2004. **98**(1): p. 47-56.

90. Zeng, J., et al., *Biodegradable electrospun fibers for drug delivery.* J Control Release, 2003. **92**(3): p. 227-31.

91. Zeng, J., et al., *Influence of the drug compatibility with polymer solution on the release kinetics of electrospun fiber formulation.* J Control Release, 2005. **105**(1-2): p. 43-51.

92. Xu, X., et al., *Ultrafine medicated fibers electrospun from W/O emulsions.* J Control Release, 2005. **108**(1): p. 33-42.

93. Huang, Z.M., et al., *Encapsulating drugs in biodegradable ultrafine fibers through co-axial electrospinning.* J Biomed Mater Res A, 2006. **77**(1): p. 169-79.

94. Chunder, A., et al., *Fabrication of ultrathin polyelectrolyte fibers and their controlled release properties.* Colloids Surf B Biointerfaces, 2007. **58**(2): p. 172-9.

95. Yannas, I.V., et al., *Synthesis and characterization of a model extracellular matrix that induces partial regeneration of adult mammalian skin.* Proc Natl Acad Sci U S A, 1989. **86**(3): p. 933-7.

96. Dagalakis, N., et al., *Design of an artificial skin. Part III. Control of pore structure.* J Biomed Mater Res, 1980. **14**(4): p. 511-28.

97. Pham, Q.P., U. Sharma, and A.G. Mikos, *Electrospun poly(epsilon-caprolactone) microfiber and multilayer nanofiber/microfiber scaffolds: characterization of scaffolds and measurement of cellular infiltration.* Biomacromolecules, 2006. **7**(10): p. 2796-805.

98. Tuzlakoglu, K., et al., *Nano- and micro-fiber combined scaffolds: a new architecture for bone tissue engineering.* J Mater Sci Mater Med, 2005. **16**(12): p. 1099-104.

99. Yang, S., et al., *The design of scaffolds for use in tissue engineering. Part I. Traditional factors.* Tissue Eng, 2001. **7**(6): p. 679-89.

100. Szentivanyi, A., et al., *Electrospun cellular microenvironments: Understanding controlled release and scaffold structure.* Adv Drug Deliv Rev. **63**(4-5): p. 209-20.

101. Brauker, J.H., et al., *Neovascularization of synthetic membranes directed by membrane microarchitecture.* J Biomed Mater Res, 1995. **29**(12): p. 1517-24.

102. Soliman, S., et al., *Controlling the porosity of fibrous scaffolds by modulating the fiber diameter and packing density.* J Biomed Mater Res A. **96**(3): p. 566-74.

103. Lowery, J.L., N. Datta, and G.C. Rutledge, *Effect of fiber diameter, pore size and seeding method on growth of human dermal fibroblasts in electrospun poly(epsilon-caprolactone) fibrous mats.* Biomaterials. **31**(3): p. 491-504.

104. Li, M., et al., *Electrospun protein fibers as matrices for tissue engineering.* Biomaterials, 2005. **26**(30): p. 5999-6008.

105. Sell, S.A., et al., *Electrospun polydioxanone-elastin blends: potential for bioresorbable vascular grafts.* Biomed Mater, 2006. **1**(2): p. 72-80.

106. McClure, M.J., et al., *Electrospinning-aligned and random polydioxanone-polycaprolactone-silk fibroin-blended scaffolds: geometry for a vascular matrix.* Biomed Mater, 2009. **4**(5): p. 055010.

107. Baker, B.M., et al., *The potential to improve cell infiltration in composite fiber-aligned electrospun scaffolds by the selective removal of sacrificial fibers.* Biomaterials, 2008. **29**(15): p. 2348-58.

108. Nam, J., et al., *Improved cellular infiltration in electrospun fiber via engineered porosity.* Tissue Eng, 2007. **13**(9): p. 2249-57.

109. McClure, M.J., et al., *The use of air-flow impedance to control fiber deposition patterns during electrospinning.* Biomaterials. **33**(3): p. 771-9.

110. Chen, Z., et al., *In vitro angiogenesis by human umbilical vein endothelial cells (HUVEC) induced by three-dimensional co-culture with glioblastoma cells.* J Neurooncol, 2009. **92**(2): p. 121-8.

111. Brown, B.N., et al., *Macrophage phenotype and remodeling outcomes in response to biologic scaffolds with and without a cellular component.* Biomaterials, 2009. **30**(8): p. 1482-91.

112. Blair, R.J., et al., *Human mast cells stimulate vascular tube formation. Tryptase is a novel, potent angiogenic factor.* J Clin Invest, 1997. **99**(11): p. 2691-700.

113. Noli, C. and A. Miolo, *The mast cell in wound healing.* Vet Dermatol, 2001. **12**(6): p. 303-13.

114. Hiromatsu, Y. and S. Toda, *Mast cells and Angiogenesis.* Microscopy research and technique, 2003. **69**: p. 60-64.

115. Rao, K.N. and M.A. Brown, *Mast cells: multifaceted immune cells with diverse roles in health and disease.* Ann N Y Acad Sci, 2008. **1143**: p. 83-104.

116. Maltby, S., K. Khazaie, and K.M. McNagny, *Mast cells in tumor growth: Angiogenesis, tissue remodelling and immune-modulation.* Biochim Biophys Acta, 2009. **1796**(1): p. 19-26.

117. Tang, L., T.A. Jennings, and J.W. Eaton, *Mast cells mediate acute inflammatory responses to implanted biomaterials.* Proc Natl Acad Sci U S A, 1998. **95**(15): p. 8841-6.

118. Metcalfe, D.D., D. Baram, and Y.A. Mekori, *Mast cells.* Physiol Rev, 1997. **77**(4): p. 1033-79.

119. Mekori, Y.A. and D.D. Metcalfe, *Mast cells in innate immunity.* Immunol Rev, 2000. **173**: p. 131-40.

120. Galli, S.J., *Complexity and redundancy in the pathogenesis of asthma: reassessing the roles of mast cells and T cells.* J Exp Med, 1997. **186**(3): p. 343-7.

121. Galli, S.J. and C.S. Lantz, *Allergy*. Fundamental Immunology, ed. W.E. Paul. 1999, Philadelphia: Lippincott-Raven Press. 1137-1184.

122. Eady, R.A., et al., *Mast cell population density, blood vessel density and histamine content in normal human skin.* Br J Dermatol, 1979. **100**(6): p. 623-33.

123. Nilsson, G., et al., *Stem cell factor is a chemotactic factor for human mast cells.* J Immunol, 1994. **153**(8): p. 3717-23.

124. Yamaguchi, H., et al., *Umbilical vein endothelial cells are an important source of c-kit and stem cell factor which regulate the proliferation of haemopoietic progenitor cells.* Br J Haematol, 1996. **94**(4): p. 606-11.

125. Coleman, J.W., et al., *Regulation of mouse peritoneal mast cell secretory function by stem cell factor, IL-3 or IL-4.* J Immunol, 1993. **150**(2): p. 556-62.

126. Galli, S.J., et al., *Reversible expansion of primate mast cell populations in vivo by stem cell factor.* J Clin Invest, 1993. **91**(1): p. 148-52.

127. Valent, P., et al., *Induction of differentiation of human mast cells from bone marrow and peripheral blood mononuclear cells by recombinant human stem cell factor/kit-ligand in long-term culture.* Blood, 1992. **80**(9): p. 2237-45.

128. Wershil, B.K., et al., *The rat c-kit ligand, stem cell factor, induces c-kit receptor-dependent mouse mast cell activation in vivo. Evidence that signaling through the c-kit receptor can induce expression of cellular function.* J Exp Med, 1992. **175**(1): p. 245-55.

129. Iemura, A., et al., *The c-kit ligand, stem cell factor, promotes mast cell survival by suppressing apoptosis.* Am J Pathol, 1994. **144**(2): p. 321-8.

130. Berton, A., et al., *Activation of fibroblasts in collagen lattices by mast cell extract: a model of fibrosis.* Clin Exp Allergy, 2000. **30**(4): p. 485-92.

131. Hatamochi, A., K. Fujiwara, and H. Ueki, *Effects of histamine on collagen synthesis by cultured fibroblasts derived from guinea pig skin.* Arch Dermatol Res, 1985. **277**(1): p. 60-4.

132. Russel, J.D., S.B. Russell, and K.M. Trupin, *The effect of histamine on the growth of cultured fibroblasts isolated from normal and keloid tissue.* J Cell Physiol, 1977. **93**(3): p. 389-93.

133. Cairns, J.A. and A.F. Walls, *Mast cell tryptase stimulates the synthesis of type I collagen in human lung fibroblasts.* J Clin Invest, 1997. **99**(6): p. 1313-21.

134. Duling, R.R., et al., *Mechanical characterization of electrospun polycaprolactone (PCL): a potential scaffold for tissue engineering.* J Biomech Eng, 2008. **130**(1): p. 011006.

135. Del Gaudio, C., et al., *Structural characterization and cell response evaluation of electrospun PCL membranes: micrometric versus submicrometric fibers.* J Biomed Mater Res A, 2009. **89**(4): p. 1028-39.

136. Pektok, E., et al., *Degradation and healing characteristics of small-diameter poly(epsilon-caprolactone) vascular grafts in the rat systemic arterial circulation.* Circulation, 2008. **118**(24): p. 2563-70.

137. Boland, E.D., et al., *Electrospinning polydioxanone for biomedical applications.* Acta Biomater, 2005. **1**(1): p. 115-23.

138. Garg, K., et al., *Angiogenic potential of human macrophages on electrospun bioresorbable vascular grafts.* Biomed Mater, 2009. **4**(3): p. 031001.

139. Smith, M.J., et al., *Suture-reinforced electrospun polydioxanone-elastin small-diameter tubes for use in vascular tissue engineering: a feasibility study.* Acta Biomater, 2008. **4**(1): p. 58-66.

140. Smith, M.J., et al., *Modulation of murine innate and acquired immune responses following in vitro exposure to electrospun blends of collagen and polydioxanone.* J Biomed Mater Res A. **93**(2): p. 793-806.

141. Smith, M.J., et al., *In vitro evaluations of innate and acquired immune responses to electrospun polydioxanone-elastin blends.* Biomaterials, 2009. **30**(2): p. 149-59.

142. Zhang, X., C.B. Baughman, and D.L. Kaplan, *In vitro evaluation of electrospun silk fibroin scaffolds for vascular cell growth.* Biomaterials, 2008. **29**(14): p. 2217-27.

143. Soffer, L., et al., *Silk-based electrospun tubular scaffolds for tissue-engineered vascular grafts.* J Biomater Sci Polym Ed, 2008. **19**(5): p. 653-64.

144. Asai, K., et al., *Regulation of mast cell survival by IgE.* Immunity, 2001. **14**(6): p. 791-800.

145. Jin, H.J., et al., *Human bone marrow stromal cell responses on electrospun silk fibroin mats.* Biomaterials, 2004. **25**(6): p. 1039-47.

146. Ryan, J.J., et al., *IL-4 inhibits mouse mast cell Fc epsilonRI expression through a STAT6-dependent mechanism.* J Immunol, 1998. **161**(12): p. 6915-23.

147. Macey, M.R., et al., *IL-4 and TGF-beta 1 counterbalance one another while regulating mast cell homeostasis.* J Immunol. **184**(9): p. 4688-95.

148. Plaut, M., et al., *Mast cell lines produce lymphokines in response to cross-linkage of Fc epsilon RI or to calcium ionophores.* Nature, 1989. **339**(6219): p. 64-7.

149. Thompson, H.L., L. Thomas, and D.D. Metcalfe, *Murine mast cells attach to and migrate on laminin-, fibronectin-, and matrigel-coated surfaces in response to Fc epsilon RI-mediated signals.* Clin Exp Allergy, 1993. **23**(4): p. 270-5.

150. Kruger-Krasagakes, S., et al., *Adhesion of human mast cells to extracellular matrix provides a co-stimulatory signal for cytokine production.* Immunology, 1999. **98**(2): p. 253-7.

151. Thompson, H.L., et al., *Laminin promotes mast cell attachment.* J Immunol, 1989. **143**(7): p. 2323-7.

152. Bianchine, P.J., P.R. Burd, and D.D. Metcalfe, *IL-3-dependent mast cells attach to plate-bound vitronectin. Demonstration of augmented proliferation in response to signals transduced via cell surface vitronectin receptors.* J Immunol, 1992. **149**(11): p. 3665-71.

153. Lam, V., et al., *IgE alone stimulates mast cell adhesion to fibronectin via pathways similar to those used by IgE + antigen but distinct from those used by Steel factor.* Blood, 2003. **102**(4): p. 1405-13.

154. Artuc, M., et al., *Mast cells and their mediators in cutaneous wound healing--active participants or innocent bystanders?* Exp Dermatol, 1999. **8**(1): p. 1-16.

155. Compton, S.J., et al., *The role of mast cell tryptase in regulating endothelial cell proliferation, cytokine release, and adhesion molecule expression: tryptase induces expression of mRNA for IL-1 beta and IL-8 and stimulates the selective release of IL-8 from human umbilical vein endothelial cells.* J Immunol, 1998. **161**(4): p. 1939-46.

156. Galli, S.J., J.R. Gordon, and B.K. Wershil, *Mast cell cytokines in allergy and inflammation.* Agents Actions Suppl, 1993. **43**: p. 209-20.

157. Goebeler, M., et al., *Interleukin-13 selectively induces monocyte chemoattractant protein-1 synthesis and secretion by human endothelial cells. Involvement of IL-4R alpha and Stat6 phosphorylation.* Immunology, 1997. **91**(3): p. 450-7.

158. Gordon, J.R. and S.J. Galli, *Mast cells as a source of both preformed and immunologically inducible TNF-/cachectin.* Nature, 1990. **346**: p. 274-6.

159. Malaviya, R., et al., *Mast cell modulation of neutrophil influx and bacterial clearance at sites of infection through TNF-alpha.* Nature, 1996. **381**(6577): p. 77-80.

160. Norrby, K., *Mast cells and angiogenesis.* Apmis, 2002. **110**(5): p. 355-71.

161. Walsh, L.J., et al., *Human dermal mast cells contain and release tumor necrosis factor alpha, which induces endothelial leukocyte adhesion molecule 1.* Proc Natl Acad Sci U S A, 1991. **88**(10): p. 4220-4.

162. McLachlan, J.B., et al., *Mast cell-derived tumor necrosis factor induces hypertrophy of draining lymph nodes during infection.* Nat Immunol, 2003. **4**(12): p. 1199-205.

163. DiPietro, L.A., et al., *MIP-1alpha as a critical macrophage chemoattractant in murine wound repair.* J Clin Invest, 1998. **101**(8): p. 1693-8.

164. Low, Q.E., et al., *Wound healing in MIP-1alpha(-/-) and MCP-1(-/-) mice.* Am J Pathol, 2001. **159**(2): p. 457-63.

165. Maurer, M. and E. von Stebut, *Macrophage inflammatory protein-1.* Int J Biochem Cell Biol, 2004. **36**(10): p. 1882-6.

166. Li, D. and Y. Xia, *Electrospinning of Nanofibers: Reinventing the Wheel?* Advanced Materials, 2004. **16**(14): p. 1151-1170.

167. Campillo-Fernández, A., et al., *Analysis of the Biological Response of Endothelial and Fibroblast Cells Cultured on Synthetic Scaffolds with Various Hydrophilic/Hydrophobic Ratios: Influence of Fibronectin Adsorption and Conformation.* Tissue Engineering: Part A, 2009. **15**: p. 1331-41.

168. Liang, D., B.S. Hsiao, and B. Chu, *Functional electrospun nanofibrous scaffolds for biomedical applications.* Adv Drug Deliv Rev, 2007. **59**(14): p. 1392-412.

169. Keselowsky, B.G., et al., *Role of plasma fibronectin in the foreign body response to biomaterials.* Biomaterials, 2007. **28**(25): p. 3626-31.

170. Clark, R.A., *Potential roles of fibronectin in cutaneous wound repair.* Arch Dermatol, 1988. **124**(2): p. 201-6.

171. Odom, S., et al., *Negative regulation of immunoglobulin E-dependent allergic responses by Lyn kinase.* J Exp Med, 2004. **199**(11): p. 1491-502.

172. Xiang, Z., et al., *Essential role of the prosurvival bcl-2 homologue A1 in mast cell survival after allergic activation.* J Exp Med, 2001. **194**(11): p. 1561-69.

173. Kawakami, T. and J. Kitaura, *Mast cell survival and activation by IgE in the absence of antigen: a consideration of the biologic mechanisms and relevance.* J Immunol, 2005. **175**(7): p. 4167-73.

174. Pham, E.A., et al., *Modification of the diphenylamine assay for cell quantification in three-dimensional biodegradable polymeric scaffolds.* J Biomed Mater Res B Appl Biomater. **92**(2): p. 499-507.

175. Panilaitis, B., et al., *Macrophage responses to silk.* Biomaterials, 2003. **24**(18): p. 3079-85.

176. Bochner, B.S., et al., *IL-13 selectively induces vascular cell adhesion molecule-1 expression in human endothelial cells.* J Immunol, 1995. **154**(2): p. 799-803.

177. Lee, C.G., et al., *Interleukin-13 induces tissue fibrosis by selectively stimulating and activating transforming growth factor beta(1).* J Exp Med, 2001. **194**(6): p. 809-21.

178. Mestas, J. and C.C. Hughes, *Of Mice and Not Men: Differences between Mouse and Human Immunology.* Journal of Immunology, 2004. **172**: p. 2731-2738.

179. Badylak, S.F., et al., *Macrophage phenotype as a determinant of biologic scaffold remodeling.* Tissue Eng Part A, 2008. **14**(11): p. 1835-42.

180. Saino, E., et al., *Effect of electrospun fiber diameter and alignment on macrophage activation and secretion of proinflammatory cytokines and chemokines.* Biomacromolecules. **12**(5): p. 1900-11.

181. Sanders, J.E., C.E. Stiles, and C.L. Hayes, *Tissue response to single-polymer fibers of varying diameters: evaluation of fibrous encapsulation and macrophage density.* J Biomed Mater Res, 2000. **52**(1): p. 231-7.

182. von Recum, A.F. and T.G. van Kooten, *The influence of micro-topography on cellular response and the implications for silicone implants.* J Biomater Sci Polym Ed, 1995. **7**(2): p. 181-98.

183. Madden, L.R., et al., *Proangiogenic scaffolds as functional templates for cardiac tissue engineering.* Proc Natl Acad Sci U S A. **107**(34): p. 15211-6.

184. Chamberlain, L.M., et al., *Phenotypic non-equivalence of murine (monocyte-) macrophage cells in biomaterial and inflammatory models.* J Biomed Mater Res A, 2009. **88**(4): p. 858-71.

185. Faffe, D.S., et al., *Interleukin-13 and interleukin-4 induce vascular endothelial growth factor release from airway smooth muscle cells: role of vascular endothelial growth factor genotype.* Am J Respir Cell Mol Biol, 2006. **34**(2): p. 213-8.

186. Gu, L., et al., *Control of TH2 polarization by the chemokine monocyte chemoattractant protein-1.* Nature, 2000. **404**(6776): p. 407-11.

187. Fairweather, D. and D. Cihakova, *Alternatively activated macrophages in infection and autoimmunity.* J Autoimmun, 2009. **33**(3-4): p. 222-30.

188. Varin, A. and S. Gordon, *Alternative activation of macrophages: immune function and cellular biology.* Immunobiology, 2009. **214**(7): p. 630-41.

189. He, Z., et al., *The interaction between different types of activated RAW 264.7 cells and macrophage inflammatory protein-1 alpha.* Radiat Oncol. **6**: p. 86.

190. Chen, S., et al., *Characterization of topographical effects on macrophage behavior in a foreign body response model.* Biomaterials. **31**(13): p. 3479-91.

191. Schutte, R.J., A. Parisi-Amon, and W.M. Reichert, *Cytokine profiling using monocytes/macrophages cultured on common biomaterials with a range of surface chemistries.* J Biomed Mater Res A, 2009. **88**(1): p. 128-39.

192. Hoh, B.L., et al., *Monocyte chemotactic protein-1 promotes inflammatory vascular repair of murine carotid aneurysms via a macrophage inflammatory protein-1alpha and macrophage inflammatory protein-2-dependent pathway.* Circulation. **124**(20): p. 2243-52.

193. Ucuzian, A.A. and H.P. Greisler, *In vitro models of angiogenesis.* World J Surg, 2007. **31**(4): p. 654-63.

194. Abbott, A., *Cell culture: biology's new dimension.* Nature, 2003. **424**(6951): p. 870-2.

195. Velazquez, O.C., et al., *Fibroblast-dependent differentiation of human microvascular endothelial cells into capillary-like 3-dimensional networks.* FASEB J, 2002. **16**(10): p. 1316-8.

196. Rao, R.R., et al., *Matrix composition regulates three-dimensional network formation by endothelial cells and mesenchymal stem cells in collagen/fibrin materials.* Angiogenesis. **15**(2): p. 253-64.

197. Dietrich, F. and P.I. Lelkes, *Fine-tuning of a three-dimensional microcarrier-based angiogenesis assay for the analysis of endothelial-mesenchymal cell co-cultures in fibrin and collagen gels.* Angiogenesis, 2006. **9**(3): p. 111-25.

198. Allen, P., J. Melero-Martin, and J. Bischoff, *Type I collagen, fibrin and PuraMatrix matrices provide permissive environments for human endothelial and mesenchymal progenitor cells to form neovascular networks.* J Tissue Eng Regen Med. **5**(4): p. e74-86.

199. Vernon, R.B. and E.H. Sage, *A novel, quantitative model for study of endothelial cell migration and sprout formation within three-dimensional collagen matrices.* Microvasc Res, 1999. **57**(2): p. 118-33.

200. Takeda, K. and S. Akira, *TLR signaling pathways.* Seminars in Immunology, 2004. **16**.

201. Yamamoto, M., et al., *Essential role for TIRAP in activation of the signalling cascade shared by TLR2 and TLR4.* Nature, 2002. **420**(6913): p. 324-9.

202. Cote, M., et al., *The critical role of the MyD88-dependent pathway in non-CNS MPTP-mediated toxicity.* Brain Behav Immun. **25**(6): p. 1143-52.

203. Geiger-Maor, A., et al., *Cells exposed to sublethal oxidative stress selectively attract monocytes/macrophages via scavenger receptors and MyD88-mediated signaling.* J Immunol. **188**(3): p. 1234-44.

204. Maa, M.C., et al., *The iNOS/Src/FAK axis is critical in Toll-like receptor-mediated cell motility in macrophages.* Biochim Biophys Acta. **1813**(1): p. 136-47.

205. van den Borne, S.W., et al., *Mouse strain determines the outcome of wound healing after myocardial infarction.* Cardiovasc Res, 2009. **84**(2): p. 273-82.

206. Yamashita, Y., et al., *Cutting edge: genetic variation influences Fc epsilonRI-induced mast cell activation and allergic responses.* J Immunol, 2007. **179**(2): p. 740-3.

207. Jain, R.K., et al., *Quantitative angiogenesis assays: progress and problems.* Nat Med, 1997. **3**(11): p. 1203-8.

208. Auerbach, R., et al., *Angiogenesis assays: problems and pitfalls.* Cancer Metastasis Rev, 2000. **19**(1-2): p. 167-72.

209. Staton, C.A., M.W. Reed, and N.J. Brown, *A critical analysis of current in vitro and in vivo angiogenesis assays.* Int J Exp Pathol, 2009. **90**(3): p. 195-221.

210. Guedez, L., et al., *Quantitative assessment of angiogenic responses by the directed in vivo angiogenesis assay.* Am J Pathol, 2003. **162**(5): p. 1431-9.

211. Kasama, T., et al., *Neutrophil-derived cytokines: potential therapeutic targets in inflammation.* Curr Drug Targets Inflamm Allergy, 2005. **4**(3): p. 273-9.

VITAE

Koyal Garg was born in Meerut, U.P., India on 29th September 1985. She received a Bachelor's of Engineering degree in Biomedical Instrumentation Engineering from Avinashilingam Deemed University, India in May 2006. In fall of 2008, she completed her Master's in Biomedical Engineering from Virginia Commonwealth University under Dr. Gary L. Bowlin. She continued with her Ph.D. work in Biomedical Engineering under the mentorship of Dr. Gary L. Bowlin and Dr. John J. Ryan from spring 2009. She had also worked as a Teaching Assistant from Fall 2006 - Spring 2012 for several courses, such as Biomedical Instrumentation, Computational Methods and Biomedical Signal Processing. During the course of her doctoral studies, she was awarded the Alex M. Clark award for excellence in Biomedical Engineering in 2012 and 2nd runner-up for the outstanding graduate teaching assistant award by Graduate School of Engineering for the academic year 2010-2011. During her graduate work at VCU, she has published eight peer reviewed journal articles and two book sections. She has also presented her work at various conferences including Annual Hilton Head Workshop, Biomedical Engineering Society (BMES) annual fall meeting, The International Society for Applied Cardiovascular Biology (ISACB) Biennial meeting and The Tissue Engineering and Regenerative Medicine International Society (TERMIS) meeting.